KINETIC AND NMR STUDIES OF SOME NITROGEN HETEROCYCLES

Lesley Marion Anderson

A Thesis Submitted for the Degree of PhD
at the
University of St Andrews

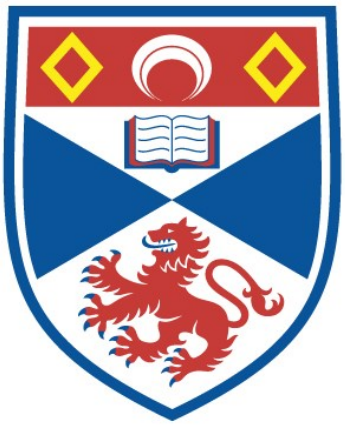

1990

M. DOWNIE & SON
Bookbinders and Printers
UNIT 2B
46 FINNIESTON ST.
GLASGOW G2 6JU
TEL: 041-221-2469

ProQuest LLC.
789 East Eisenhower Parkway
P.O. Box 1346
Ann Arbor, MI 48106 – 1346

Kinetic and NMR Studies of Some Nitrogen Heterocycles

A Thesis presented for the degree of

DOCTOR OF PHILOSOPHY

in the Faculty of Science of the

University of St. Andrews

by

Lesley Marion Anderson

September 1989

United College of
St. Salvator and St. Leonard,
St. Andrews.

听 而 忘

见 而 忆

作 而 明

I hear, and I forget

I see, and I remember

I do, and I understand.

-Traditional Chinese saying.

DECLARATION

I, Lesley Marion Anderson, hereby certify that this thesis has been composed by myself, that it is a record of my own work, and that it has not been accepted in partial or complete fulfilment of any other degree or professional qualification.

Lesley Anderson

I was admitted to the Faculty of Science of the University of St. Andrews under Ordinance General No. 12 on 1st October 1986 and as a candidate for the degree of Ph.D. on 1st October 1987.

Lesley Anderson

I hereby certify that the candidate has fulfilled the conditions of the Resolution and Regulations appropriate to the degree of Ph. D.

Supervisor

COPYRIGHT

ACKNOWLEDGEMENTS

I would like to thank a number of people who have been connected with this work during the past three years.

Firstly, in St. Andrews, thanks are due to Dr. R. K. Mackie for running the two-dimensional nmr spectra and for valuable assistance in interpreting them, Melanja Smith for running many of the other nmr spectra, Dr. C. Glidewell for help with the MNDO calculations and Dr. K. Harris for advice on solid state nmr spectroscopy..

I am grateful also to the following for the use of equipment and for their advice: Drs. I. Sadler and D. Reed (SERC Regional NMR Service at the University of Edinburgh), Drs. B. J. Say and D. Apperly (SERC/UDIRL NMR Service at the University of Durham), Dr. L. Williams and technical staff (University of Durham), Dr. N. Isaacs (University of Reading), Dr. P. Boyle (Trinity College, Dublin) and Dr. P. Sorensen (Technical University of Copenhagen).

Finally, and most importantly, my thanks go to my supervisor, Dr. A. R. Butler, for his enthusiasm and support throughout my research and to the Rollo Trust for the provision of a Research Studentship during 1986-1989.

CONTENTS

ABSTRACT

The work carried out in this thesis involves the investigation of some reactions of heterocyclic compounds by a wide range of spectroscopic and kinetic techniques.

Chapter 1 describes several methods, including stopped-flow spectrophotometry, high pressure kinetics and MNDO calculations, which are used to analyse the mechanism of the reaction of imidazole with diazonium ions. Chapter 2 describes the use of the temperature-jump technique to follow the extremely fast protonation of pyrroles. Diazonium ions are further investigated in Chapter 3 which examines the structure of p-nitrobenzenediazonium tetrafluoroborate by X-ray crystallography. The nature of other benzenediazonium ions and some of their complexes is also investigated by solid state ^{15}N nmr spectroscopy.

Chapter 4 switches the emphasis to nmr spectroscopy. The reactive intermediates of reactions of benzil with nitrogen heterocycles are investigated using ^{13}C nmr spectroscopy in a kinetic application. Chapters 5 and 6 continue the use of nmr spectroscopy in the structural assignment of bilirubin and the determination of the nature of bilirubin inclusion complexes. Chapter 6 also examines by spectrophotometry the reaction used in the clinical analysis of bilirubin and the effect on this reaction of binding agents such as albumin and α-cyclodextrin.

Chapter 1

Study of the Mechanism of Imidazole Coupling with Diazonium Ions.

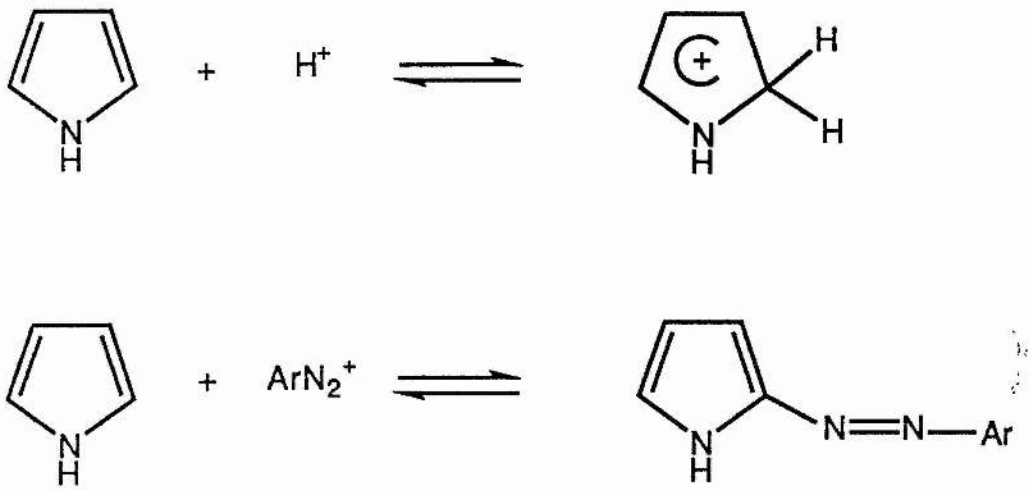

Scheme 1. Mechanism for diazotisation.

1.1 INTRODUCTION

Extensive studies have been carried out on the reaction of pyrroles and various pyrrole derivatives with diazonium ions. Butler, Pogorzelec and Shepherd[1] studied the kinetics and products of the reaction of pyrrole and substituted derivatives and proposed the mechanism shown in Scheme 1. Imidazole and its methylated derivatives also react with diazonium ions to give highly coloured products. As part of an extension of the investigation into the reactions of pyrrole reactions with diazonium ions, the mechanism of the imidazole reaction was compared with that of pyrrole. It was expected that the two mechanisms would be similar, the extra ring nitrogen present in imidazole having little effect except to reduce the susceptibility of the ring to electrophilic attack. One of the most important previous studies is that due to Ridd et al[2]. In 1953 they reported an investigation into the kinetics of the diazo-coupling reaction of imidazole and proposed that reaction proceeds via an anionic intermediate. Preliminary kinetic studies confirmed that imidazole reacts more slowly with diazonium ions than pyrrole, consistent with the electron withdrawing effect of the second nitrogen. Further kinetic work, however, did not confirm a mechanism of the type shown in Scheme 1 but was consistent with reaction via the imidazole anion. The aim of this work was to confirm the anionic intermediate by the use of a variety of experimental techniques not available to Ridd et al. in 1953.

1.2 KINETIC STUDY

Kinetic studies were carried out using stopped-flow spectrophotometry. Pyrrole is known to be protonated only at the α-carbon[3] so attack by the diazonium ion was expected to occur solely at this position. The observance of only one product by nmr spectroscopy confirmed this prediction and the mechanism proposed is shown in Scheme 1. Although the pyrrole kinetics were studied under acid conditions, no evidence was found for reaction of protonated pyrrole with diazonium

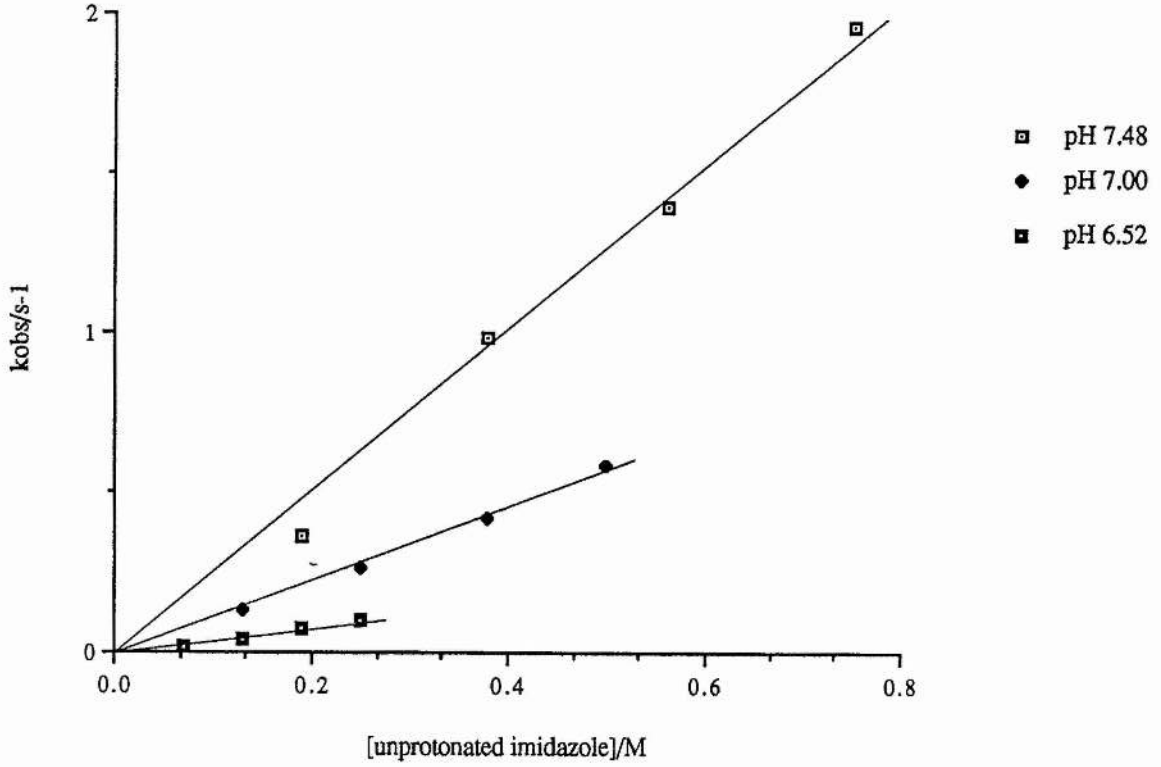

Figure 1.

Rate of reaction of unprotonated imidazole [ImH] with 4-nitrobenzenediazonium ion.

Table 1.

Rate data for rate of reaction of imidazole and methylated imidazoles with 4-nitrobenzenediazonium ion. 1M solutions in 0.5M HCl were diluted with 0.5M KCl to concentrations stated.

Imidazole	conc./M	k_{obs}/s^{-1}
	1.00	0.58
	0.75	0.42
	0.50	0.26
	0.25	0.13
2-Methylimidazole	1.00	3.00
	0.75	2.38
	0.50	1.50
	0.25	0.81
1-Methylimidazole	1.00	0.060
	0.75	0.036
	0.50	0.022
	0.25	0.007
1,2-Dimethylimidazole	1.00	0.070
	0.75	0.055
	0.50	0.037
	0.25	0.016

ion. The conditions under which imidazole was reacted with 4-nitrobenzenediazonium ion were rather different from those used in the investigation of the pyrrole reaction. Imidazole buffers were prepared at three different pH's by addition of HCl to imidazole in solution. Each buffer was diluted with KCl solution to give a series of solutions of constant pH and ionic strength but different buffer concentrations. The rate constant for reaction of each of these buffers with 4-nitrobenzenediazonium ion was measured by monitoring the change in absorbance at 410nm, with both neutral and protonated imidazole present in large excess over the diazonium ion. The rate data for these reactions are shown in Table 1. The concentration of neutral imidazole present in each buffer was calculated from the pK_a of imidazole acting as a base (7.10) as shown in Table 2. Assuming the reaction mechanism for imidazole to be the same as that for pyrrole, a plot of k_{obs} against concentration of neutral imidazole, [ImH], should be linear, having points from all three buffers on a single straight line. From Figure 1, it can be seen that this is not the case. However, if the concentration of imidazole anion,[Im^-], present in each buffer is calculated from the pK_a of imidazole acting as an acid (14.5)[4](Table 2), then a plot of k_{obs} against imidazole anion concentration does have the required linearity (Figure 2). This result suggests that the reactive species in the coupling of imidazole with benzenediazonium ion is the anion. The proposed mechanism is shown in Scheme 2.

1.3 VOLUME OF ACTIVATION

The value of the volume of activation for a reaction ($\Delta V^{\neq}$) is characteristic of the mechanistic processes taking place. $\Delta V^{\neq}$ is defined as the difference in partial molar volumes between the transition state and the reactants. $\Delta G^{\neq}$ is related to the rate constant, k , by the Eyring equation:

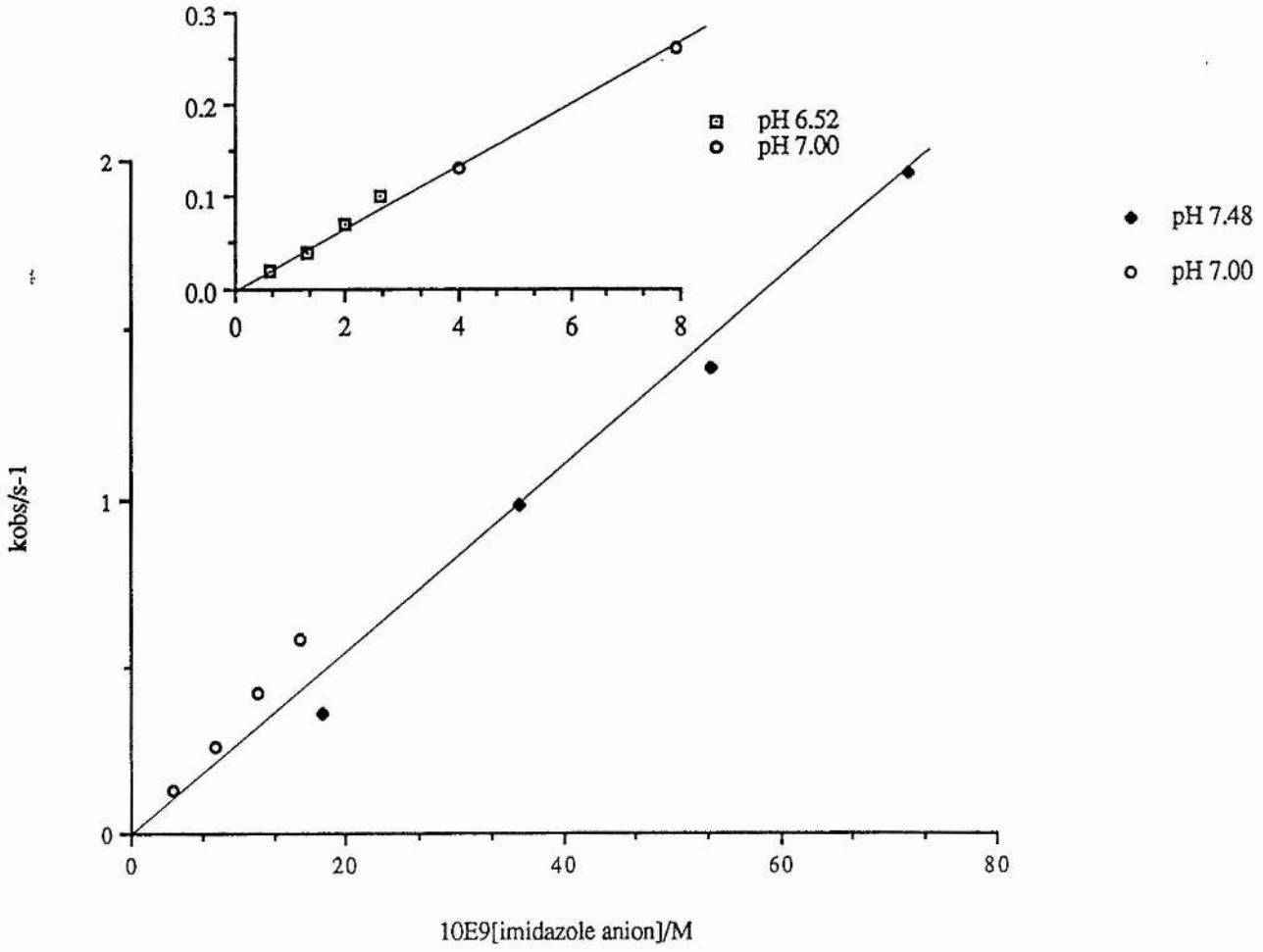

Figure 2.

Rate of reaction of anionic imidazole [Im-] with 4-nitrobenzenediazonium ion.

Table 2.
Rate of reaction of calculated amounts of unprotonated (ImH) and anionic (Im^-) imidazole with 4-nitrobenzenediazonium ion at three pH's.

pH	[ImH]/M	k_{obs}/s^{-1}	$10^9[Im^-]/M$
7.48	0.75	1.96	71.6
	0.56	1.39	53.7
	0.38	0.98	35.8
	0.19	0.36	17.9
6.52	0.25	0.10	2.62
	0.19	0.07	1.96
	0.13	0.04	1.31
	0.07	0.019	0.65
7.00	0.50	0.58	15.8
	0.38	0.42	11.9
	0.25	0.26	7.90
	0.13	0.13	4.00

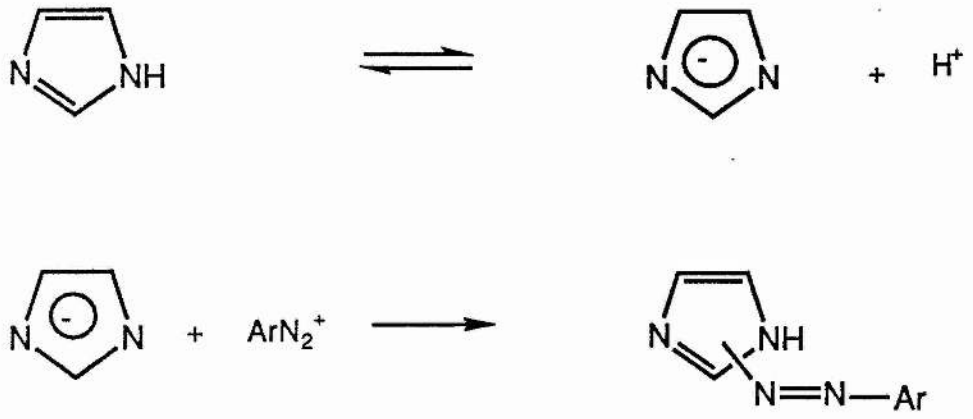

Scheme 2. Proposed mechanism for reaction of imidazole with benzenediazonium ion.

$$k = \frac{k_o T}{h} \exp\left(\frac{-\Delta G^{\neq}}{RT}\right) \frac{\gamma \text{reagents}}{\gamma^{\neq}} \qquad (1)$$

where k_o is Boltzman's constant and h is Planck's constant. From this can be derived:

$$\frac{\delta \ln k}{\delta p} = -\frac{\delta \Delta G^{\neq}}{\delta p} \cdot \frac{1}{RT} = -\frac{\Delta V^{\neq}}{RT} \qquad (2)$$

Thus $\Delta V^{\neq}$ may be calculated from the slope of a plot of lnk against p where k is the observed second order rate constant and p is the pressure. Table 3 shows the characteristic values of $\Delta V^{\neq}$ for the reaction of benzenediazonium ions with anionic species[5]. These values are quite different from those obtained for benzenediazonium coupling with neutral species. The kinetics of reaction of 4-methoxybenzenediazonium ion with imidazole were studied at various pressures up to 1000bar. The 4-methoxy compound was used in order to control the rate of reaction to a rate suitable for the apparatus available. The rate constants obtained over this range of pressures, shown in Table 4, were used to obtain a value for the volume of activation by plotting lnk against p according to equation (2) (Figure 3). The plot is linear up to 600 bar with a slope of 1.1934×10^{-3} bar^{-1}. From equation (2) $\Delta V^{\neq}$ is calculated to be $-29 cm^3 mol^{-1}$(+/-5) taking $R=80.98 cm^3$ and T=303K. This value is too large to be consistent with bond formation alone. Additional solvation must be occurring in the transition state. This proposal would be consistent with initial dissociation of neutral imidazole to the anion, with water acting as the base, followed by attack by the benzenediazonium ion on the anionic species (Scheme 2). The first step of this proposed mechanism, dissociation of neutral nitrogen bases has $\Delta V^{\neq}$

Table 3.
Volumes of activation for reaction of aryldiazonium ions with nucleophiles in water at 25°C.

aryldiazonium ion	**nucleophile**	**$\Delta V^{\neq}$/cm^{3}mol^{-1}**
$C_6H_5N_2^+$	N_3^-	+2.2
$C_6H_5N_2^+$	HSO_3^-	-9.1
$C_6H_5N_2^+$	SO_3^{2-}	-8.9
p-$NO_2C_6H_4N_2^+$	$PhSO_2^-$	-1.7
p-$MeOC_6H_4N_2^+$	p-nitrobenzoate	-15.0

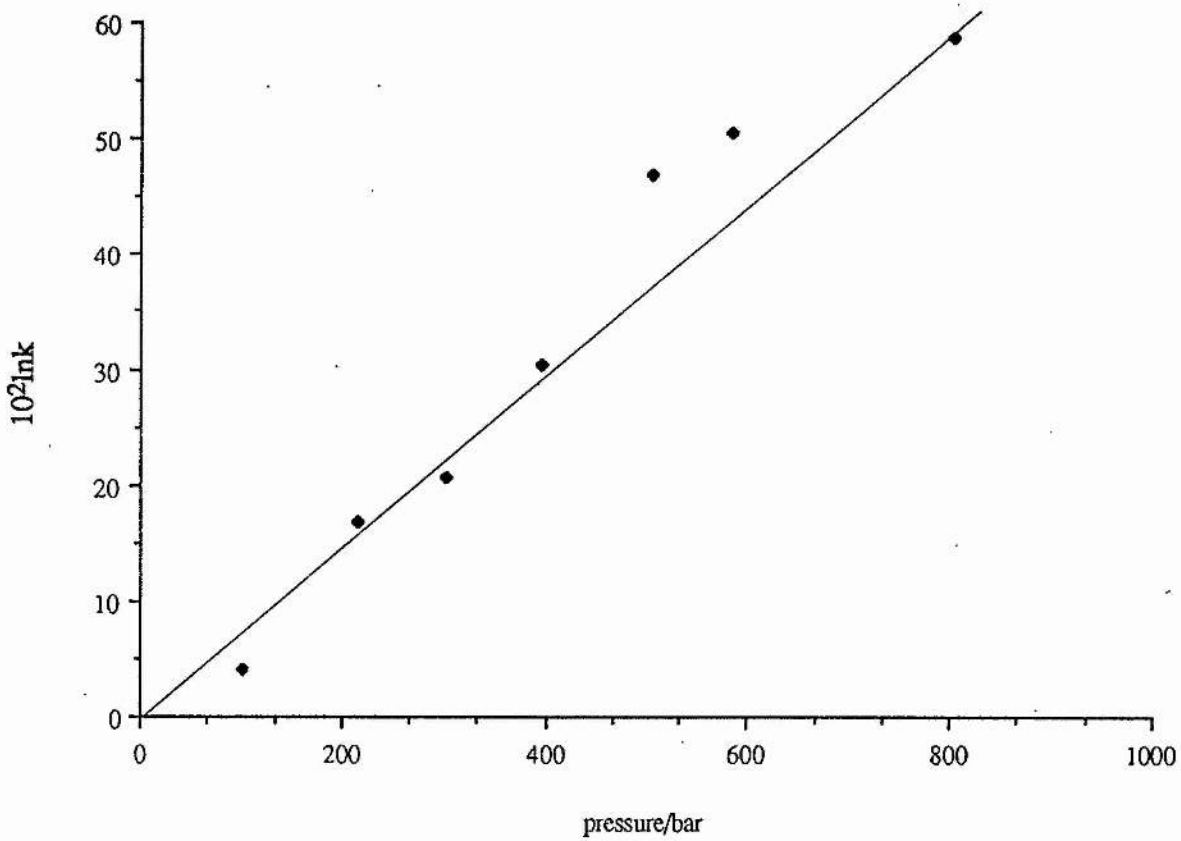

Figure 3.

Plot of **lnk** against pressure.

Table 4.
Rate constants for the reaction of 4-methoxybenzenediazonium ion with imidazole at various pressures.

pressure/bar	$10^2 \ln k_{obs}$
102.5	4.06
215	16.72
302.5	20.55
395	30.44
505	46.77
582.5	50.47
802.5	58.63

Attack by proton on neutral pyrrole:

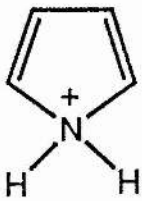

+890

(1)

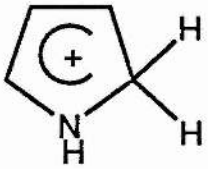

+826

(2)

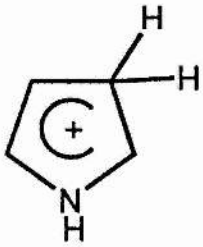

+834

(3)

Attack by proton on neutral imidazole:

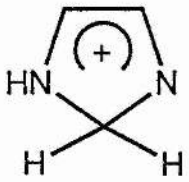

+903

(4)

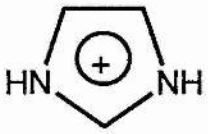

+784

(5)

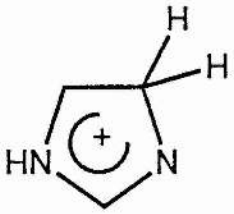

+896

(6)

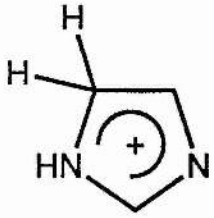

+872

(7)

Figure 4. Heats of formation units of species formed by attack by proton on pyrrole and imidazole.

around -25cm^{3}mol^{-1}, and would make the largest contribution to $\Delta V^{\neq}_{obs}$. The second step involves bond formation, contributing -10cm^{3}mol^{-1}, and a spreading of the charge with solvent relaxation[6] which would reduce the final value by about 5cm^{3}mol^{-1}. The resulting value, -30cm^{3}mol^{-1}, agrees well with the experimentally obtained value of -29cm^{3}mol^{-1}. It is not justifiable to claim that this analysis proves the proposed mechanism as the estimates were made after the experimental values were known, but a $\Delta V^{\neq}$ of -29cm^{3}mol^{-1} is certainly consistent with the proposed mechanism.

1.4 MNDO CALCULATIONS

Heats of formation (ΔH_f^o/kJ) were calculated by MNDO (Modified Neglect of Differential Overlap)[7,8] for species relevant to this investigation and are shown in Figures 4 and 5. The values obtained for protonation of pyrrole agree with the experimentally observed preference for α-protonation over N-protonation. Therefore the values obtained for other species were treated with confidence. For benzenediazonium ion (PhN_2^+) attack on pyrrole the reactive intermediates have very similar heats of formation. The difference of 15kJmol^{-1}, however, is sufficient for species (8) in Figure 5 to be the preferred intermediate as only substitution at the 2-position is observed in the product. A similar difference (14kJmol^{-1}) is observed when MNDO calculations are applied to attack of PhN_2^+ on neutral imidazole, species (10) to (14) in Figure 5. This indicates that attack by PhN_2^+ on the neutral species should result in formation of only one product, namely that with 4(5)-substitution (12). On examination of the product of reaction of 4-nitrobenzenediazonium ion and imidazole by nmr spectroscopy, it was found that substitution had occurred at both the 2- and the 4(5)-positions. This contradictory

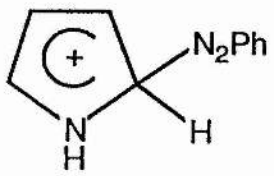

+1100

(8)

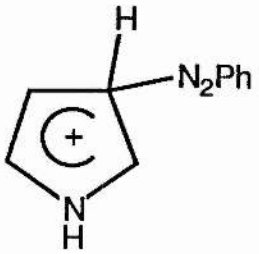

+1115

(9)

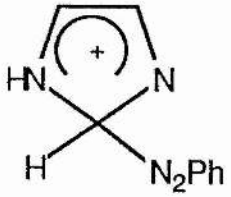

+1156

(10)

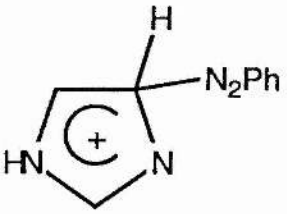

+1156

(11)

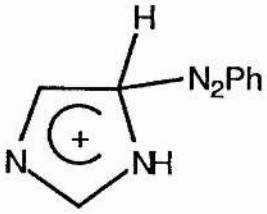

+1142

(12)

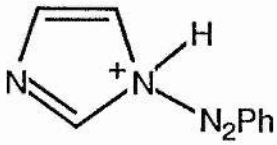

+1284

(13)

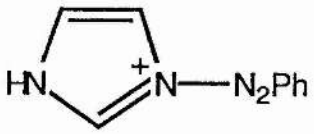

+1081

(14)

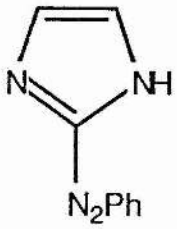

+450

(15)

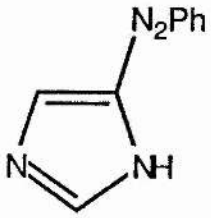

+451

(16)

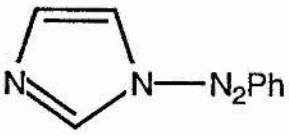

+513

(17)

Figure 5. Heats of formation units for attack by PhN_2^+ on pyrrole and imidazole.

evidence suggests that reaction does not occur via the neutral species. Calculated values of ΔH_f^o for intermediates obtained by attack of PhN_2^+ on the imidazole anion (15 and 16) are very similar. These values indicate that two products would be formed in this instance, as is observed experimentally, and suggest that the imidazole anion is the reactive species. The values of ΔH_f^o for species (15) and (16) are very low indicating that the anionic pathway is very favourable. However, the concentration of imidazole anion in the buffer is also very low. Reaction can probably occur via both the neutral and anionic pathways, but the anionic is greatly favoured except perhaps under rather acid conditions.

1.5 EFFECT OF N-METHYLATION

The reactions of 1-methyl- and 1,2-dimethylimidazole with 4-nitrobenzenediazonium ion were examined by stopped-flow spectrophotometry. The conditions were the same as those used previously, with the imidazoles acting as their own buffer. The rate constants obtained for these reactions are shown in Table 1. The effect of N-methylation is illustrated in Figure 7 where the stoichiometric amount of 2-methyl- and 1,2-dimethylimidazole present in the buffered solutions has been calculated and plotted against the observed rate constant. The reactions of 1-methyl- and 1,2-dimethylimidazole with the 4-nitrobenzenediazonium ion are slower than the range of the stopped-flow spectrophotometer so these reactions were investigated futher by a scanning spectrophotometer. The initial stages of the reactions were monitored (from 0 to 10 seconds after mixing) using the same buffered solutions as before. First order kinetics were still observed on this time scale and rate constants obtained previously were therefore assumed to be accurate.

The decrease in the observed rate of reaction (Figure 7) on N-methylation is clear and consistent with reaction via an anionic pathway because an anionic form of the molecule is not possible once it has been N-methylated. Some reaction does

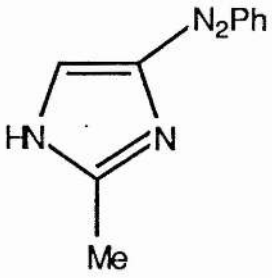

(18)

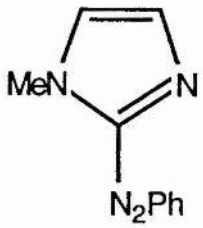

(19)

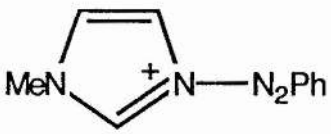

(20)

Figure 6. Possible products formed by attack of PhN_2^+ on 1-methyl- and 2-methylimidazole.

occur between the N-methylated species and the diazonium ion, however, indicating that reaction can still occur via the neutral forms as well as via the anionic forms. A complex mixture of products was obtained from the reaction of imidazole and methylated imidazole with 4-nitrobenzenediazonium ion. The crude product mixtures were examined by ^{13}C and ^{1}H nmr and by mass spectroscopy. Reaction of imidazole resulted in a crude product with a large peak in the mass spectrum at 217. This could be the result of formation of either (15) of (16) or both. In the ^{1}H nmr spectrum, a major signal was observed at 7.40ppm which is consistent with (15). Two smaller signals also occured at 7.50 and ca. 8.2ppm, indicating the presence of smaller amounts of (16). The highly complicated ^{13}C nmr spectrum is consistent with the presence of both (15) and (16). The product of reaction of 4-nitrobenzenediazonium ion with 2-methylimidazole has a molecular ion peak at 231 and there is one singlet in the ^{1}H nmr spectrum at around 8ppm. This is consistent with the formation of (18). The mass spectra of products of reaction of imidazole and 2-methylimidazole also contained small signals corresponding to coupling after elimination of nitrogen that is, phenylation. The crude product obtained from the reaction of 1-methylimidazole with 4-nitrobenzenediazonium ion gave very complicated nmr spectra. Several peaks were observed corresponding to methyl groups in different environments indicating that a mixture of products had been formed. This was supported by the occurrence of a number of peaks in the mass spectra corresponding to the products of coupling and phenylation. In order to clarify the situation, an attempt was made to isolate the products by column chromatography. A large number of highly coloured fractions were obtained, some in very small quantities and it was not thought worthwhile to try to separate and identify each one. It is clear, however, that N-methylation has a marked effect on the reaction pathway.

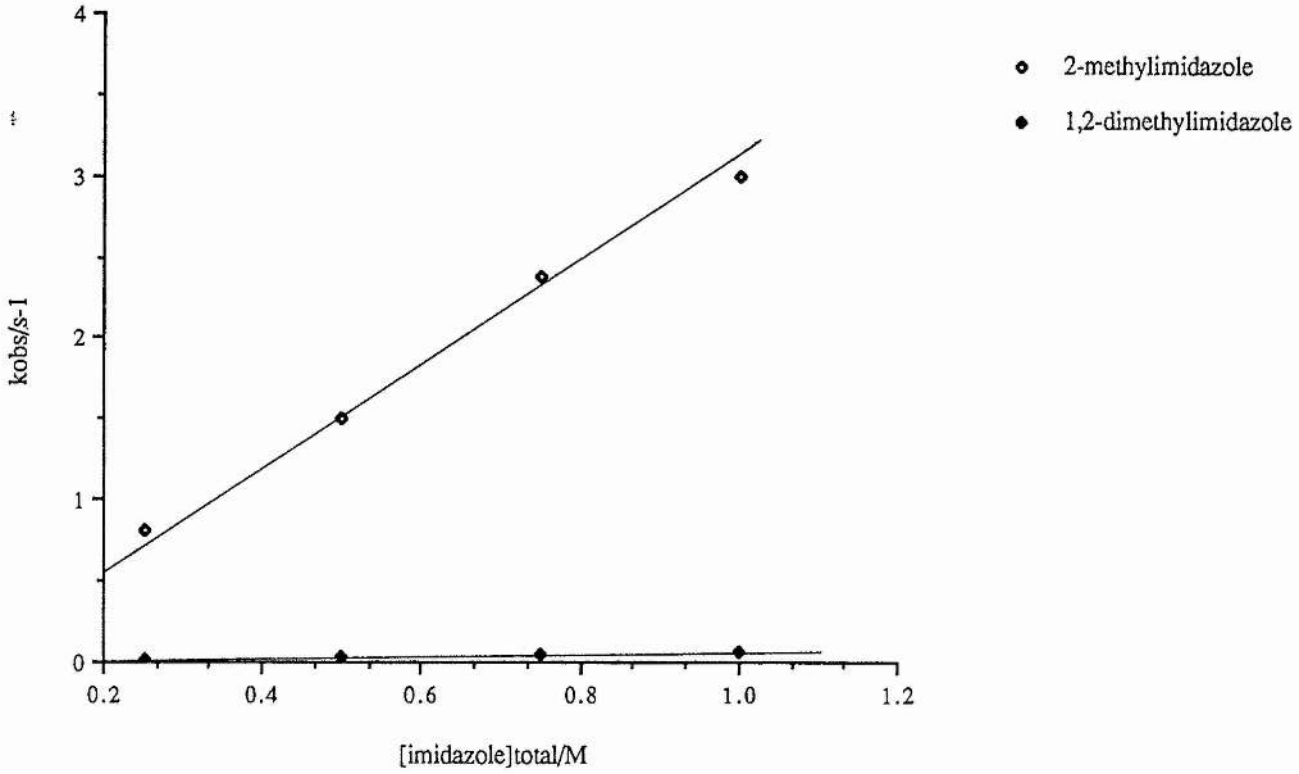

Figure 7.

Effect of N-methylation on the rate of reaction
of methylated imidazole with 4-nitrobenzenediazonium ion

1.6 DISCUSSION

From Scheme 2 it can be seen that for imidazole the essential step in the reaction pathway is that involving interaction of the imidazole anion and the cationic benzenediazonium ion. This step should be encounter-controlled. Calculations using the modified Smoluchowski[9] equation for encounter-controlled reactions in water at 25°C give a value for the second order rate constant of $7.4 \times 10^9 lmol^{-1}s^{-1}$. Because of electrostatic interactions this value should be adjusted slightly to about $2 \times 10^{10} lmol^{-1}s^{-1}$. From the data in Figure 2, a lower value of $2.7 \times 10^7 lmol^{-1}s^{-1}$ is obtained, suggesting either that the proposed mechanism in Scheme 2 is incorrect or that some other factor is reducing the rate constant for an encounter reaction. Imidazole differs from pyrrole in two important ways: firstly pyrrole is a weaker acid than imidazole, having a pK_a of 16.5 compared with 14.5 for imidazole. This difference is too small to have a dramatic effect on the reaction path. Secondly, as demonstrated by the MNDO calculations, imidazole favours N-protonation rather than C-protonation. Assuming that, in the reaction being considered here, the benzenediazonium ion behaves as a proton, then the product of reaction with neutral imidazole should be (14) (Figure 5). The values of ΔH_f^o shown in Figure 4 confirm that (14) is indeed the most favourable product. This means that encounter between neutral imidazole and a benzenediazonium ion will rarely result in attack on carbon. However, formation of (14) by attack on nitrogen, is a reversible process and will not result in an isolable product but reduces the opportunity for irreversible coupling following attack on carbon. Formation of (14) as the initial product on addition of 4-nitrobenzenediazonium ions to an imidazole buffer could not be detected as the uv spectrum is dominated by absorption of protonated imidazole. The heats of formation of species (15), (16) and (17) (Figure 5) show that for encounter between the imidazole anion and benzenediazonium ions, nitrogen is not the preferred site of attack. Attack on carbon results in irreversible formation of product and this is the

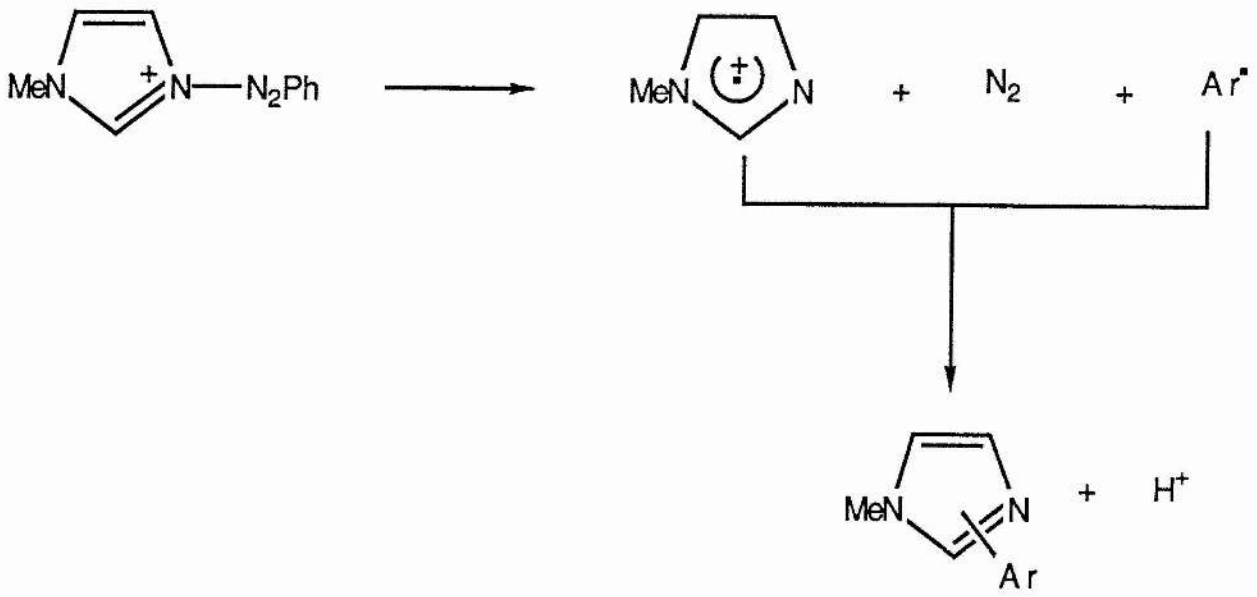

Scheme 3. Proposed decomposition mechanism for the attack by PhN_2^+ on N of N-methylimidazole.

dominant reaction pathway. This difference in pathways helps to explain the low encounter-controlled rate constant obtained for the reaction. The availability of benzenediazonium ion is reduced because the cation attacks neutral imidazole at nitrogen forming (14), reducing the amount of cation available for reaction via the anion. The encounter-controlled pathway exists but with a lowered encounter-controlled rate constant. 1-Methyl- and 1,2-dimethylimidazole cannot react via an anionic intermediate so (18) and (19) (Figure 6) must be formed via attack at carbon of the neutral species.

This process is much slower than reaction with the anion and therefore species such as (20) (Figure 6) will probably be able to decompose by an alternative pathway. This decomposition (Scheme 3) can be compared to the reaction of benzenediazonium ion with aminopyridine[10], and could produce nitrogen, a radical and a radical cation. The phenylated product observed in the reaction mixture could then be formed by dimerisation of the radical and radical cation with the loss of a proton. The large number of products of reaction between 4-nitrobenzenediazonium ions and N-methylimidazole makes the kinetics of the reaction complex but the data obtained can be analysed to give a first order rate constant. From Figure 7 it can be deduced that N-methylation results in a marked decrease in rate. This result substantiates the view of Ridd that coupling of imidazole with benzenediazonium ions occurs via the anion.

1.7 EXPERIMENTAL

All pyrroles and imidazoles were purchased from Aldrich. The tetrafluoroborate salts of 4-nitro- and 4-methoxybenzenediazonium ions were prepared according to the method of Starkey[11]. p-Nitroaniline, or p-anisole for the methoxy compound, (0.025 moles) was dissolved in fluroboric acid (10ml). The solution was stirred in an ice-bath and a solution of $NaNO_2$ (1.725g) in water (5ml) was added dropwise. The solution was stirred for a further few minutes and filtered

by suction on sintered glass. The product was washed once with cold fluoroboric acid (5ml), twice with ethanol and several times with ether.

Kinetic studies were carried out on a Hi-Tech SF-3L stopped-flow spectrophotometer and SF-40C photomutiplier, Data-Lab DL 901 transient recorder and a DT V12-14 Farnell oscilloscope. For the pyrrole experiments, a solution of the pyrrole (0.0005M in 0.05M HCl) was placed in one arm and the diazonium ion (0.01M im 0.05M HCl) in the other. The imidazole buffered solutions were prepared by dissolving a known amount of the required imidazole in water and partially neutralising with HCl. KCl was added to bring the ionic strength to 0.10M. The pH was measured and the solution diluted with KCl to give a series of imidazole buffers with constant pH but containing various amounts of unprotonated imidazole. Two other imidazole buffers of different pH's were prepared in the same way. The imidazole solution was placed in one arm of the stopped-flow spectrophotometer and the benzenediazonium ion (0.00025M in H_20) in the other. The reaction mixture was monitored at 410nm and 25°C. Data acquisition and processing were carried out by an Apple II Plus microcomputer using a Hi-Tech system software kinetics package. Rate constants were calculated by a computer program using the Kedzy-Swinbourne[12] method.

High pressure kinetics were carried out on a solution containing 0.05M imidazole, 0.0025M HCl and 0.005M 4-methoxybenzenediazonium tetrafluoroborate. A sliding cell of the type described by LeNoble[13] was filled with the solution and placed in a Nova Swiss high pressure optical cell used in a Beckman 25 spectrophotometer.

A Hi-Tech Spectra Scan MG-3000 linked to a Hi-Tech stopped-flow spectrophotometer SF-3L and SF3C photomultiplier control unit was used to study the kinetics of N-methyl and 1,2-dimethylimidazole. Rate constants were calculated by an Apple II computer. A Phillips PU 8720 UV/VIS scanning spectrophotometer was used to look at the reactions over a longer time-scale.

Preparation of coupling products was by the method described by Fargher et al[14]. The appropriate imidazole was dissolved in saturated sodium carbonate solution and an equimolar amount of 4-nitrobenzenediazonium tetrafluoroborate was added. After 30 minutes the coloured product was filtered off and washed with water.

^{1}H and ^{13}C nmr spectra were run on a Bruker 360 or on a Bruker AM300 spectrometer. Samples were dissolved in d_6-DMSO and referenced to TMS.

1.8 REFERENCES

1. A.R. Butler, P. Pogorzelec and P.T. Shepherd, *J. Chem. Soc., Perkin II*, 1977, 1452.
2. R.D. Brown, H.C. Duffin, J.C. Maynard and J.H. Ridd, *J. Chem. Soc.*, 1953, 3937.
3. Y. Chiang and E.B. Whipple, *J. Amer. Chem. Soc.*, 1963, **85**, 2763.
4. H. Walba and R.W. Insensee, *J. Org. Chem.*, 1961, **26**, 2789.
5. N.S. Isaacs, T.S. Najen and R. Van Eldik, *Tet. Lett.*, 1987, **28**, 3043.
6. N.S. Isaacs, *'Liquid Phase High Pressure Chemistry'*, Wiley, Bath, 1981, p188.
7. M.J.S. Dewar and W. Thiel, *J. Am. Chem. Soc.*, 1977, **99**, 4899 and 4907.
8. J.J.P. Stewart, Quantum Chemistry Program Exchange, Bloomington, Indiana, QCPE No. 455.
9. M.W. Austin and J.H. Ridd, *J. Chem. Soc.*, 1963, 4204.
10. G. Fillipi, G. Vernin, H.J.M. Dou, J. Metzger and M.J. Perkins,*Bull. Soc. Chem. France*, 1974, 1075.
11. E.B. Starky, 'Organic Synthesis' Collective Vol.II, Wiley, New York, 1943, p.225.
12. F.J. Kezdy, J. Jaz and P. Bruylants, *Bull. Soc. Chim. Belges*, 1958, **67**, 687.
13. W.J. LeNoble and R. Schlott, *Rev. Sci., Instr.*, 1976, **47**,770.
14. R.G. Fargher and F.L. Pyman, *J. Chem. Soc.*, 1919, **115**, 217.

Chapter 2

Kinetic Study of Pyrrole Protonation

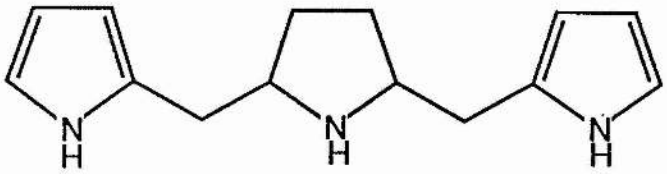

(a)

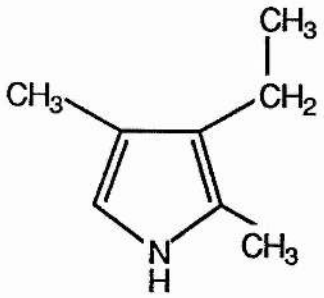

(b)

Figure 1.

2.1 INTRODUCTION

The basicity of pyrrole has been variously estimated to be between -1.7 and +0.3 on the pK_a scale[1], with basicity increasing rapidly on increasing alkyl substitution. However, problems of pyrrole stability in acid solution have been encountered, implying that pyrrole is a weaker base than expected. Chiang and Whipple[2] endeavoured to overcome the problem by carrying out measurements on a series of methylated pyrroles in concentrated H_2SO_4, a medium which is acidic enough to ensure complete protonation. These experiments gave the pK_a of pyrrole as -3.8, a value considerably lower than those previously calculated. Dilute solutions of pyrrole in aqueous sulfuric acid are rather stable but the use of concentrated H_2SO_4 solutions meant that the ratio of protonated to unprotonated base was very different to that used in other studies.

In spite of the fact that pyrrole is an extremely weak base, a certain amount of protonation occurs when pyrrole is added to acid. The protonated ion of pyrrole is highly unstable and undergoes polymerisation very readily, one of the main products being the trimer, 2,5-dipyrrolypyrrolidine[3] (Figure 1a). The formation of polymers even in moderately strong acid solutions has been the main difficulty in the direct determination of the pK_a of the very weak base.

Alexander and Butler[4] studied the mechanism of hydrogen exchange of pyrrole in aqueous buffer. Using pyrrole methylated at the nitrogen and one ring carbon to ensure protonation at only one site, they found that, contrary to previous reports, the α-position in pyrroles is not substantially more reactive than the β-position. The study also confirmed that the product of reaction is determined by thermodynamic rather than kinetic factors. The relative reactivity of the α- and

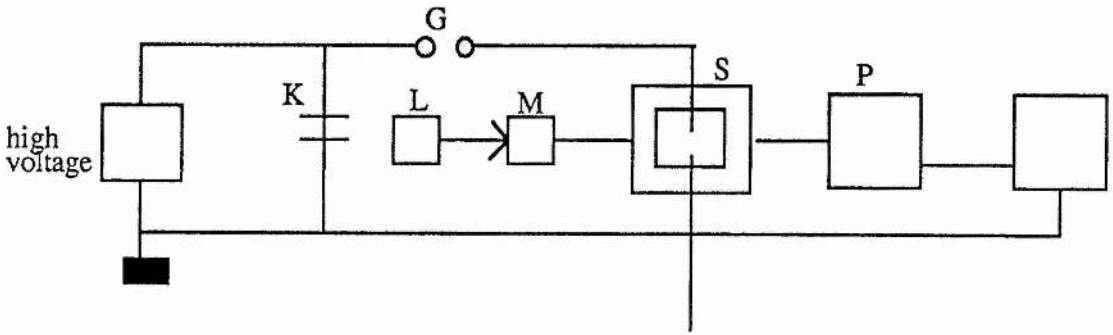

Figure 2. Temperature-jump apparatus.

β-positions was also noted by Whipple, Chiang and Hinman[5] who observed competitive β-protonation by nmr spectroscopy.

To investigate further the rate of α-protonation in pyrrole, a preliminary study was carried out on 3-ethyl-2,4-dimethylpyrrole. By the nature of the substitution in this molecule, protonation must only occur at the α-position. A buffered system was used to minimise polymerisation and stability problems. Two fast reaction spectrophotometric techniques, stopped-flow and temperature-jump, were used in the investigation.

2.2 EXPERIMENTAL

3-Ethyl-2,4-dimethylpyrrole was obtained from Aldrich. A stock solution was prepared by dissolving 3-ethyl-2,4-dimethylpyrrole (10μl) in CH_3CN (1ml). The stock solution (100μl) was then diluted in buffer (10ml, 0.75/0.25M, HOAc/ OAc^-). The resulting solution had an ionic strength of 0.25M and a pH of 4.03. The rate of the reaction was expected to be on the interface of detection for both temperature-jump and stopped-flow and was therefore observed by both methods.

The temperature-jump technique used in the experiments was one involving spectrophotometric detection developed originally by Eigen[6]. The temperature perturbation was produced by a high current of short duration flowing through a solution of electrolyte: this is known as Joule heating. The principle of the apparatus can be seen in Figure 2. The condenser, K, was charged to a high voltage U_o. The spark gap was then reduced until the voltage discharged through the cell S containing the solution to be investigated. During the discharge the current I is given by the equation:

$$I = \frac{U_o}{R} \exp\left(\frac{-t}{RC}\right)$$

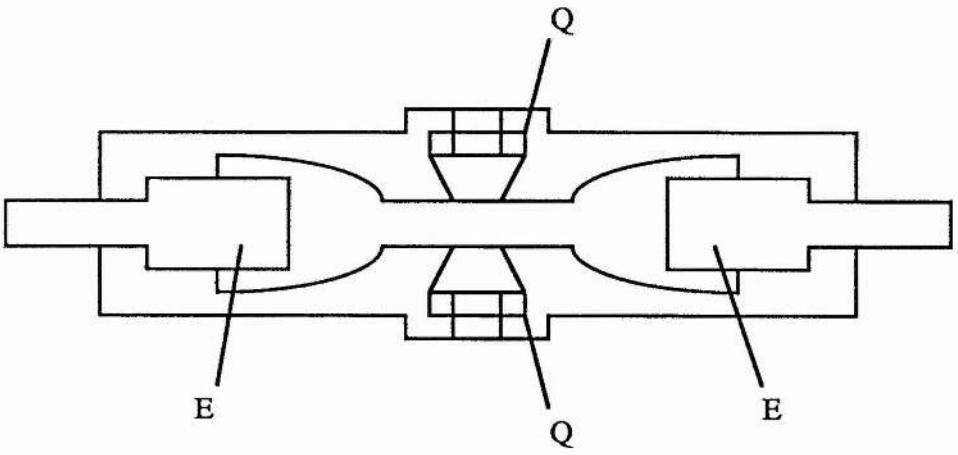

Figure 3. Cross-section of temperature-jump sample cell

where R is the resistance if the cell and C is the capacitance of the condenser. Under these conditions a temperature jump of 5°C was produced for aqueous solutions. The temperature changes exponentially with the time constant RC/2 where R is the resistance of the cell. Therefore, the electrical conductivity of the solution had to be high in order to get a fast discharge of voltage. This was acheived by adding an inert electrolyte, in this case 0.2M KCl, so that the temperature jump could be completed within a few microseconds.

In the apparatus used and illustrated in Figure 2, the absorption of light was used to determine the change in concentration. L was a high intensity light source with constant luminosity, M was a monochromator and P a photomultiplier whose output was recorded on an oscilloscope. The fluctuation in the light intensity of the lamp was compensated for by splitting the light beam between the monochromator and the sample cell. The intensity of the reflected beam was compared with that of the light passing through the solution. During each experiment, a wavelength was chosen so that the absorbance changes were as much as possible a result of the experiment being examined.

The temperature-jump cell used is shown in Figure 3. The cell had a volume of a few mls and an optical pathlength of 1cm. The incident light beam was focused in the middle of the cell using quartz windows Q. To obtain a uniform temperature increase, the volume heated was greater than that required for observation. The reactions were monitored at 261nm and two runs were made for each sample.

Stopped-flow experiments were recorded on a Hi-Tech SF-3L stopped-flow spectrophotometer. A solution of the pyrrole (0.01M in HCl) was placed in one arm and the acetate buffer (either 0.75/0.25M HOAc/OAc^- or 0.25/0.75M HOAc/OAc^-) in the other. The final ratios of HOAc/OAc- in each solution are noted in Table 1. The reaction mixture was monitored at 261nm and 25°C. Rate constants

Table 1.

[buffer$_t$][a]/M	Ratio HOAc/OAc$^-$	pH	$k_{obs}/\mu s^{-1}$	method
1.00	3/1	4.03	5.69,5.76	t-jump
0.50	3/1(approx.)	3.95	2.93,2.92	stopped-flow
1.00	>3/1	3.44	4.46,4.83	t-jump
0.50	1/3(approx.)	4.98	5.64,5.23	stopped-flow

a. total acetate buffer concentration.

were calculated by the Kedzy-Swinbourne[7] method.

2.3 RESULTS AND DISCUSSION

The protonation reaction of 3-ethyl-2,4-dimethylpyrrole in acetate buffer occurs on a time-scale at the slow end of the t-jump range and the fast end of the stopped-flow range. Both techniques were used to observe the reaction and the collected results are contained in Table 1. Peaks were observed by uv spectrophotometry at 261 and 225nm and the reaction was monitored at 261nm. The trace shown in Figure 4 was observed for a temperature jump of 5°C from 20 to 25°C.

These preliminary results demonstrate that this system can be studied successfully by temperature-jump and stopped-flow techniques and a pK_a of approximately 3.5 was obtained. This is in excellent agreement with the value of 3.8 for pyrrole obtained in previous investigations. The rate constants obtained indicate that the stopped-flow technique may be rather more suitable than temperature-jump. However, further experiments using a range of buffers and buffer ratios are required to establish a firm relationship between pH and k_{obs}.

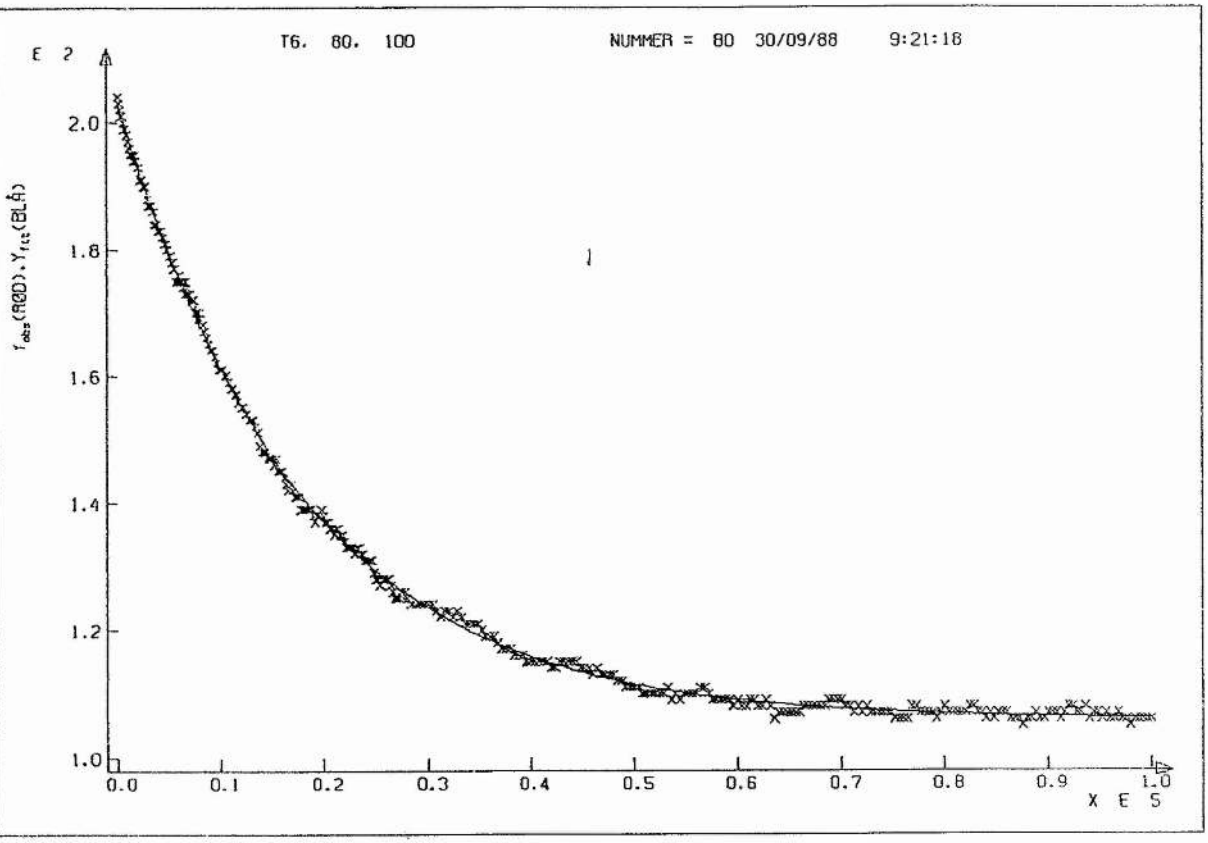

Figure 4. Kinetic curve obtained in temperature-jump experiment.

2.4 REFERENCES

1. N. Naqvi and Q. Fernando, *J. Org. Chem.*, 1960, **25**, 551.
2. Y. Chiang and E.B. Whipple, *J. Am. Chem. Soc.*, 1963, **85**, 2763.
3. H.A. Potts and G.F. Smith, *J. Chem. Soc.*, 1957, 4018.
4. R.S. Alexander and A.R. Butler, *J. Chem. Soc. Perkin Trans. II*, 1980, 110.
5. E.B. Whipple, Y. Chiang and R.L. Hinman, *J. Am. Chem. Soc.*, 1963, **85**, 26.
6. E.F. Caldin, 'Fast Reactions in Solution', Blacknell, London, 1964.
7. F.J. Kezdy, J. Jaz and P. Bruylants, *Bull. Soc. Chim. Belges*, 1958, **67**, 687.

Chapter 3

Structure of Benzenediazonium Ions

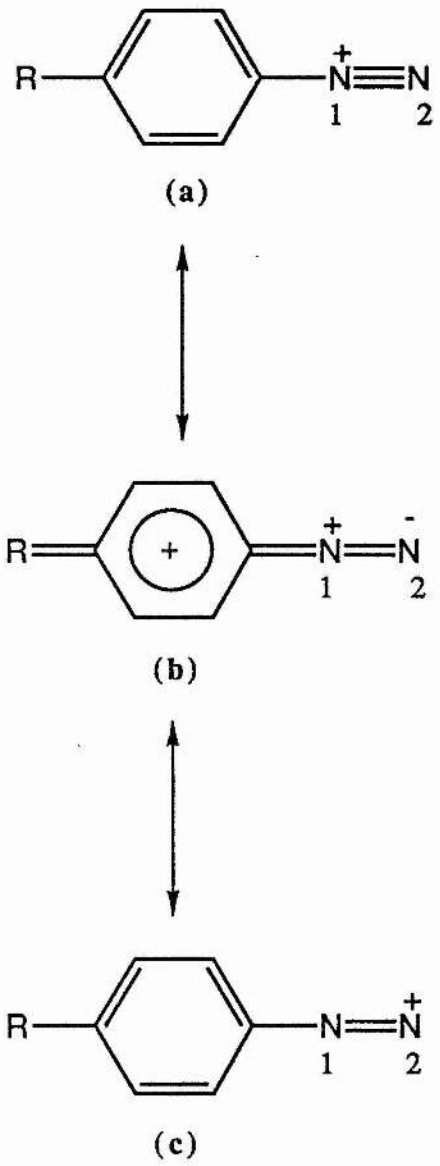

Figure 1. Canonical forms of benzenediazonium ion

3.1 INTRODUCTION

The structure of benzenediazonium ions can be represented by a number of canonical forms as shown in Figure 1. To establish what contribution each of these structures makes to the overall structure of the benzenediazonium ion, Romming carried out an X-ray crystallographic study of benzenediazonium chloride. A preliminary study[1], demonstrated that the orthorhombic crystals of benzenediazonium chloride grown in ethanol are ionic in nature, containing benzenediazonium ions and chloride ions. The nitrogen-nitrogen triple bond and the carbon-nitrogen bonds were of the expected length but the distance between carbons C1 and C4 across the ring was shorter than in benzene (Figure 2a). The N2-N1-C1 arrangement is strictly linear and the benzenediazonium ion is planar.

Romming[2] also examined the structure of the 4-sulphobenzenediazonium ion (Figure 2b). These monoclinic crystals are obtained by recrystallisation from water. Apart from the sulphonate group, which is a distorted tetrahedron, the benzenediazonium ion is almost planar. The orientation of the nearly trigonal SO_3 group about the carbon-sulphur bond is probably mainly determined by the crystal forces. The benzenediazonium ion is very similar to the previously investigated benzenediazonium chloride. The charge distribution on the molecule was discussed by Romming for both the chloride and the 4-sulpho- species. Consideration of the geometry as determined by the X-ray structure analysis of the benzenediazonium chloride led Romming to suggest that the positive charge is shared between the two nitrogen atoms (Figure 1c) rather than the classical view in which the inner nitrgen carrys the full positive charge (Figure 1a). Calculations on benzenediazonium sulphate upheld Romming's proposal, with the charges on the inner and outer nitrogens found to be 0.31 and 0.12 respectively. The same calculations were also applied to

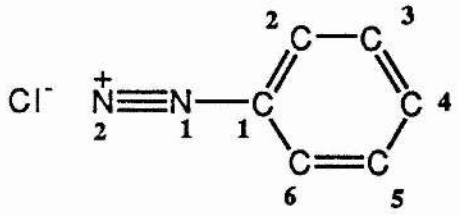

(a)

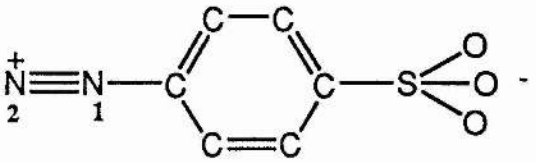

(b)

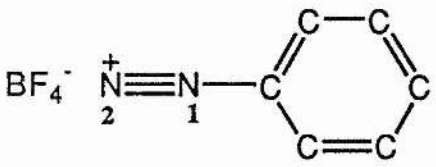

(c)

Figure 2.

benzenediazonium chloride[3] and a similar pattern of charge distribution on the two nitrogens established. The rest of the positive charge is distributed evenly between the phenyl atoms.

In 1982, Cygler et al[4] published the crystal structure of benzenediazonium tetrafluoroborate (Figure 2c). This structure agreed very well with Romming's structure of benzenediazonium chloride. The bond lengths of the nitrogen-nitrogen triple bond and the carbon-nitrogen bond again point to 1(a) as the dominant canonical form. Also in agreement with Romming, Cygler et al found that the positive charge is shared between the two nitrogens. Four tetrafluoroborate ions were shown to be arranged around the azo part of the molecule. Each nitrogen atom makes four short contacts with a fluorine of each of the four anions. The formation of nitrogen-fluorine contacts between both nitrogens and the counteranions indicates the sharing of the positive charge between the two nitrogen atoms. Cygler et al deduced from this that the resonance structure 1(c) may also make some contribution to the benzenediazonium ion structure.

It is possible that valence tautomerism of the benzenediazonium ion (Figure 3) could give a spiro structure (Figure 3b) resulting in scrambling of the nitrogens at positions 1 and 2. Evidence has been obtained from ^{15}N labelling experiments to support such scrambling. Evidence of isotopic rearrangement was obtained by Lewis and Insole[5,6] from mass spectral analysis of the decomposition products of benzenediazonium ions. The techniques involved in this analysis were elaborate and prevented further investigation into the nature of the intermediate involved. This conclusion was rejected by Bose and Kugajevsky[7] on evidence gained from nmr spectroscopy experiments. Comparison of the areas under the ^{15}N-^{1}H doublet and the ^{14}N-^{1}H singlet indicated that 96.5% of ^{15}N was in the position adjacent to the phenyl ring (position N1). The ^{15}N content of the nitrogen in this position in the starting material was shown to be 96.6%. No noticeable isotopic rearrangement was deemed to

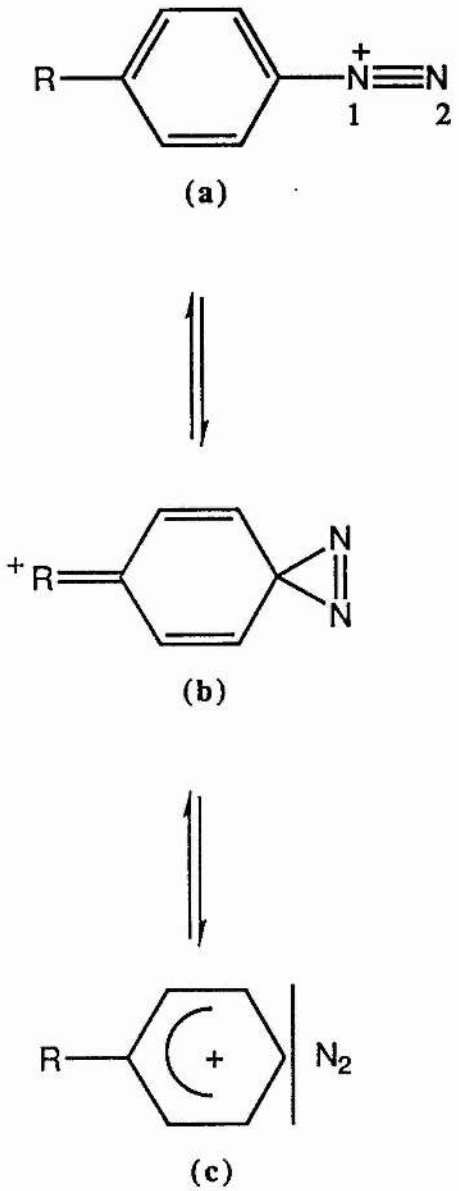

Figure 3.

have taken place. Lewis and Kotcher[8] replicated Bose and Kugajevskys' nmr experiments on the 4-methoxybenzenediazonium ion labelled with ^{15}N. In contrast to Bose and Kugajevsky's results, however, they reported that the ^{15}N did migrate to the N2 position thus reconfirming Lewis' previous conclusion.

Swain et al[9] found by use of mass spectroscopy that benzenediazonium ion in 1% sulphuric acid undergoes 1.6% nitrogen rearrangement. Prompted by this result they proposed a phenyl cation-dinitrogen pair (Figure 3c) intermediate rather than the spiro structure (Figure 3b). Nitrogen rearrangement has also been found in a series of studies by Zollinger et al[10-13]. The existence of intermediate 3(c) has been strengthened by evidence for incorporation of isotopically different di-nitrogen. A more recent investigation using the now routine technique of ^{15}N nmr spectroscopy, incorporated ^{15}N into benzenediazonium tetrafluoroborate salts by the use of 98% ^{15}N-labelled sodium nitrite[14]. Only one signal was observed in the ^{15}N nmr spectrum, suggesting that ^{15}N is present only in one position, most plausibly N2. No scrambling was observed after leaving the sample overnight.

The present work concentrated mainly on the 4-nitrobenzenediazonium ion, a species used in the kinetic studies of pyrrole and imidazole azo-coupling (Chapter 1). A solid state ^{15}N nmr study of the benzenediazonium ion was undertaken to confirm incorporation of ^{15}N into one position only. The effect of the complexation of diazonium ions with crown ethers was also examined as it is known that benzenediazoniumions form inclusion complexes with these macrocycles. The crown either sits on the azo part of the benzenediazonium ion and complexation reduces the rate of the azo-coupling reaction (Figure 6c)[15,16]. Complexation can be detected by its effect on the chemical shift of the nitrogens. This phenomenon has been investigated by natural abundance ^{15}N nmr spectroscopy[17] and by enriching the benzenediazonium ion with ^{15}N[14].

It has been shown that dicyclohexyl-18-crown-6 is an excellent phase transfer catalyst for the reaction of benzenediazonium ions with aromatic compounds[18]. Two compounds of this nature were also examinedby solid state nmr spectroscopy.

3.2 EXPERIMENTAL

3.2.1 X-RAY CRYSTAL STRUCTURE

The 4-nitrobenzenediazonium tetrafluoroborate was prepared from 4-nitroaniline according to the method of Starky[19]. 4-Nitroaniline (0.025 moles) was dissolved in fluroboric acid (10ml). The solution was stirred in an ice-bath and a solution of $NaNO_2$ (1.725g) in water (5ml) was added dropwise. The solution was stirred for a further few minutes and filtered by suction on sintered glass. The product was washed once with cold fluoroboric acid (5ml), twice with ethanol and several times with ether. The crude product was dried in vacuuo and recrystallised from acetonitrile. Crude product was dissolved in the minimum amount of hot acetonitrile and the resulting solution left overnight. Off-white, striated needles were obtained on evaporation of the solvent. Crystals deteriorated slowly on the open bench but showed no loss of intensity during the data collection when mounted in Lindemann glass capillaries. A Stoe Stadi-II diffractometer was used. The crystal had dimensions 0.61x0.26x0.25mm and was aligned along the c-axis. The unit cell was refined from 20 precisely set reflections with $12<2\theta<15^{o}$. 1418 measured reflections gave 886 unique data ($R_{int} = 0.070$). index range $-6<h<27$, $-2<k<37$, $0<l<5$, $1<2\theta<50^{o}$. 732 reflections with $F_o>2\theta_F$ used in the refinement. The programs used in the data analysis were; SHELX 86[20], SHELX 76[21], XANADU[22] and PLUTO[23]. Atomic scattering factors were obtained from SHELX 76.

The structure was solved by routine direct methods. Refinements minimised

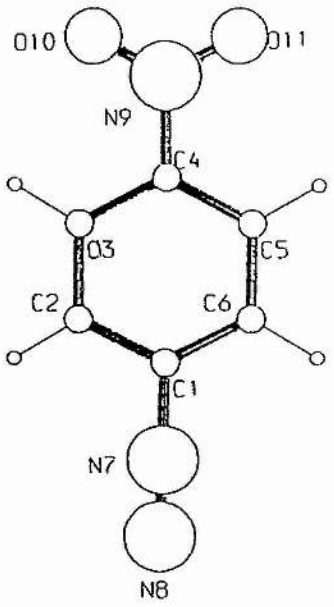

Figure 4.
X-ray structure of 4-nitrobenzenediazonium cation.

Table 1.

p-Nitrobenzenediazonium tetrafluoroborate coordinates x 10^4 for non-hydrogen atoms with estimated standard deviations in parentheses. $U_{eq} x 10^3$

$$U_{eq} = (1/3)\mathbf{E}_i\mathbf{E}_j U_{ij} a^*_i a^*_j \mathbf{a}_i.\mathbf{a}_j$$

atom[a]	x/a	y/b	z/c	Ueq
C1	849(3)	771(2)	112(18)	45(2)
C2	1228(4)	837(2)	2088(18)	53(2)
C3	1576(4)	490(3)	2803(20)	57(2)
C4	1528(3)	106(2)	1449(18)	45(2)
C5	1144(3)	52(2)	-527(18)	52(2)
C6	794(3)	395(2)	-1204(18)	53(2)
N7	494(3)	1125(2)	-554(14)	46(2)
N8	223(3)	1407(2)	-1066(20)	73(2)
N9	1914(3)	-248(2)	2181(21)	66(2)
O10	2178(3)	-222(2)	4079(18)	100(3)
O11	1943(3)	-553(2)	797(20)	96(3)
B12	540(1)	4193(1)	9046[b]	57(3)
F13	555(1)	4201(1)	6477(1)	83(2)
F14	-16(1)	4075(1)	9830(1)	110(3)
F15	671(1)	4593(1)	9957(1)	162(5)
F16	947(1)	3902(1)	9918(1)	197(6)
F14A	1105(1)	4310(1)	9742(1)	134(21)
F15A	416(1)	3795(1)	10001(1)	212(34)
F16A	145(1)	4487(1)	9957(1)	229(36)

a. see Figure 4 for atom labels.

b. fixed coordinate.

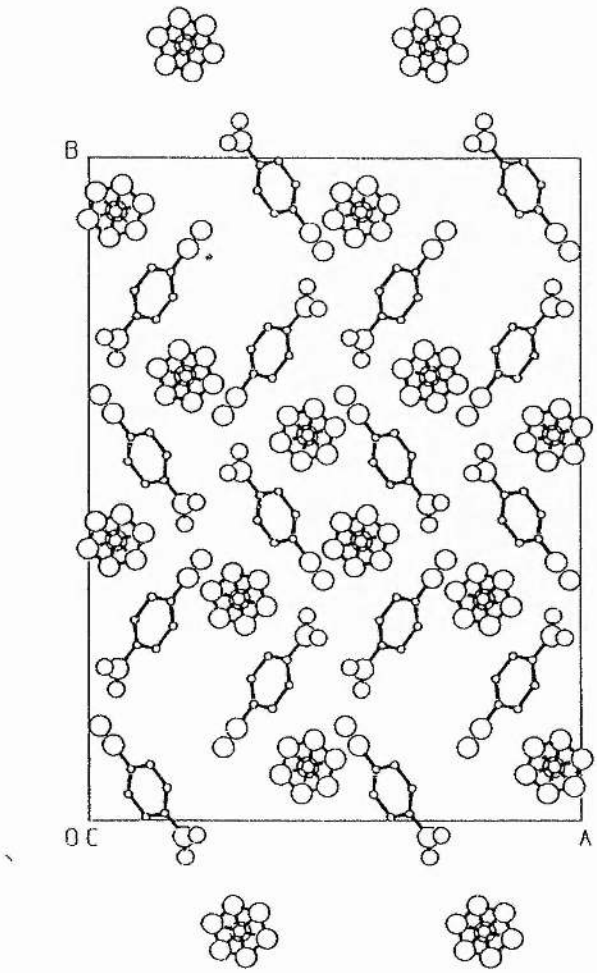

Figure 5.
X-ray packing structure of 4-nitrobenzenediazonium tetrafluoroborate.

Table 2.

p-Nitrobenzenediazonium tetrafluoroborate interatomic distances (Å) and angles (°) in the cation with estimated standard deviations in parentheses.

interatomic distances/(Å)[a]

C2 ---C1	1.373(11)	C6 ---C1	1.367(11)
N7 ---C1	1.408(10)	C3 ---C2	1.388(11)
C4 ---C3	1.398(11)	C5 ---C4	1.374(11)
N9 ---C4	1.458(10)	C6 ---C5	1.377(10)
N8 ---N7	1.103(8)	O10 ---N9	1.177(11)
O11 ---N9	1.204(10)		

angles/°

C6 -C1 C2	125.4(7)	N7 -C1 -C2	115.5(7)
N7 -C1 -C6	119.2(7)	C3 -C2 - C1	116.5(7)
C4 -C3 -C2	118.5(8)	C5 -C4 -C3	123.4(7)
N9 -C4 -C3	117.4(7)	N9 -C4 -C5	119.2(8)
C6 -C5 -C4	117.8(8)	C5 -C6 -C1	118.4(8)
N8 -N7 -C1	178.8(7)	O10 -N9 -C4	118.7(9)
O11 -N9 -C4		117.6(9)	O11 -N9 -O10
123.7(9)			

a. see Figure 4 for atom labels.

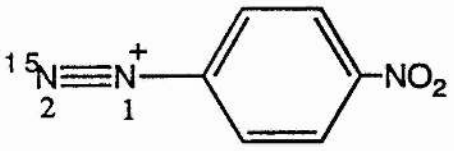

(a)

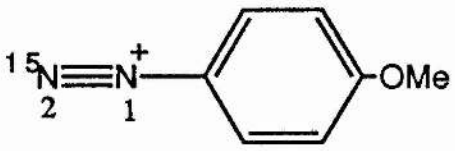

(b)

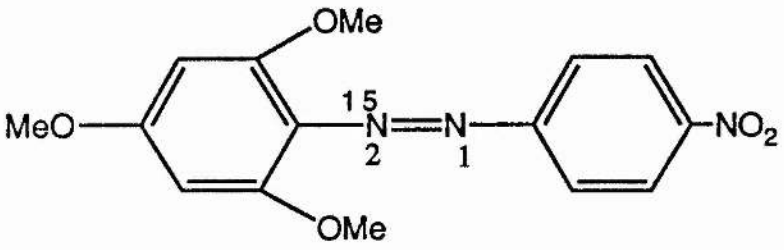

(c)

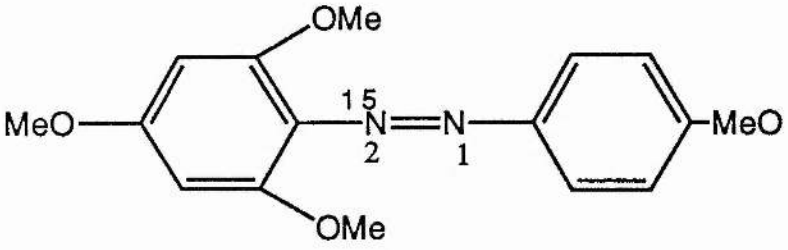

(d)

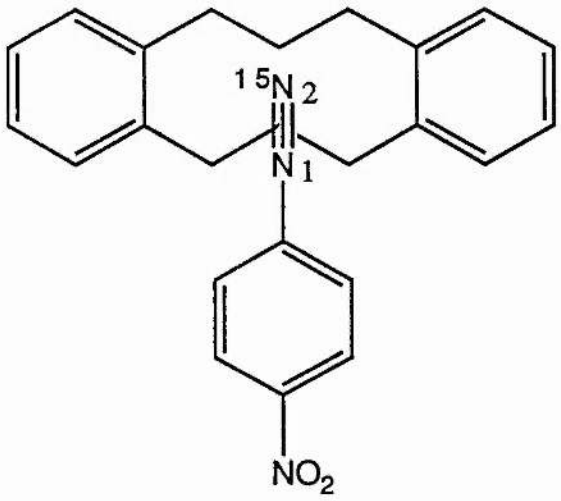

(e)

Figure 6.

$\Sigma w/F_o-/F_c//^2$ to R = 0.081, wR = 0.095. The difference map showed alternative positions for F(14), F(15) and F(16) by rotation about F(13)-B(12), which is almost parallel with the c-axis. The majority position was refined as a rigid tetrahedron with the boron-fluorine bond equal to 1.370Å. All non-hydrogen atoms were anisotropic except for the minority positions F(14A), F(15A) and F(16A). U(H) was refined to 0.069(12)$Å^2$ for the hydrogen atom on the calculated position. 141 refined parameters, $w=[2.6856/\sigma^2(F)+0.000438F^2]$;max. Δ/σ 0.021; max. features on final difference map 0.32, -0.29e$Å^{-3}$.

Final coordinates are given in Table 1 with bond lengths and angles of the cation in Table 2. The cation is shown in Figure 4 and a packing diagram in Figure 5. There is no suggestion of disorder in the cation but the disorder if the anion is probably more complicated than the model used here. The crystals did not diffract strongly and attempts at more elaborate treatments did not succeed with the limited data available.

3.2.2 SOLID STATE ^{15}N NMR SPECTROSCOPY

Solid state ^{15}N nmr spectra were recorded of compounds (a) to (e) in Figure 6. The two labelled benzenediazonium tetrafluoroborates were prepared by the use of 98% ^{15}N labelled sodium nitrate according to the method of Starky [19].These salts were coupled with trimethoxybenzene in acetonitrile to give products 6(c) and 6(d). A complex of ^{15}N labelled 4-nitrobenzenediazonium tetrafluoroborate and dibenzyl 18-crown-6 6(e) was prepared by dissolving equimolar amounts of each reactant in acetonitrile and allowing the acetonitrile to evaporate off overnight.

All solid state ^{15}N nmr spectra were recorded on a Varian VXR 300MHz spectrometer with solid state attachment and wide bore Oxford magnet at the SERC/UDIRL solid state nmr service at the University of Durham. The spectra were recorded at 30.405MHz using Cross Polarisation Magic Angle Spinning (CPMAS).

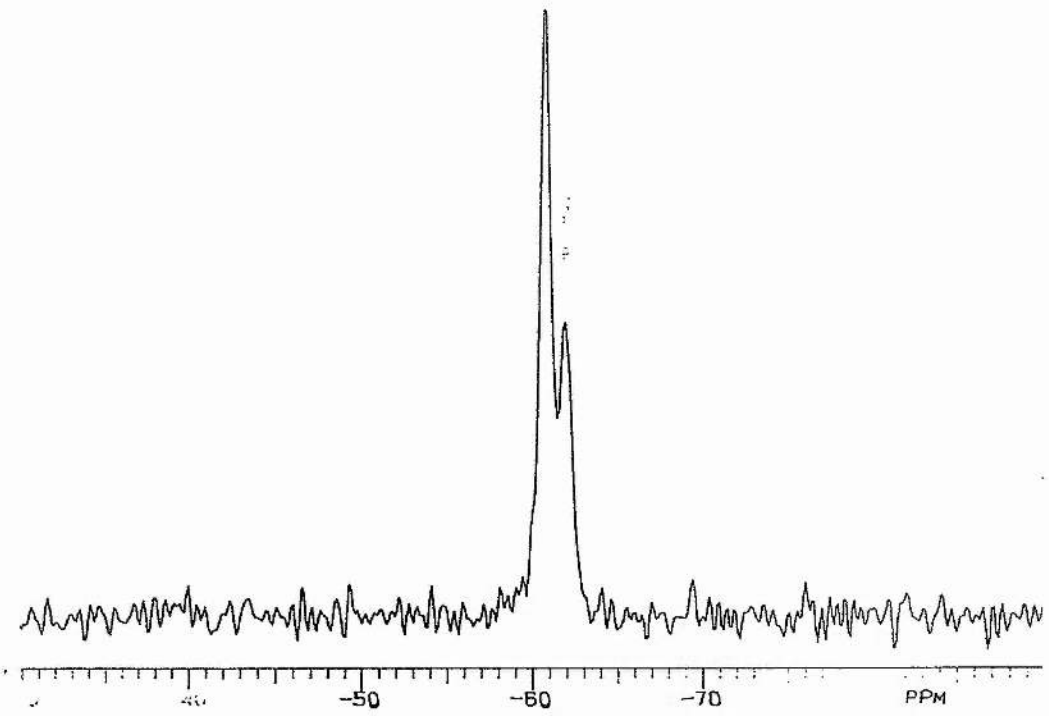

Figure 7.
Solid state ^{15}N nmr spectrum of 4-nitrobenzenediazonium tetrafluoroborate.

3.3 RESULTS AND DISCUSSION

The solid state ^{15}N nmr spectra of 4-nitro- and 4-methoxybenzenediazonium tetrafluoroborate were compared with the solution state spectra reported previously[14]. The chemical shifts for both solution and solid state are shown in Table 3. Normally a straightforward comparison can be made between solution and solid state nmr and the CPMAS technique provides a bridge between X-ray crystal structures and those existing in solution. Two signals are observed in the solid state spectrum of 4-nitrobenzenediazonium ion (Figure 7). This is an unexpected result as the solution state nmr exhibits only one signal indicating the existence of only one ^{15}N environment. From the solid state spectrum, it is possible that ^{15}N is present in two environments in crystalline 4-nitrobenzenediazonium tetrafluoroborate. Furthermore, the solid state spectrum of the dibenzyl 18-crown-6/4-nitrobenzenediazonium ion complex contains three signals at chemical shifts at least 5ppm removed from the 4-nitrobenzenediazonium ion shifts. This is an intriguing observation as it was expected that only one ^{15}N environment would exist in the dibenzyl 18-crown-6 complex with all the diazonium ion expected to be held within the crown cavity. Any diazonium ion remaining outside the crown would have a chemical shift the same as that observed for the 4-nitrobenzenediazonium ion sample with no crown added. An explanation for these unexpected nmr results was sought by solving the X-ray crystal structure of 4-nitrobenzenediazonium tetrafluoroborate. Solving this structure should help to clarify the solid state ^{15}N nmr spectrum of this species and possibly also of the 4-methoxy species, for which three signals are observed in the ^{15}N solid state nmr spectrum (Figure 9).

The final solution of the crystal structure of p-nitrobenzenendiazonium tetrafluoroborate does not indicate that the diazonium ion has more than one orientation. However, there is considerable disorder in the anion (BF_4^-) and two alternative

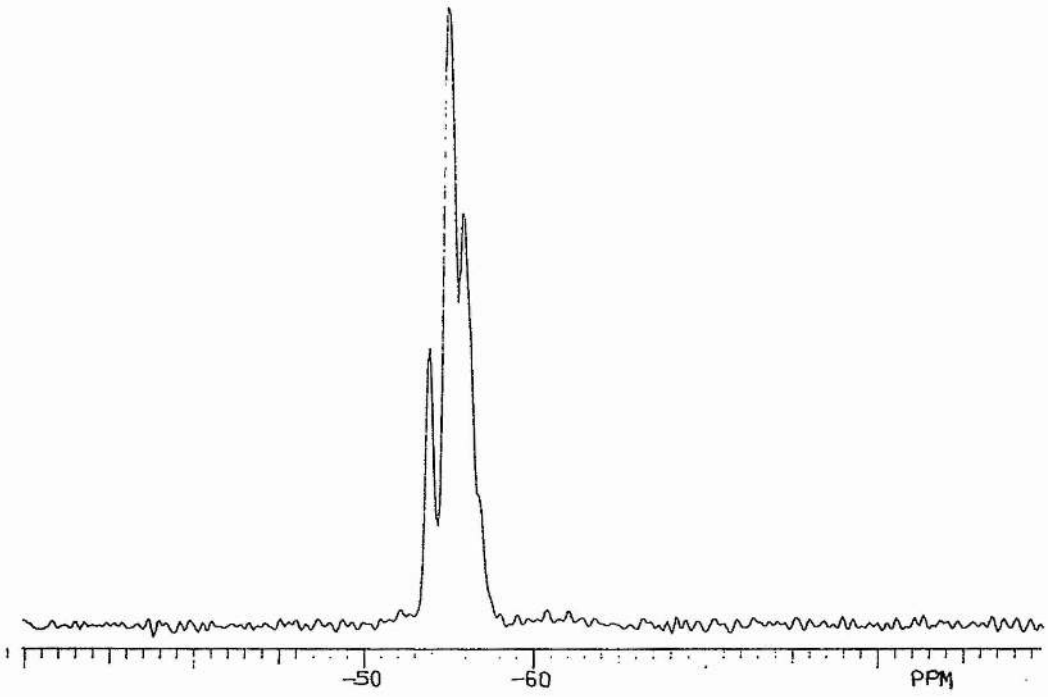

Figure 8.
Solid state ^{15}N nmr spectrum of 4-nitrobenzenediazonium tetrafluoroborate complexed to dibenzyl 18-crown-6.

Table 3.

	Solution state [a]	Solid state[b]
p-$NO_2C_6H_4N_2^+BF_4^-$	-65.2	60.826 61.951
p-$MeOC_6H_4N_2^+BF_4^-$	-57.2	53.939 55.279 56.190
p-$NO_2C_6H_4N_2^+BF_4^-$/18-C-6[c]	-62.9[d] -64.5[e]	53.993 55.105 56.003
p-$NO_2C_6H_4N_2C_6H_2(MeO)_3$	–	16.854 17.752
p-$MeOC_6H_4N_2C_6H_2(MeO)_3$	–	53.899 55.011

a. chemical shift in ppm relative to nitromethane.
b. chemical shift in ppm.
c. dibenzyl 18-crown-6.
d. dibenzyl 18-crown-6 in excess.
e. p-$NO_2C_6H_4N_2BF_4^-$ in excess.

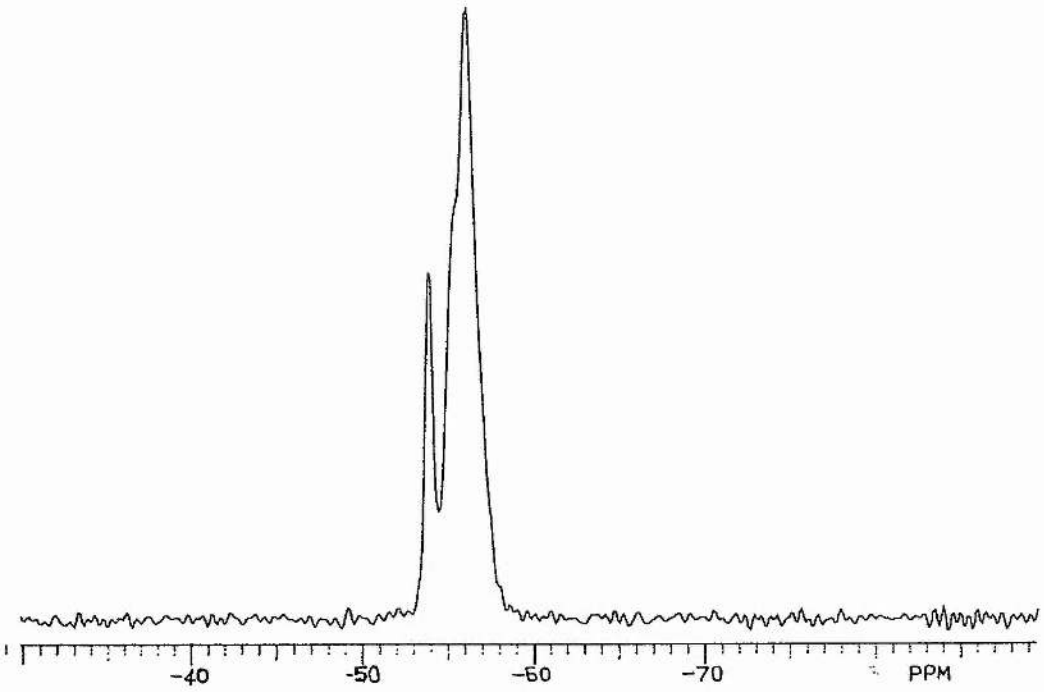

Figure 9.
Solid state ^{15}N nmr spectrum of 4-methoxybenzenediazonium tetrafluoroborate.

positions are defined for F14, F15 and F16 about the B-F13 axis, although the situation is possibly even more disordered than this. It can be imagined that the occurrence of at least two anion orientations may alter the environment of the ^{15}N label in the diazonium ion to the extent that two signals are observed in the solid state ^{15}N nmr spectrum. The crystal structure of 4-methoxybenzenediazonium tetrafluoroborate was not analysed but it is possible that a similar situation to the 4-nitro compound may exist, leading to more than one peak in the solid state ^{15}N nmr spectrum.

In the solution state, addition of dibenzyl 18-crown-6 to 4-nitrobenzenediazonium tetrafluoroborate changes the chemical shift according to the amount of crown added (Table 3). Only one signal is observed, indicating rapid exchange between free and complexed diazonium ion. In the solid state, exchange is not possible and only one signal, corresponding to complexed diazonium, is expected. Three signals are in fact observed in the solid state spectrum of a sample containing equimolar amounts of crown and diazonium ion (Figure 8). This result may also be clarified in the light of the anion disorder in the crystal structure. The presence of the crown changes the chemical shift from around 61ppm to around 55ppm. This indicates that the environment of all the ^{15}N present is affected by the crown. If all the ^{15}N was complexed within the crown cavity, only one peak would be expected in the solid state nmr spectrum as all the environments would be identical and unaffected by the anion disorder. However, if some ^{15}N in each of the original two environments caused by anion disorder remains outwith the crown, two solid state ^{15}N nmr signals would be expected for the two ^{15}N observed in the spectrum without any crown. These signals would correspond to the two ^{15}N environments observed in the original 4-nitrobenzenediazonium tetrafluoroborate sample. These ^{15}N would still have a different environment and therefore different chemical shift, because they are in close proximity to the crown and the chemical shifts would be in a similar place to the fully complexed ^{15}N.

Although the X-ray crystal structure data are recorded from a single unit crystal,

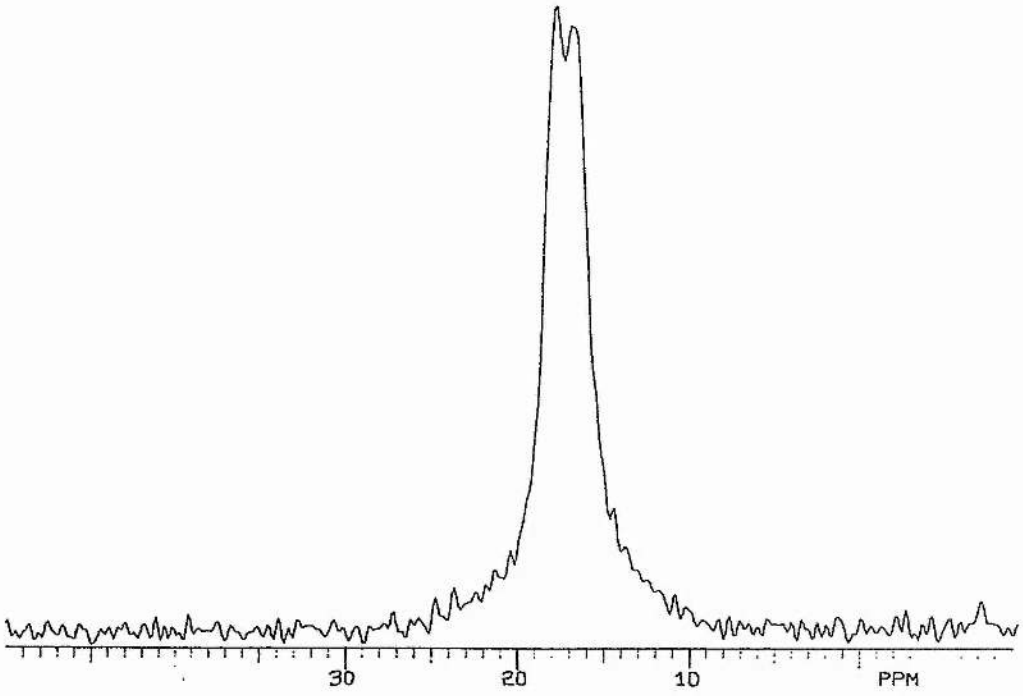

Figure 10.
Solid state ^{15}N nmr spectrum of 4-nitrobenzenediazonium tetrafluoroborate coupled to trimethoxybenzene.

the sample used for the solid state ^{15}N nmr may contain more than one type of unit crystal. A mixture of crystal types may result in the observance of different ^{15}N environments in the solid state ^{15}N nmr spectrum. Thus, although a single cation orientation is observed in the X-ray structure, a number of orientations may exist in a sample containing a mixture of unit cell types. To verify this idea, the sample would have to be analysed by X-ray powder diffraction to establish the actual number of cation orientations present.

A further explanation of the signal pattern observed in the ^{15}N solid state nmr spectrum of 4-nitrobenzenediazonium tetrafluoroborate is found by consideration of the nature of the nuclei to which the ^{15}N is bound. Some solid state nmr spectra exhibit coupling between the nucleus being observed and other nuclei, particularly if the latter are quadrupolar. This coupling has been investigated for a number of nuclei including ^{14}N directly bonded to ^{13}C[24] and ^{13}C directly bonded to ^{2}H[25]. The occurrence of ^{14}N directly bonded to ^{13}C is very common in nature and the effects have been observed by a number of groups[26,27]. The resonances of ^{13}C bonded to ^{14}N are split into broadened asymmetric doublets. This results from the ^{14}N nuclear quadrupole moment interfering with the ability of magic angle spinning to average out carbon-nitrogen dipolar interactions.

The molecule being observed in this experiment contains ^{14}N (I=1) directly bonded to ^{15}N (I=1/2) and therefore is comparable to the situation where ^{13}C is directly bonded to ^{2}H. It is therefore likely that the two peaks observed in the ^{15}N spectrum are in fact the result of a splitting of one signal caused by residual dipolar coupling. This effect could be confirmed by further experiments at a variety of field strengths, allowing a measurement of the coupling constants involved.

The complications encountered in the analysis of the structure of the 4-nitrobenzenediazonium ion limited the analysis of the other solid state ^{15}N nmr

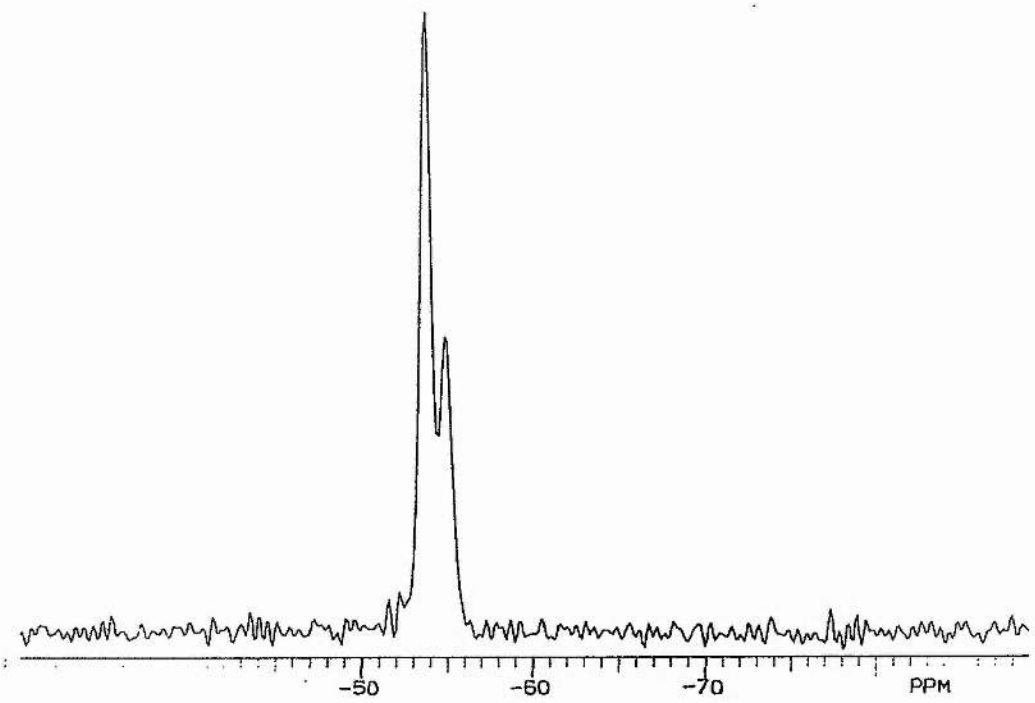

Figure 11.
Solid state ^{15}N nmr spectrum of 4-methoxybenzenediazonium tetrafluoroborate coupled to trimethoxybenzene.

spectra obtained. It is possible that residual dipolar coupling also occurs in the 4-methoxybenzenediazonium ion, which exhibits three signals in its solid state ^{15}N nmr spectrum (Figure 9). The solid state ^{15}N nmr spectra of the coupled products 6(c) and 6(d) also cannot be confidently assigned at this stage (Figures 10 and 11). An extension of this work involving further solid state ^{15}N nmr experiments is necessary to complete the structural investigation of these compounds.

3.4 REFERENCES

1. C. Romming, *Acta Chem.Scand.*, 1959, **13**, 1260.
2. C. Romming, *Acta Chem.Scand.*, 1972, **26**, 523.
3. C. Romming, *Acta Chem.Scand.*, 1963, **17**, 1444.
4. M. Cygler, M. Przybylska and R.M. Elofson, *Can. J. Chem.*, 1982, **60**, 2852.
5. J.M. Insole and E.S. Lewis, *J. Am. Chem. Soc.*, 1963, **85**, 122.
6. E.S. Lewis and J.M. Insole, *J. Am. Chem. Soc.*, 1963, **86**, 32.
7. A.K. Bose and I.Kugajevsky, *J. Am. Chem. Soc.*, 1966, **88**, 2325.
8. E.S. Lewis and P.G. Kotcher, *Tetrahedron*, 1969, **25**, 4873.
9. C.G. Swain, J.E. Sheats and K.G. Harbison, *J. Am. Chem. Soc.*, 1975, **97**, 796.
10. R.G. Bergstrom, R.G.M. Landells, G.H. Wahl and H. Zollinger, *J. Am. Chem. Soc.*, 1976, **98**, 3301.
11. I. Szele and H. Zollinger, *J. Am. Chem. Soc.*, 1978, **100**, 2811.
12. Y. Hashida, R.G.M. Landells, G.E. Lewis, I. Szele and H. Zollinger, *J. Am. Chem. Soc.*, 1978, **100**, 2816.
13. I. Szele and H. Zollinger, *Helv. Chim. Acta*, 1981, **64**, 2728.
14. L.M. Anderson, A.R. Butler and A.S. McIntosh, *J. Chem. Soc. Perkin Trans. II*, 1987, 1239.
15. P.N. Juri and R.A. Bartsch, *J. Org. Chem.*, 1979, **44**, 143.
16. T. Kuokkanen and P.O.I. Virtanen, *Acta Chem.Scand.*, 1979, **B33**, 725.
17. C. Casewit, J.D. Roberts and R.A. Bartsch, *J. Org. Chem.*, 1982, **47**, 2875.
18. A.R. Butler and P.T. Shepherd, *J. Chem. Res.*, 1978 (S), 1978 (M) 4471.
19. E.B. Starky, 'Organic Synthesis' Collective Vol.II, Wiley, New York, 1943, p.225.
20. G.M. Sheldrick, 1986, SHELX86. Program for crystal structure

determination. University of Gottingen, Federal Republic of Germany.

21. G.M. Sheldrick, 1976, SHELX76. Program for crystal structure determination. University of Cambridge, England.
22. P. Roberts and G.M. Sheldrick, 1975, XANADU. Program for crystallographic calculations. University of Cambridge, England.
23. W.D.S. Motherwell and W. Clegg, 1978, PLUTO. Program for plotting molecular and crystal structures. University of Cambridge, England.
24. P. Jonsen, *J. Magn. Res.*, 1988, **77**, 348.
25. D. Swanson, S. Ganapathy and R.G. Bryant, *J. Magn. Res.*, 1987, **73**, 239.
26. M.H. Frey and S.J. Opella, *J. Chem. Soc. Chem. Commun.*, 1980, 474.
27. C.J. Grommbridge, R.K. Harris, K.J. Packer, B.J. Say and S.F. Tanner, *J. Chem. Soc. Chem. Commun.*, 1908, 174.

Chapter 4

Kinetic Study by ^{13}C NMR Spectroscopy of Some Reactions Involving Benzil

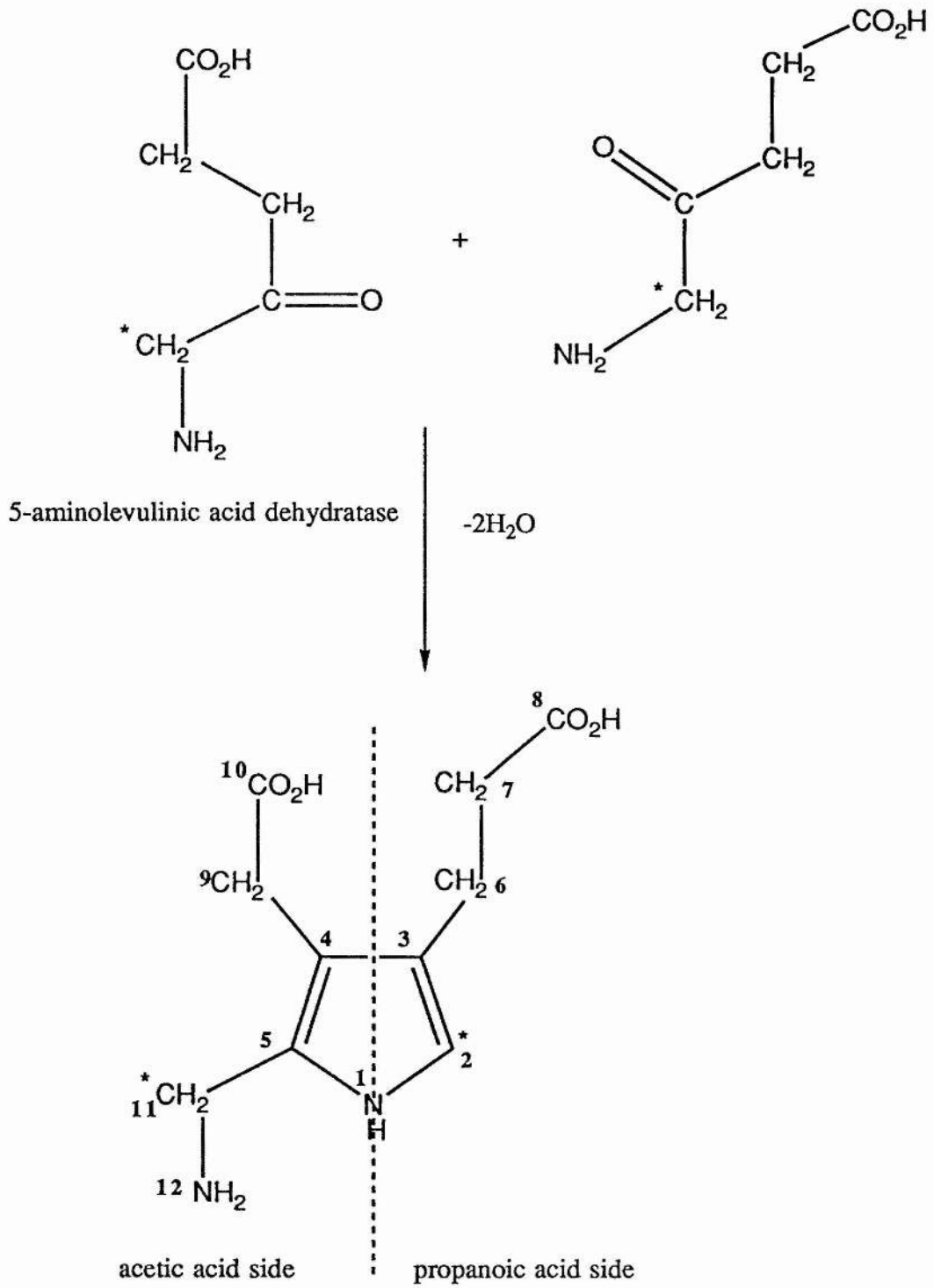

Scheme 1. Formation of porphobilinogen from two molecules of 5-aminolevulinic acid.

4.1 INTRODUCTION

The advantage of ^{13}C nmr as a probe for the investigation of a wide range of biochemical problems has been highlighted by the use of the technique to demonstrate the existence of transient or labile species in systems where a non-invasive approach is essential. The sensitivity of the ^{13}C nucleus to its chemical environment enables direct observation of intermediates in enzymatic reactions and the elucidation of metabolic pathways in the biosynthesis of natural products from ^{13}C enriched precursors.

The mechanism of action of 5-aminolevulinic acid dehydratase, an enzyme in the porphyrin biosynthetic pathway, has been investigated by this technique[1]. This enzyme catalyses the formation of porphobilinogen from two molecules of 5-aminolevulinic acid (Scheme 1). Previous studies[2] of the dehydratase from *Rhodopseudomonas spheroides* established the participation of a Schiff base linkage between the substrate and an amino group on the enzyme. To understand the events occurring at the enzyme active site, the two substrate molecules which combine to give porphobilinogen must be distinguishable in the final product. This is done by synthesising the porphobilinogen from two molecules of 5-aminolevulinic acid specifically labelled at the C-5 position. These carbons will end up at positions 2 and 11 in the product molecule (Scheme 1), positions which have very different ^{13}C environments and therefore different chemical shifts. By this method the investigators established that the first molecule of 5-aminolevulinic acid bound to the enzyme is the one giving rise to the propanoic acid side of porphobilinogen (Scheme 1). The further reactions of porphobilinogen to urogen I and urogen III have also been extensively studied by ^{13}C labelling experiments[3,4]. More recently, ^{13}C nmr spectroscopy has been used to observe the equilibrium complex of ^{13}C labelled

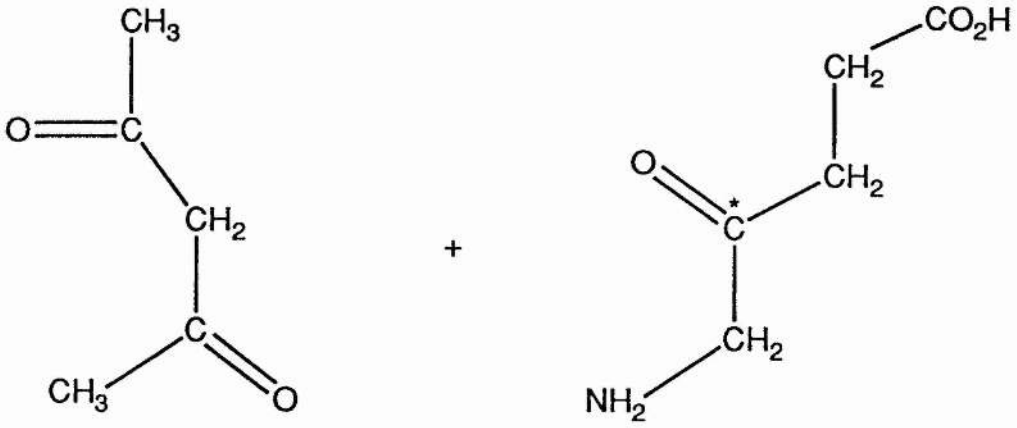

acetylacetone

5-aminolevulinic acid

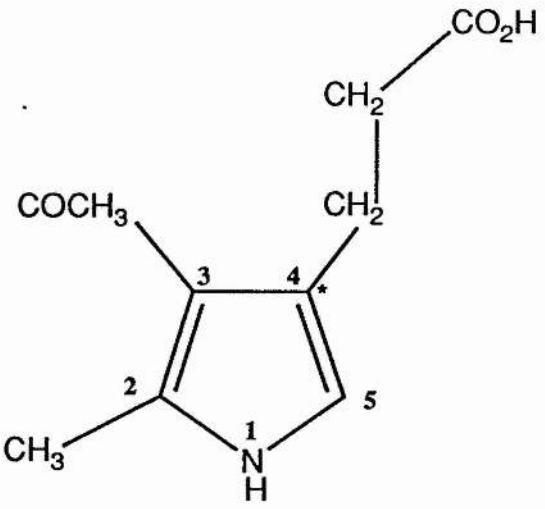

* denotes position of ^{13}C label

Scheme 2. Reaction of acetyl acetone with 5-aminolevulinic acid

5-aminolevulinic acid bound to 5-aminolevulinic acid dehydratase[5]. This work led to the investigation of the chemistry of the substrate and product bound to the enzyme and the ^{13}C nmr shifts of porphobilinogen itself were investigated as functions of pH and a variety of organic solvents[6]. By enriching a reactant molecule with ^{13}C at a specific position, ^{13}C nmr spectroscopy can also be used to study the kinetics of a reaction. By taking ^{13}C nmr spectra at regular intervals over the duration of the reaction, the progress of the ^{13}C label can be monitored as it changes environment from reactant molecule to intermediates and products. For a particular species, the intensity of the peaks observed in ^{13}C nmr spectroscopy are directly proportional to the amount of ^{13}C label present. Thus as the intensity of the ^{13}C labelled peak decreases, this particular labelled species must be being consumed on reaction to form another species which will contain the ^{13}C label in a new environment.

In the present investigation, it was intended to study firstly a model non-enzymatic condensation reaction which parallels the formation of porphobilinogen. The chosen reaction involved one molecule of acetylacetone reacting with one molecule of 5-aminolevulinic acid labelled with ^{13}C at position 4 (Scheme 2). This position was chosen because the carbonyl ^{13}C signal is distinctive and removed from the other ^{13}C signals in the spectrum. Examination of this reaction by ^{13}C nmr should indicate the mechanism involved. As the reaction proceeds, the 5-aminolevulinic acid will be used up and therefore the ^{13}C signal of the carbonyl in this molecule will diminish. The label will be incorporated into intermediates and consequently into the pyrrole product molecule. The change in environment of the ^{13}C label will be reflected in its change in chemical shift as the reaction proceeds. By examining this change and assigning the new chemical shift, the nature of the

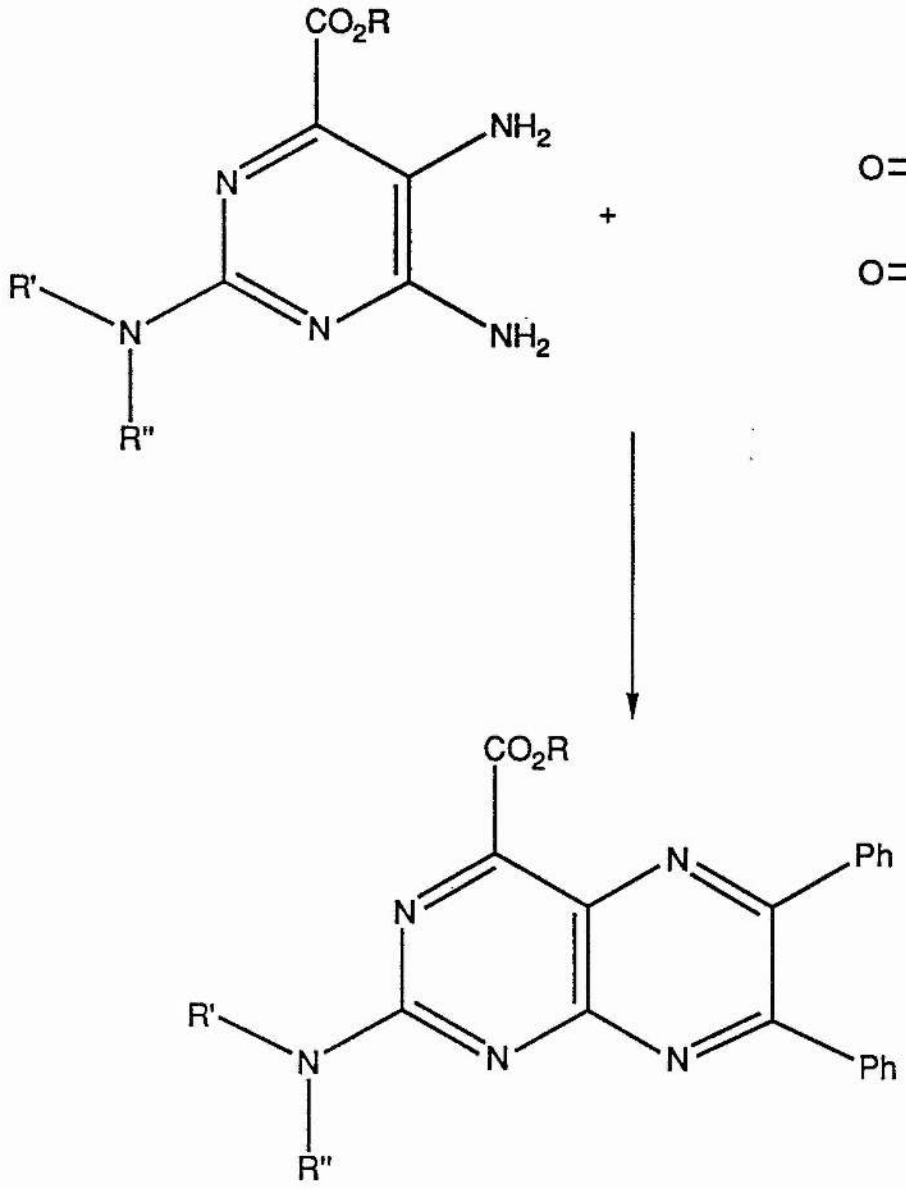

Scheme 3. Reaction of benzil with 6-alkoxy pyrimidine.

intermediates of the reaction should be identified.

These experiments will only be successful if the intermediates can be detected by ^{13}C nmr spectroscopy. It is essential that the rate determining step occurs at a stage in the reaction which allows the accumulation of intermediates to a level at which they give rise to signals in the ^{13}C nmr spectrum. If the rate determining step occurs in the latter stages of the mechanism, the intermediate-forming steps will be fast resulting in a build-up of intermediates which could be detected by nmr before being converted by a slower rate determining step to the products. On the other hand, if the early intermediates are formed slowly via a rate determining step and then quickly converted to product there will be no significant amount of intermediate present at any one point and detection will not be possible by nmr spectroscopy.

The results obtained from the comparatively simple reaction of acetylacetone with 5-aminolevulinic acid can be used in the analysis of the reaction of two molecules of ^{13}C-4 labelled 5-aminolevulinic acid. Both of these reactions required the synthesis of ^{13}C labelled 5-aminolevulinic acid from a convenient and readily available ^{13}C labelled starting material. From a survey of reported procedures in the literature, the method of Pichat and Herbert[7] was selected. This preparation starts with glycine labelled at C-1 and after four steps results in formation of 5-aminolevulinic acid labelled at C-4.

Before proceeding with the 5-aminolevulinic acid experiment, the technique was tried out on a related system.

It has been reported that 6-alkoxycarbonyl-2,4,5-triaminopyrimidines condense readily *in situ* with benzil to give a series of 4-alkoxypteridines[8] (Scheme 3). Reaction of a 50% molar excess of benzil with the pyrimidine occurs on refluxing in methanol for 2-4 hours. By carrying out the reaction at room temperature it was

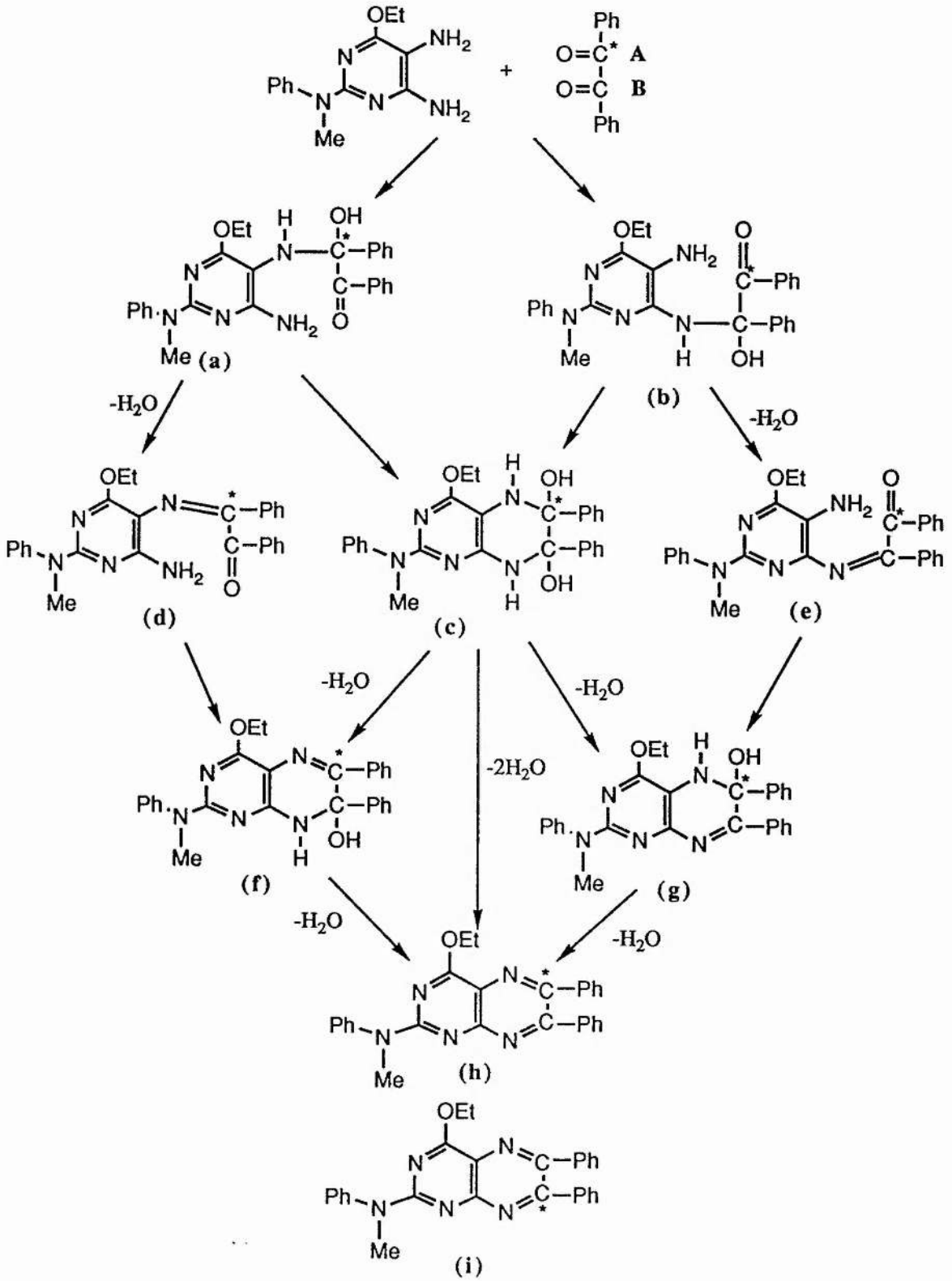

Scheme 4. Proposed mechanisms for the reaction of ^{13}C labelled benzil with 6-methoxy-2,4,5-triaminopyrimidine.

hoped to lengthen the reaction time to around 15 hours, the required time for the ^{13}C nmr kinetics experiment. The use of benzil labelled with ^{13}C at one carbonyl will enable the reaction to be followed easily.

The proposed mechanisms for this reaction are shown in Scheme 4. The unsymmetrical nature of 6-ethoxy-2,4,5-triaminopyrimidine leads to the formation of a large number of intermediates and the labelling of benzil with ^{13}C increases the complexity of the results. A simpler system, the reaction of the symmetrical o-phenylenediamine with ^{13}C labelled benzil, was therefore examined in a preliminary study. The enrichment of the benzil carbonyl with ^{13}C enables this signal to be observed easily. Other signals arising from natural abundance ^{12}C environments can also be seen in the spectra. For this study, however, the fate of the ^{13}C label was followed during the reaction. The amount of intermediates present at any one time will be very small and only observed by virtue of the presence of the ^{13}C label.

Several possible mechanisms for the reaction of benzil with o-phenylenediamine were postulated for this reaction (Scheme 5). The presence of the ^{13}C label in benzil renders it unsymmetrical and increases the number of possible intermediates. As illustrated in Scheme 5, these mechanisms overlap, making determination of the correct pathway rather complex. Only the intermediates containing the ^{13}C label will be detected because it is probable that only very small amounts of intermediate will be formed. To differentiate between the various reaction pathways, the nature of the intermediates and the order in which they are formed has to be established. The ^{13}C label is placed in benzil at a position which has different environments in each of the intermediates (a) to (g) (Scheme 5). An

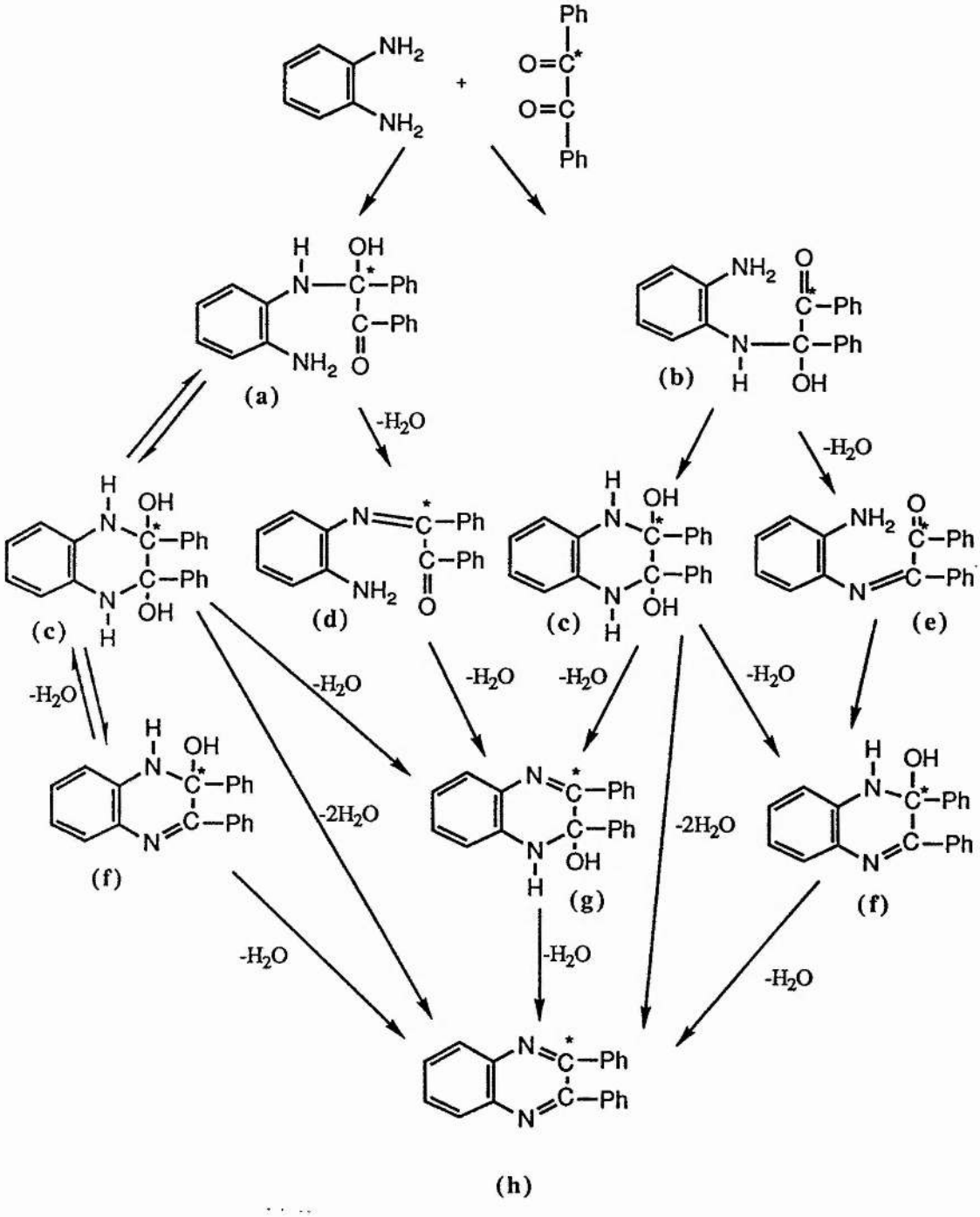

Scheme 5. Proposed mechanisms for the reaction of ^{13}C labelled benzil with o-phenylenediamine.

intermediate containing a carbon-nitrogen single bond must be formed first in all pathways (a) or (b), but this step may be followed either by immediate loss of one water molecule, to give (d) or (e), or by formation of a saturated cyclic intermediate (c). It should be possible by following the ^{13}C labelled atom to determine which of these intermediates is formed. Once this has been established, it may also be possible to observe formation of (g) or (f). If no evidence is found for formation of (g) or (f) it must follow that loss of the two water molecules occurs simultaneously rather than sequentially. The findings from this study can then be applied to the reaction of benzil with 6-methoxy-2,4,5-triaminopyrimidine to elucidate this reaction mechanism.

4.2 EXPERIMENTAL

Benzil labelled with ^{13}C at one carbonyl was synthesised according to the method of Butler and Broan[9]. o-Phenylenediamine and p-phenylenediamine were obtained from Aldrich. o-Phenylenediamine was treated with charcoal and recrystallised from water before use. A sample of 6-methoxy-2,4,5-triaminopyrimidine was kindly donated by Peter Boyle of Trinity College, Dublin. Deuteriated methanol (d_4-CD_3OD) and tetrahydrofuran (THF- d_8) for use in ^{13}C nmr spectroscopy were obtained from MSD isotopes.

Preliminary experiments to determine the approximate rate of the reactions were carried out on a Pye-Unicam SP8-100 spectrophotometer at 25°C.

Samples for nmr were made up in 5mm tubes with TMS as reference. The spectra were run on a Bruker AM-300 spectrometer at 25°C. A spectrum was recorded every hour for fifteen hours. Each spectrum was accumulated for 15 minutes, resulting in 320 scans per spectrum, followed by a delay of 45 minutes

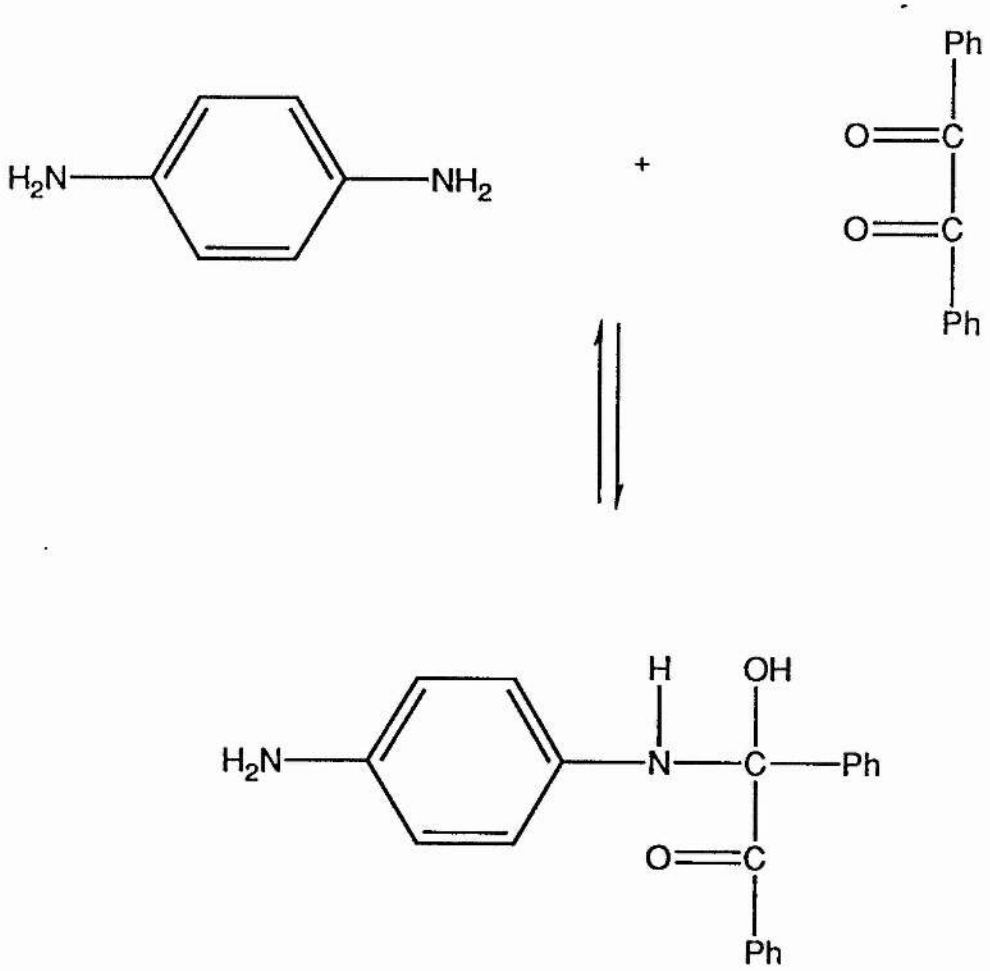

Scheme 6.

before the next accumulation. The TMS reference peak was used to normalise the peak intensities when the spectra were transformed.

The data from the spectra was analysed on an Apple Macintosh computer using a BASIC ^{13}C data-handling program devised by Broan[10].

4.3 RESULTS AND DISCUSSION

The ^{13}C nmr spectra obtained over a period of 15 hours for the reaction of 0.2M o-phenylenediamine and 0.2M ^{13}C-labelled benzil in methanol, indicated that the reaction was occurring too quickly for any useful information to be obtained. The ^{13}C label on the benzil carbonyl appears at 196.3ppm in methanol. This signal disappeared after one hour and a new signal at 155.1ppm, due to transferal of the ^{13}C label to an new environment, was observed increasing to a maximum also after one hour. The experiment was repeated at several lower concentrations but the disappearance of the benzil signal intensity at 196.3ppm after only one or two hours indicated that the reaction was still going too fast. To solve the problem, the solvent was changed from methanol to tetrahydrofuran.

The reaction was examined first by uv spectrophotometry to establish optimum conditions. Absorbance at wavelengths of 304 and 344 nm were observed to increase steadily over a period of 15 hours when both reactants were present at a concentration of 0.2M. A similar experiment was carried out on equimolar amounts of ^{13}C labelled benzil and p-phenylenediamine. In this case no absorbance of any significance were observed indicating that no reaction was taking place. This would seem a reasonable assumption because, as can be seen in Scheme 6, the $-NH_2$ groups in p-phenylenediamine are not in a favourable position to react with the carbonyl groups of benzil. It is possible an intermediate of the type

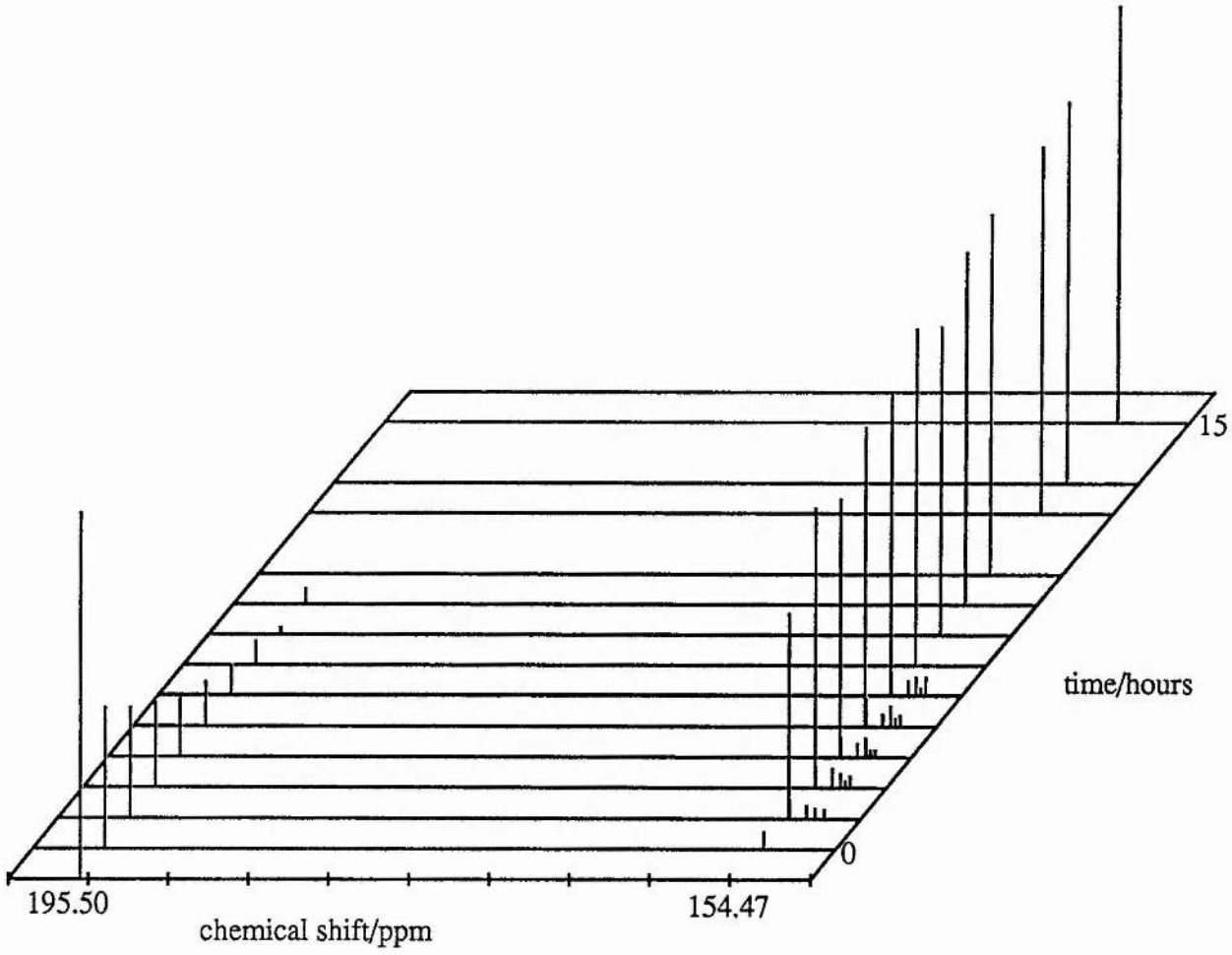

Figure 1. Three-dimensional array of ^{13}C nmr spectra.

shown in Scheme 6 may be formed, but only in a very low equilibrium concentration.

The ^{13}C nmr kinetics experiment was carried out on 0.2M o-phenylenediamine and ^{13}C labelled benzil in THF-d_8. The variation of signal intensity with time for relevant species is shown in Table 1. The spectra obtained showed the intensity of the ^{13}C enriched benzil signal, now at 195.50ppm, decreasing to zero over a period of 12 hours, indicating that all the benzil reacts in this time. The decrease in the ^{13}C benzil signal was compared with the increasing intensity of a new signal at 154.47ppm. The three-dimensional plot in Figure 1 illustrates the change in intensity of the signals at 154.47 and 195.50ppm during the 15 hour experiment. Analysis of the spectra by the ^{13}C data-handling program enabled a direct comparison of the changing intensities of the two signals (Figure 2). A plot of intensity against time was drawn for each signal (Figure 2a) and the 154.47ppm plot inverted. When overlaid on the plot of the 195.50ppm signal intensity, the 154.47ppm plot does not exactly coincide (Figure 2b). During the first 1-2 hours of reaction, the benzil signal (195.50ppm) decreases more rapidly than the 154.47ppm signal increases. This suggests that intermediate species are formed first from benzil and these then react further to the product molecule.

The formation of intermediates is also indicated by the appearance and disappearance during the 15 hour experiment period of a cluster of signals between 80 and 90ppm. These are illustrated in the three-dimensional plot in Figure 3. Figure 4 demonstrates that these intermediates are formed in the first two hours of the experiment, as the benzil signal rapidly decreases. It should be noted that the intensities of these signals have been normalised and therefore are not quantitative relative to each other. The appearance of intermediates in the region of 80-90ppm is

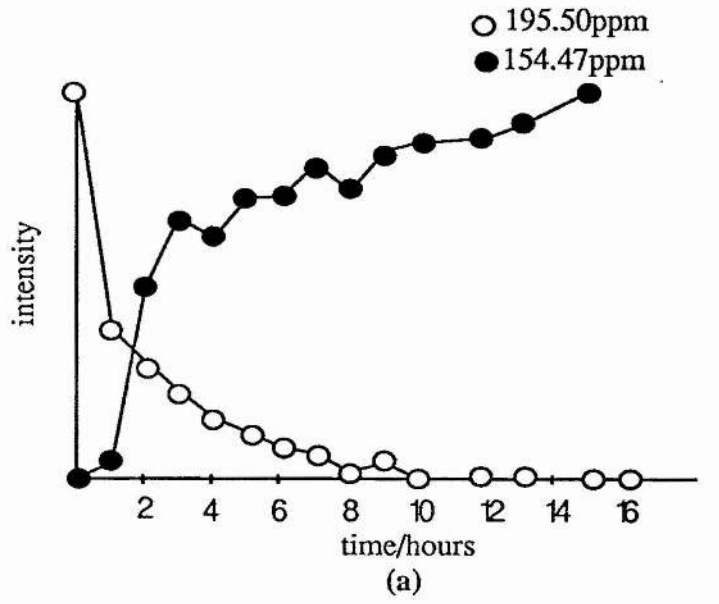
195.50ppm
154.47ppm
intensity
2
4
6
8
10
12
14
16
time/hours
(a)

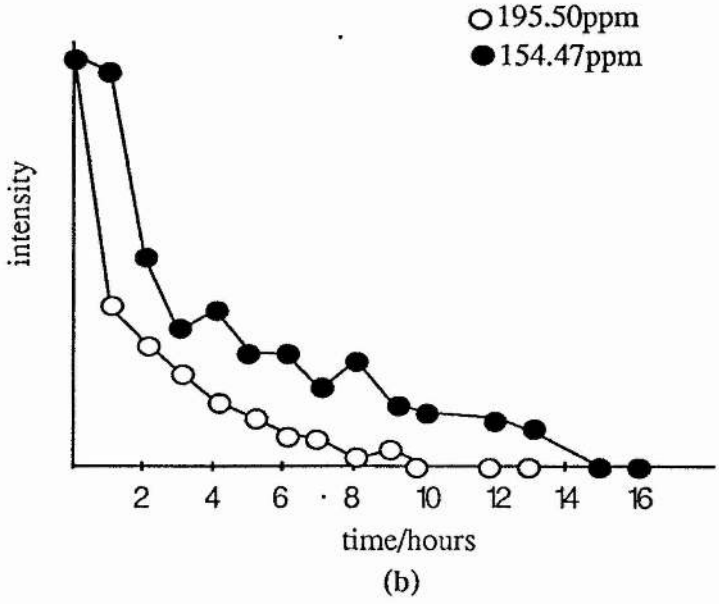
195.50ppm
154.47ppm
intensity
2
4
6
8
10
12
14
16
time/hours
(b)

Figure 2.

Table 1.
Reaction of ^{13}C benzil with o-phenylenediamine.
Intensities of relevant signals in the ^{13}C spectrum over a 15 hour period.

	Time/hours				
chemical shift/ppm	**0**	**1**	**2**	**3**	**4**
195.50	13.672	6.176	4.989	3.653	2.532
154.47	0.000	0.751	9.346	12.177	11.520
154.41	0.000	0.000	0.870	0.878	0.863
84.56	0.000	3.539	1.542	0.338	0.000
84.06	0.000	1.449	0.421	0.241	0.000
chemical shift/ppm	**5**	**6**	**7**	**8**	**9**
195.50	1.917	1.278	0.990	0.261	0.623
154.47	13.171	13.302	14.571	12.000	15.344
154.41	1.206	0.993	0.000	0.000	0.000
84.56	0.000	0.000	0.000	0.000	0.000
84.06	0.000	0.000	0.000	0.000	0.000
chemical shift/ppm	**10**	**12**	**13**	**15**	
195.50	0.000	0.000	0.000	0.000	
154.47	15.853	15.934	16.345	18.139	
154.41	0.000	0.000	0.000	0.000	
84.56	0.000	0.000	0.000	0.000	
84.06	0.000	0.000	0.000	0.000	

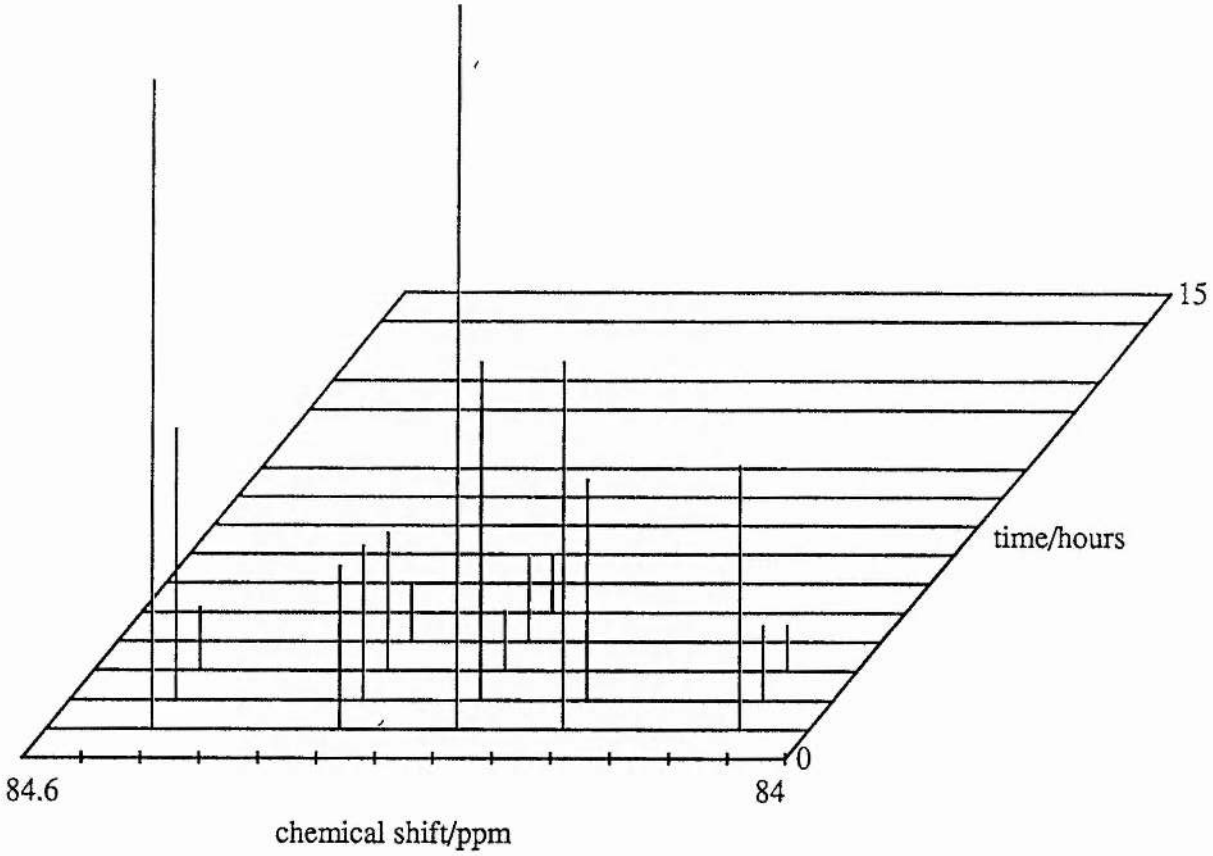

Figure 3. Expansion of the region between 84 and 84.6ppm

consistent with the formation of intermediates (a) and (b) in Scheme 5. These species contain a carbon atom singly bonded to a nitrogen. This type of carbon characteristically has a chemical shift between 80 and 100ppm. However, these intermediates are formed in low concentrations and as a result only species (a), containing the ^{13}C label in the carbon-nitrogen bond will be observed. The ^{13}C label in (b) is still in the carbonyl and is not distinguishable from the benzil ^{13}C carbonyl signal. From Figures 4 and 5 it is clear that the intermediates giving rise to the signals in the 80-90ppm region are formed in the first 2 hours of reaction, before those in the 154-155ppm region. This is consistent with the formation of intermediate (a) (Scheme 5) as the first step in the reaction mechanism.

Having established (a) as the first species formed in the pathway, the next step must either be loss of one water molecule to form a carbon-nitrogen doublebond (d), or formation of a saturated cyclic intermediate (c). Formation of species (d) results in a molecule containing a carbon-nitrogen double bond. This species would subsequently form a cyclic intermediate (g) containing one carbon-nitrogen double bond and one carbon-nitrogen single bond.This order of intermediate formation would give rise to a signal for a carbon-nitrogen double bond appearing in the ^{13}C spectra (in the 150-160ppm region) at the same time as the appearance of the final carbon-nitrogen single bond (in the 80-100ppm region). No signals were observed in the 150-160ppm region until after all the signals in the 80-100ppm region had appeared. From this evidence it seems likely that intermediate (a) forms a cyclic intermediate (c) rather than the carbon-nitrogen double bond containing species (d).

Examination of the signals observed (Table 1) shows that two signals are observed in the 80-100ppm region. The reaction pathway through intermediates (a) and (c) involves two species containing carbons singly bonded to nitrogen but in

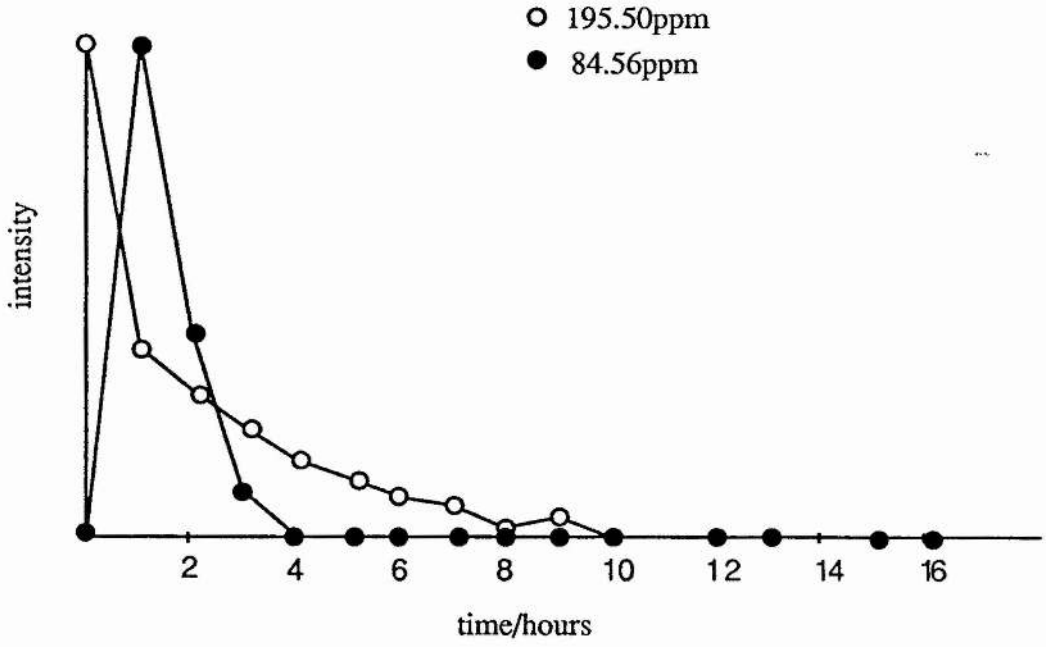

Figure 4.

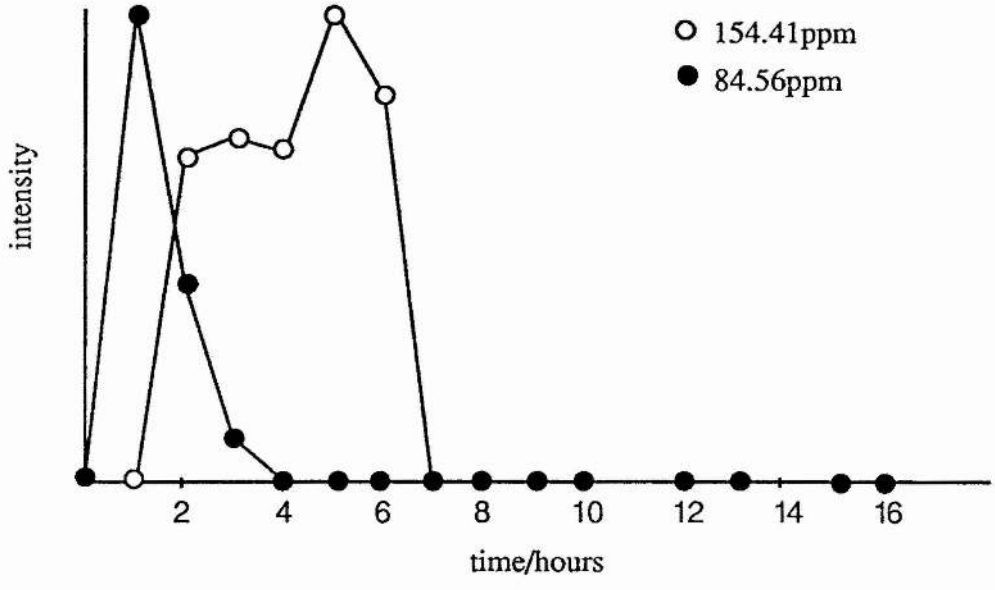

Figure 5.

different environments and therefore with different chemical shifts. The two signals which are observed rise and fall in parallel. This behaviour may be due to the existence of an equilibrium between the intermediate species.

Assuming that the pathway follows the route from (a) to (c), formation of the product (h) now follows either simultaneous or sequential loss of two water molecules. Three signals are expected to be observed in the 80-90ppm region corresponding to the three species, (a), (c) and (f), containing carbon-nitrogen single bonds. As previously observed, only two signals appear in this region of the spectrum. More than one explanation for this result can be proposed. It is possible that only two out of the three signals are detected because only very low levels of intermediate are present. If it is assumed that (a) and (c) are formed, then (f) may not be detected as it is present in such a low equilibrium concentration. However, it could be possible that (f) is not actually formed at all and that two water molecules are lost simultaneously to give product (h). It is not possible to determine which of these explanations is correct from the evidence gathered in the present study. The other deductions made, however, have allowed the number of intermediates to be reduced and the order of their formation at least partially determined. The proposed mechanism based on these deductions is that shown in Scheme 7.

The reaction of benzil with 6-methoxy-2,4,5-triaminopyrimidine is also very complex (Scheme 8). The non symmetrical nature of the pyrimidine means there are twice as many possible intermediates in this reaction pathway as there are in the reaction of benzil with o-phenylenediamine (Scheme 5) and more routes to these intermediates are possible. The situation is further complicated by the consideration that carbon B of benzil rather than carbon A may contain the ^{13}C label. This inversion must double the number of possible intermediates. In the light of this

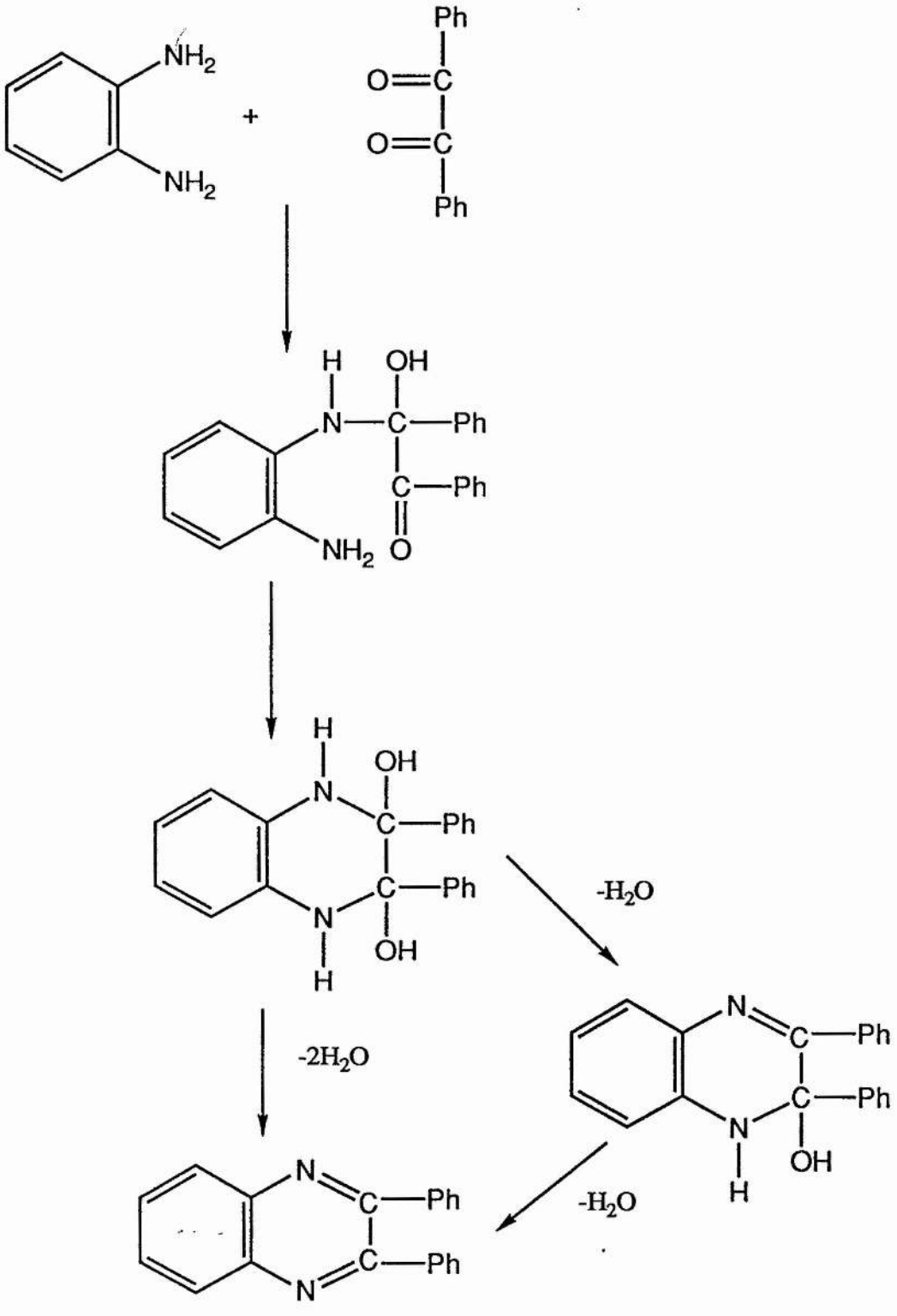

Scheme 7. Mechanism for reaction of benzil with o-phenylenediamine.

complexity, a full analysis of the mechanism seemed a daunting task, but as with the previous analysis the determination of the order of intermediate formation should be enable at least partially elucidation of the pathway.

The reaction of ^{13}C labelled benzil with 6-methoxy-2,4,5-triamino-pyrimidine in d_4-methanol was analysed by taking a spectrum every hour for 15 hours. Reaction was not complete after this time and a further spectrum was run after 23 hours. In this spectrum the benzil signal had disappeared completely indicating completion of reaction. The intensities of relevant signals over this period of time are recorded in Table 2. Figure 6 shows the comparison of the ^{13}C benzil signal (196.23ppm) with a signal at 152.37ppm. This latter signal rises from zero to a maximum over 23 hours and occurs in the correct chemical shift region for a species containing a carbon-nitrogen double bond. A second signal in this region (162.06ppm) also increases from zero to a maximum during the reaction. The non-symmetrical nature of the pyrimidine means that the ^{13}C label is incorporated into the product molecule in two distinct carbon-nitrogen double bond environments. The two signals at 152.37 and 162.06ppm are assigned to the two different carbon-nitrogen double bond environments in the product molecules (h) and (i) in Scheme 8. Figure 7 shows the parallel increase in the intensities of these signals over the 23 hour reaction period, indicating that the molecules containing these signals are formed at the same rate. This indicates that products (h) and (i) are formed at the same rate and it will not be possible to distinguish the reaction pathway of benzil labelled at carbon A from that of benzil labelled at carbon B. This study therefore concentrates on benzil labelled at carbon A as indicated in Scheme 8. The signal at 152.37ppm is thus assigned to the ^{13}C labelled carbon in product (h).

The comparison of reactant (196.23ppm) and product (152.37ppm) signals

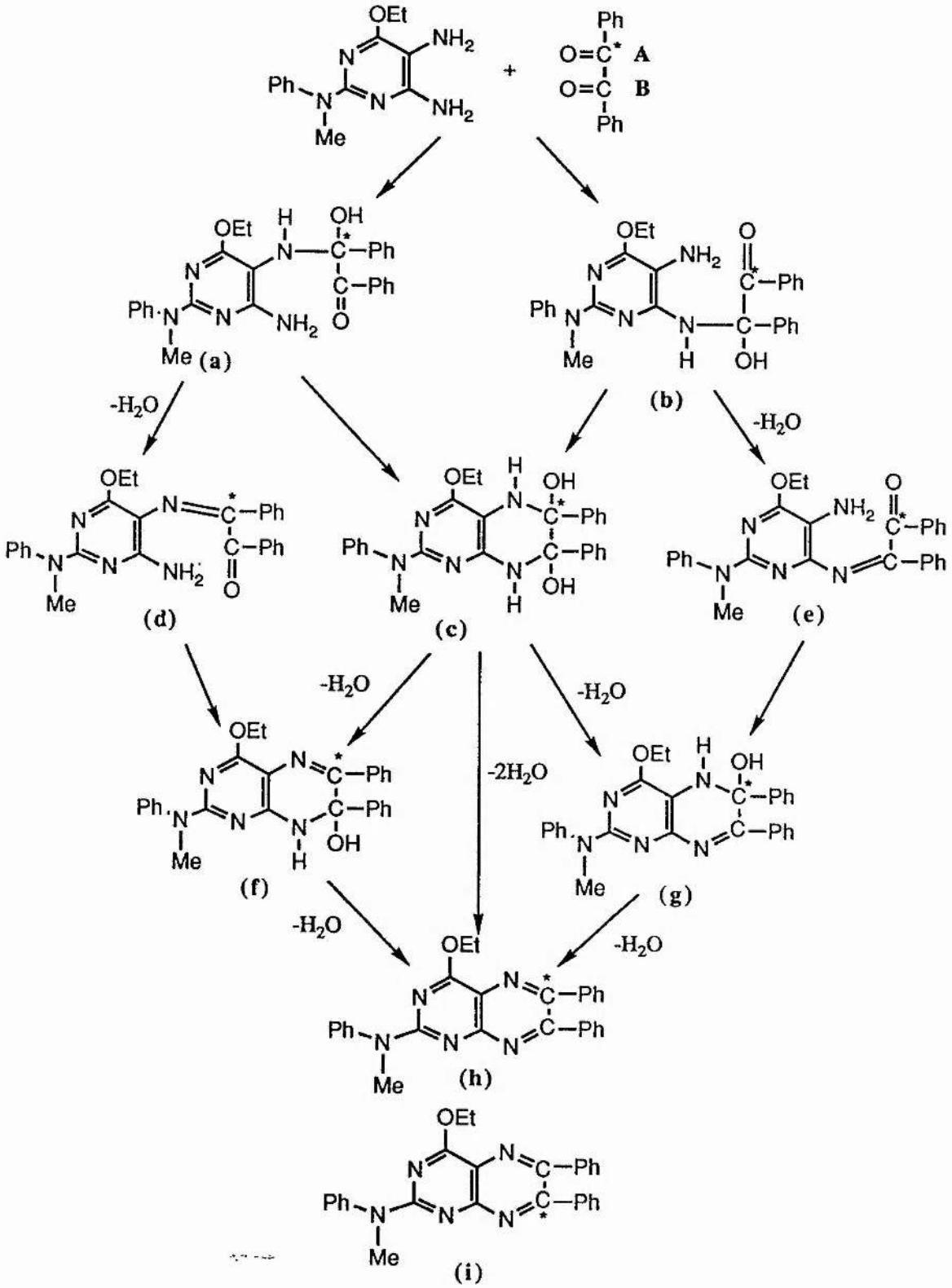

Scheme 8. Proposed mechanisms for the reaction of ^{13}C labelled benzil with 6-methoxy-2,4,5-triaminopyrimidine.

Table 2.

Reaction of ^{13}C benzil with 6-methoxy-2,4,5-triaminopyrimidine. Intensities of relevant signals in the ^{13}C spectrum over a 23 hour period

	Time/hours				
chemical shift/ppm	**1**	**2**	**3**	**4**	**5**
196.23	30.456	24.629	21.711	19.204	17.432
162.06	0.000	0.904	3.592	6.990	10.420
156.85	0.000	2.618	4.264	3.986	3.595
155.64	0.000	0.487	0.988	1.408	1.717
152.37	0.000	0.983	4.081	7.295	10.625
85.35	0.963	2.676	1.887	1.592	1.248
85.13	1.118	2.846	2.328	1.734	1.676
83.98	1.868	3.734	3.087	2.379	1.719
83.78	1.724	2.882	2.723	3.016	2.128
82.00	0.000	0.615	1.004	1.721	1.684
chemical shift/ppm	**6**	**7**	**8**	**9**	**10**
196.23	13.850	14.010	11.961	11.910	10.589
162.06	14.299	15.307	18.568	21.304	22.671
156.85	3.137	2.466	2.138	1.698	1.544
155.64	1.978	2.163	1.885	2.224	2.147
152.37	14.441	15.748	19.783	20.344	20.493
85.35	0.839	0.640	0.598	0.744	0.000
85.13	1.268	0.674	0.634	0.000	0.000
83.98	1.323	0.935	0.971	0.757	0.000
83.78	2.227	2.088	01.717	1.573	1.514
82.00	1.916	2.089	2.321	1.906	1.988
chemical shift/ppm	**11**	**12**	**13**	**14**	**15**
196.23	8.938	8.647	8.366	7.463	6.890
162.06	22.380	22.668	25.466	27.158	28.144
156.85	1.104	0.965	0.000	0.000	0.755
155.64	1.787	1.869	2.015	1.985	2.003
152.37	22.989	25.362	26.069	25.366	25.827
85.35	0.000	0.000	0.000	0.000	0.000
85.13	0.000	0.000	0.000	0.000	0.000
83.98	0.971	0.757	0.000	0.000	0.000
83.78	1.452	1.439	1.065	1.079	0.000
82.00	1.892	1.837	1.906	1.705	2.050
chemical shift/ppm	**23**				
196.23	1.013				
162.06	30.051				
152.37	27.733				

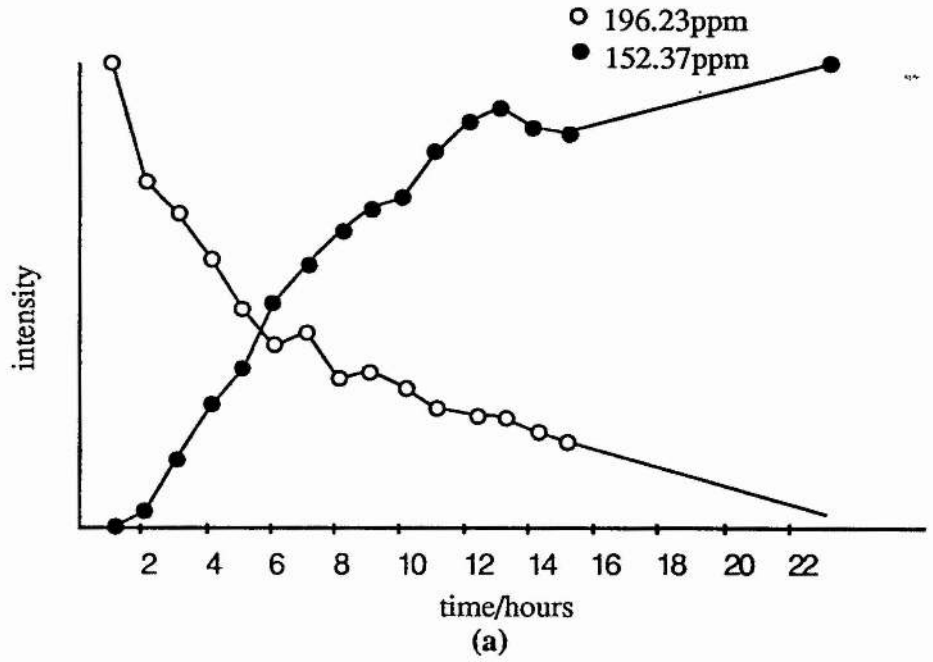
196.23ppm
152.37ppm
intensity
2 4 6 8 10 12 14 16 18 20 22
time/hours
(a)

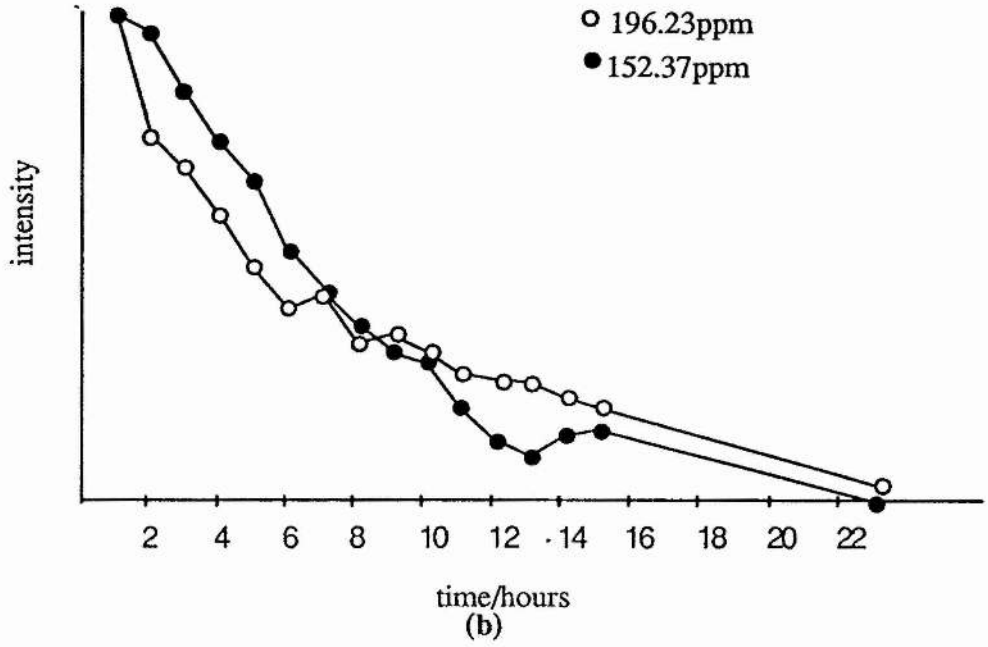
196.23ppm
152.37ppm
intensity
2 4 6 8 10 12 14 16 18 20 22
time/hours
(b)

Figure 6.

in Figure 6(b) again indicates that the benzil is being consumed more quickly than the product is being formed. Intermediates must be being formed on reaction of 6-methoxy-2,4,5-triaminopyrimidine with benzil before the product is formed. Figure 8 illustrates the formation of an intermediate species at a chemical shift of 85.13ppm during the first 4 hours of reaction as benzil is depleted. In fact a cluster of signals in the 80-90ppm region is observed as it was in the o-phenylenediamine reaction. These are illustrated in the 3-dimensional plot in Figure 9. As in the previous study these signals are due to the formation of carbon-nitrogen single bonds containing the ^{13}C label.

The first step in the reaction must be the formation of an intermediate containing one carbon-nitrogen single bond as illustrated in Scheme 8. Considering only the situation where the ^{13}C label is in carbon A in benzil, the two intermediates (a) and (b) are formed. The ^{13}C carbonyl signal of intermediate (b) will not be distinguishable from the benzil ^{13}C carbonyl and the carbon-nitrogen single bond in this intermediate will not be detected as it does not contain a ^{13}C label. As before both intermediates will be formed but only (a) is detected.

Having determined that formation of (a) is the first step in the pathway, the next step involves either loss of one water molecule, to give (d), or formation of the saturated cyclic intermediate (c). Evidence was found to support the existence of a species containing two carbon-nitrogen single bonds. This is illustrated in Figure 10 which shows two signals in the 80-90ppm range increasing and decreasing at the same rate indicating that they belong to the same molecule. These signals are observed in the first four hours of reaction and are probably formed immediately after (a). This evidence supports the formation of (c) which can have ^{13}C incoporated in both carbon-nitrogen positions. However, unlike the

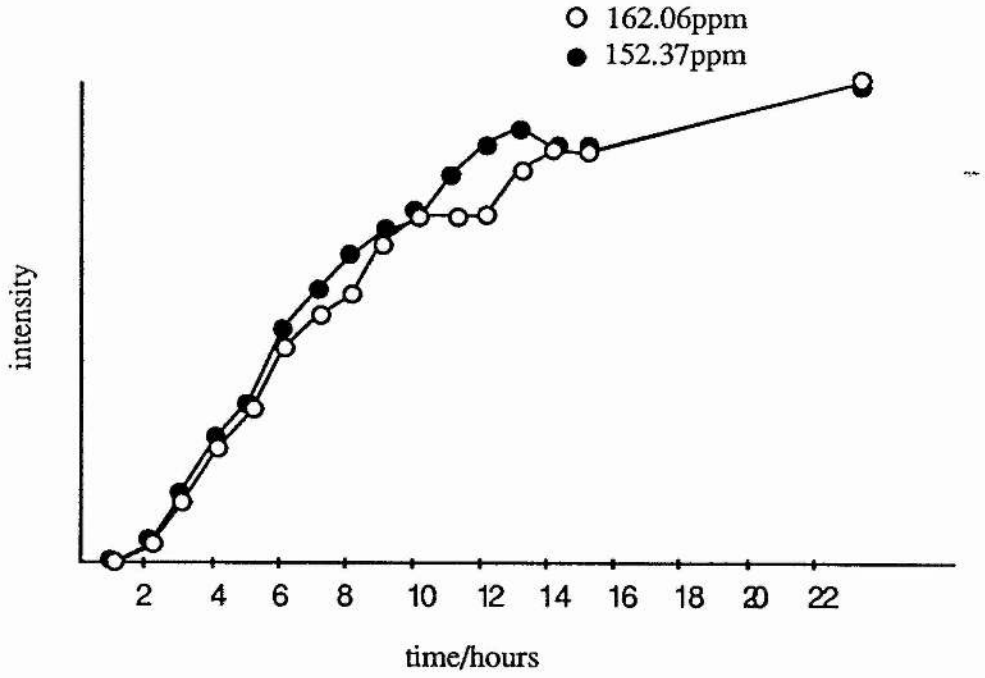

Figure 7.

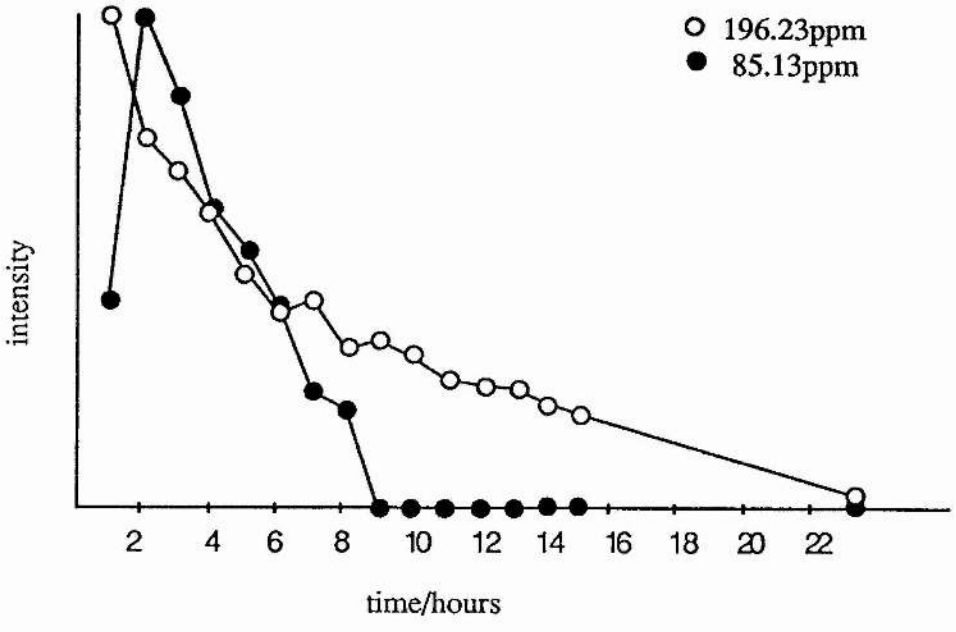

Figure 8.

o-phenylenediamine reaction, evidence was also found which indicated the existence of a species containing both a carbon-nitrogen single bond and a carbon-nitrogen double bond (Figure 11). This species is formed during the first 8 hours of reaction and persists until the end of the 15 hour experiment. From this evidence it appears that in this experiment, unlike the o-phenylenediamine experiment, levels of intermediate (f), which contains both a carbon-nitrogen single bond and a carbon-nitrogen double bond, are high enough to be detected by ^{13}C nmr. Figure 12 compares a signal in the carbon-nitrogen single bond region (85.35ppm) with a signal in the carbon-nitrogen double bond region (156.85ppm) and shows that the species containing a carbon-nitrogen single bond is formed before that containing a carbon-nitrogen double bond. This is consistent with formation of (f) as the subsequent step after formation of the unsaturated cyclic intermediate (c). Detection of (f) indicates that rather than two water molecules being lost simultaneously from (c), as is possible in the o-phenylenediamine reaction, two sequential steps are necessary to lose the two water molecules from the cyclic intermediate (c). A similar reaction scheme to that proposed for the reaction of o-phenylenediamine is therefore supported by the evidence found in this analysis. This pathway is illustrated in Scheme 9. The two schemes for o-phenylenediamine and the pyrimidine are very similar except for the determination of the loss of water in the final stages of the reactions.

The limited amount of information gained from the reaction of benzil with o-phenylenediamine reaction restricts the analysis of the 6-methoxy-2,4,5-triaminopyrimidine reaction pathway. However, it has been possible to eliminate some of the possible intermediates from the proposed mechanism and to determine the order of formation of most of the remaining species. Further complications may

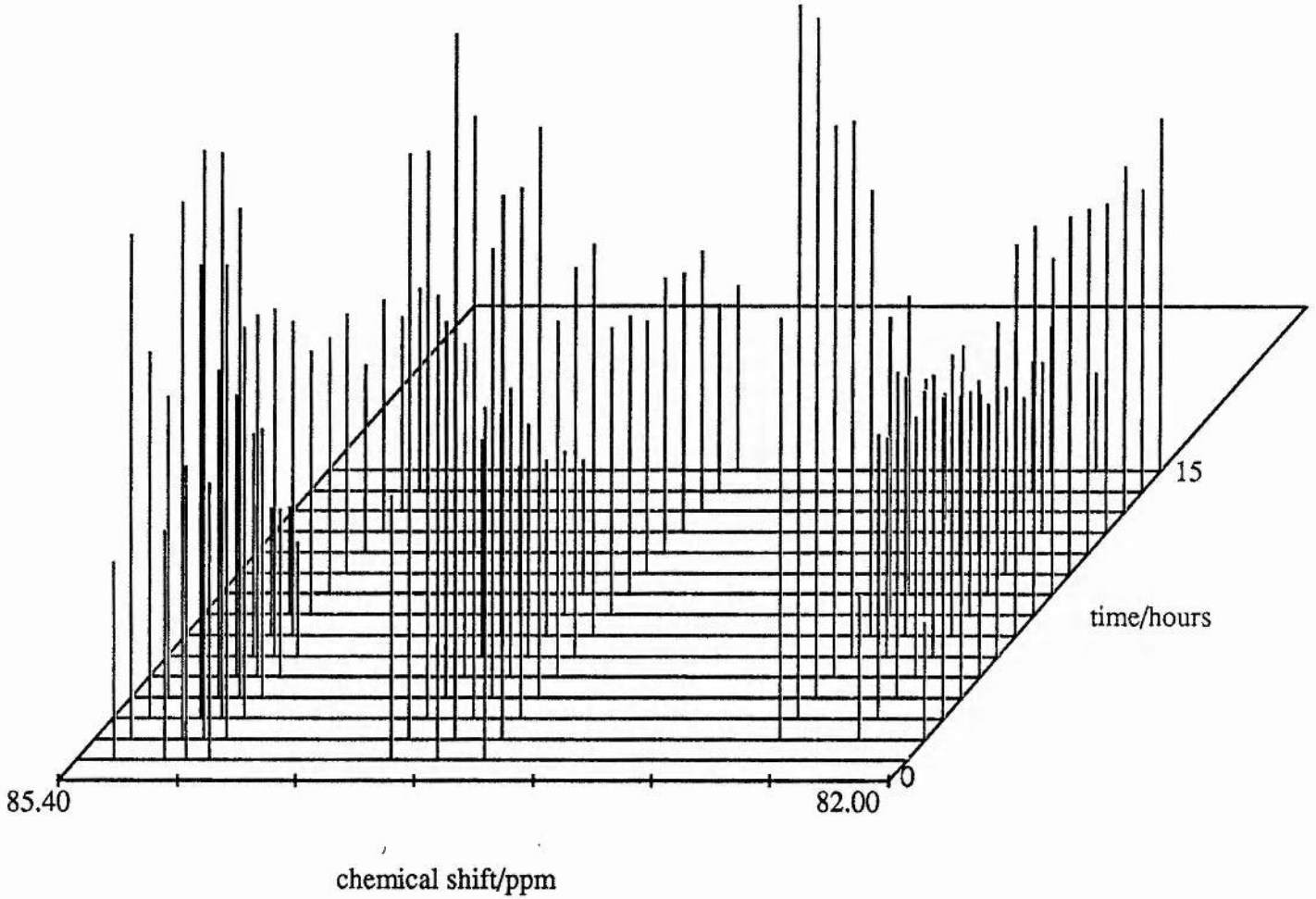

Figure 9.

be encountered when considering the alternative incorporation of the ^{13}C label at the position shown in product (i) in Scheme 8. These have not been included in the determination of the mechanism proposed here which has been simplified in order to illustrate the usefulness of the ^{13}C labelling technique in elucidating mechanism by nmr spectroscopy.

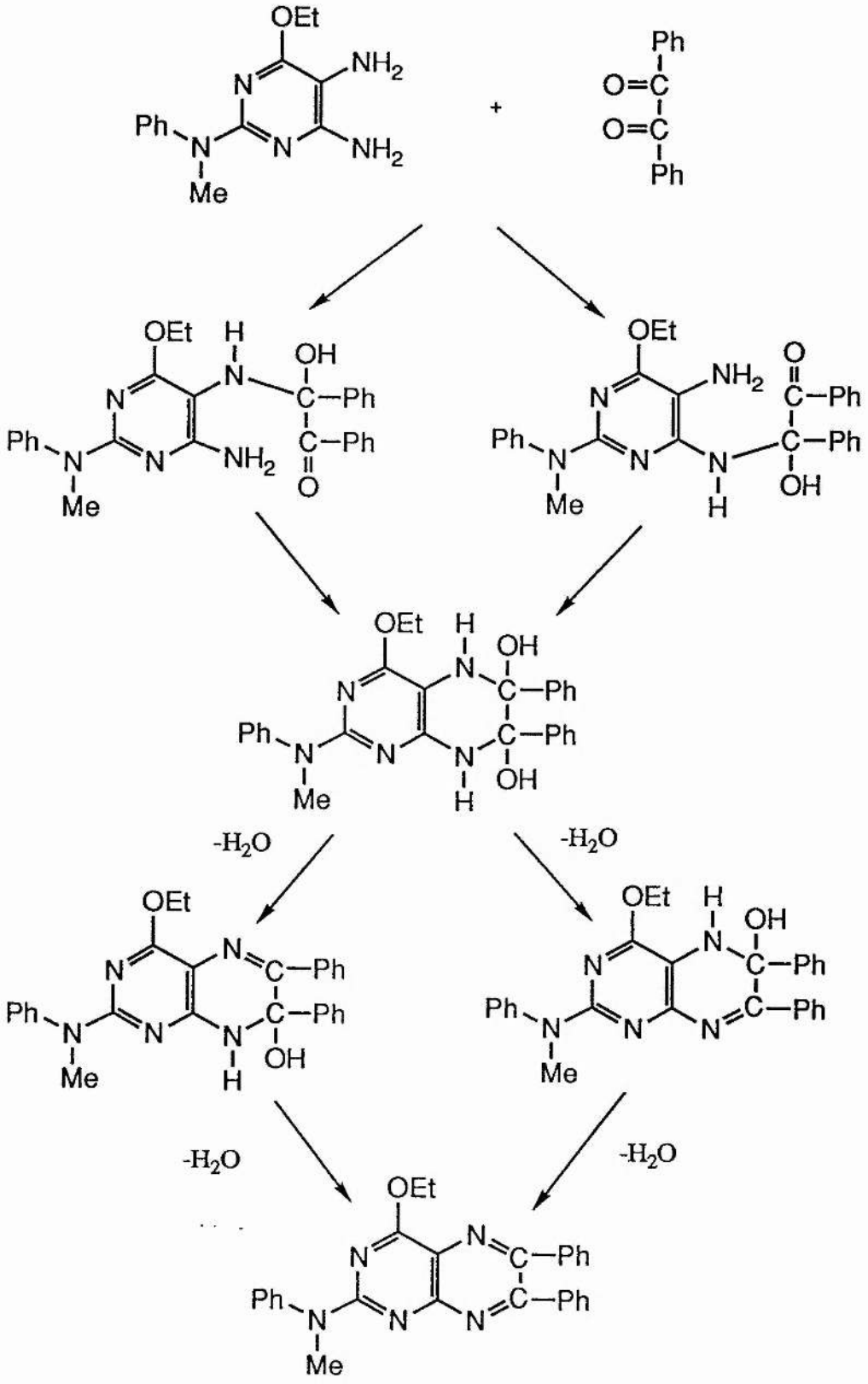

Scheme 9. Mechanism for reaction of benzil with 6-methoxy-2,4,5-triaminopyrimidine.

4.4 REFERENCES

1. P.M. Jordan and J.S. Seehra, *FEBS Lett.*, 1980, **114**, 283.
2. D.L. Nandi and D. Shemin, *J. Biol. Chem.*, 1968, **243**, 1236.
3. G. Burton, P.E. Fagerness, S. Hosozawa, P.M. Jordan and A.I. Scott, *J. Chem. Soc. Chem. Commun.*, 1979, 202.
4. P.M. Jordan, G. Burton, H. Hordlove, M.M. Schneider, L. Pryde and A.I. Scott, *J. Chem. Soc. Chem. Commun.*, 1979, 204.
5. E.K. Jaffe and G.D. Markham, *Biochemistry*, 1987, **26**, 4258.
6. E.K. Jaffe and G.D. Markham, *Biochemistry*, 1988, **27**, 4475.
7. L. Pichat and M. Herbert, *Bull. Soc. Chim. Fr.*, 1957, 673.
8. P.H. Boyle and R.J. Lockhart, *J. Org. Chem.*, 1985, **50**, 5127.
9. C.J. Broan and A.R. Butler, *J. Chem. Soc. Perkin Trans. II*, 1989, 731.
10. C.J. Broan, Ph.D. Thesis, St. Andrews, 1988.

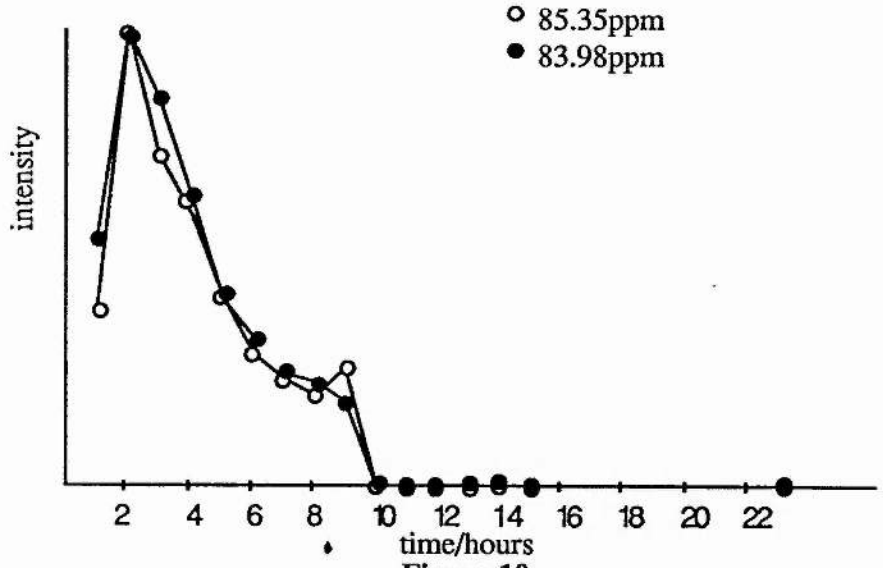

Figure 10.

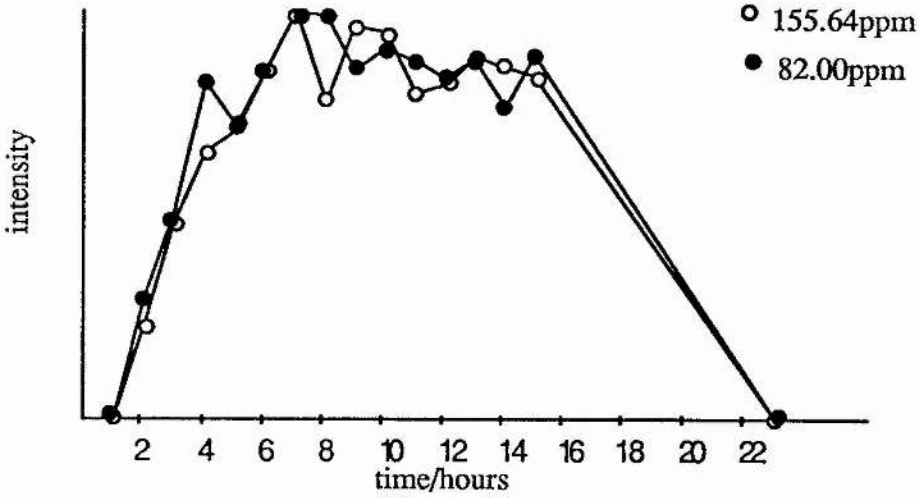

Figure 11.

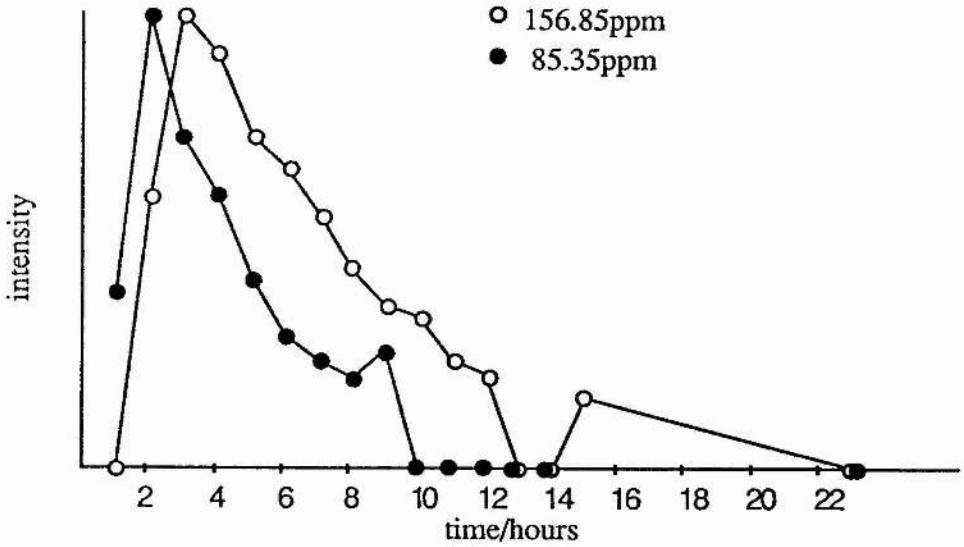

Figure 12.

Chapter 5

NMR Study of the Structure and Conformation of Bilirubin

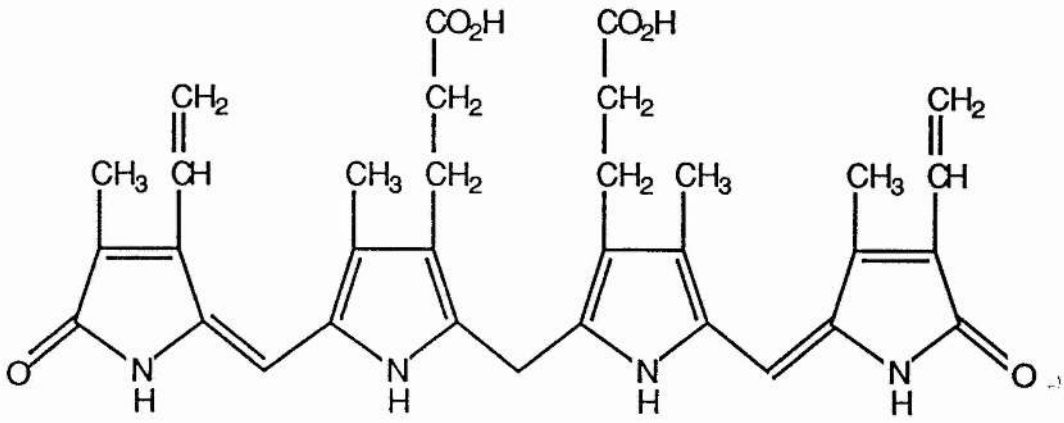

Figure 1. Structure of bilirubin.

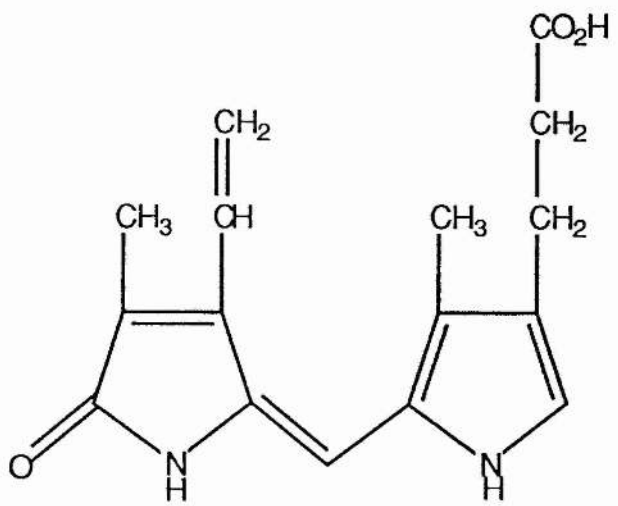

Figure 2. [3-vinyl]neoxanthobilirubinic acid

5.1 INTRODUCTION

Bilirubin is an important biological molecule formed mainly by the catabolic degradation of haem[1]. The build up of serum bilirubin as a result of metabolic disorder leads to the development of jaundice, a condition particularly prevalent in newborn babies[2]. The need to understand the role of bilirubin in neonatal jaundice has prompted investigations into its structure by a variety of techniques[3,4]. The structure of bilirubin (Figure 1) has been known for many years but its stereochemical and tautomeric conformations in the crystalline state and in solution were in doubt. A large number of ^{1}H and ^{13}C nmr studies have been undertaken to investigate the behaviour of the molecule in solution[5]. Initially the low solubility of bilirubin in most solvents limited its study by continuous wave nmr to routine measurements of ^{1}H spectra. These spectra, combined with proton exchange experiments, helped to establish that in solution bilirubin exists predominantly in the bis-lactam form (Figure 1)[6,7]. A variable temperature ^{1}H nmr study provided evidence that a dynamic equilibrium exists in solution between two conformers of bilirubin[8]. The development of high-field Fourier transform spectrometers expanded the range of useful solvents for nmr studies of bilirubin. More detailed assignments of the structure could now be accomplished by the use of ^{1}H nmr techniques such as nuclear Overhauser enhancements[9] and by ^{13}C nmr. The majority of studies, however, still relied on comparison of bilirubin spectra with those of model compounds such as bilirubin mono- and dimethylesters[10,11] and mono- and bisdimethylamides[12]. The ^{13}C nmr studies undertaken also used a number of model compounds, notably [3-vinyl]neoxanthobilirubinic acid[13,14] and bilirubin dimethyl ester[15-17] to assign the majority of carbon atoms in bilirubin itself. Hansen et al[19] used ^{13}C nmr to determine acidity constants for bilirubin. The quaternary ring carbons of related bile pigments were assigned by Wray et al [20] using ^{13}C enriched compounds. These assignments were then used to assign more complex porphyrin

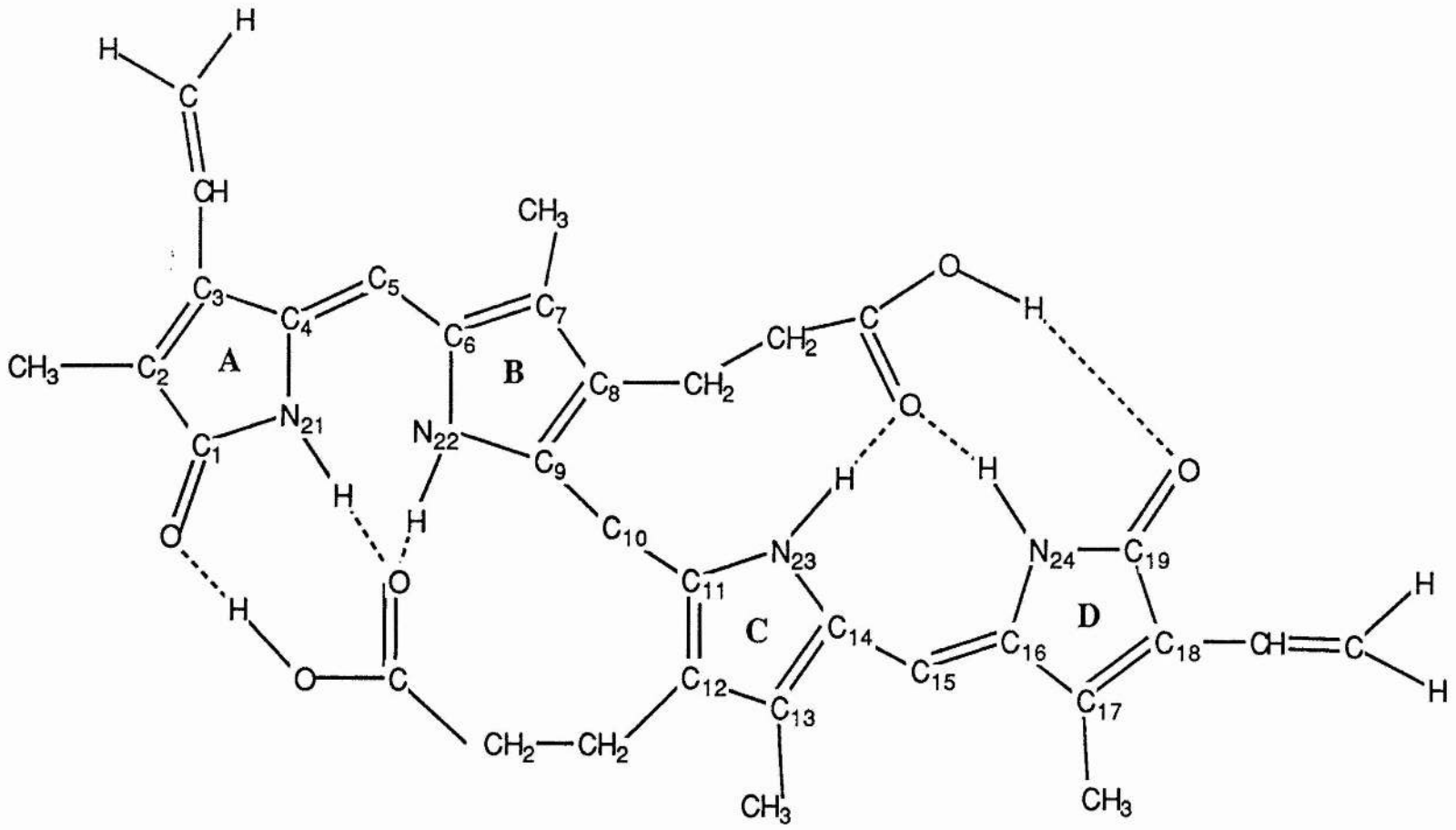

Figure 3. Conformation of bilirubin from crystal structure.

related molecules including bilirubin dimethyl ester.

The crystallographic structure solved by Bonnett et al (1976)[21,22] established that the solid state conformation of bilirubin is that shown in Figure 3. This structure confirms the bis-lactam form previously postulated by Kuenzle et al.[6] and the predominant isomeric form is shown to be that with Z-configuration at C4-5 and C14-15. The X-ray data also demonstrated that crystalline bilirubin has a bent or 'ridge-tile' structure in which each propionic acid side chain is hydrogen bonded to the pyrrolic and lactam sites in the opposite half of the molecule. Because of the very low solubility of bilirubin, however, the majority of nmr spectra in this investigation were run in d_6-dimethylsulphoxide (d_6-DMSO) in which most of these intramolecular hydrogen bonds will be destroyed. A variety of nmr techniques were employed in order to obtain a full and unambiguous assignment of bilirubin in d_6-DMSO without reference to other molecules.

5.2 ^{1}H NMR SPECTROSCOPY

The ^{1}H nmr spectrum of bilirubin in d_6-DMSO is shown in Figure 4 and the initial assignments in Table 1. The four methyl groups can be clearly seen but at this stage cannot be specifically assigned. The signal at 4.00ppm arise from the two protons on the central methylene bridge (C10). The vinyl proton resonances give rise to complex splitting patterns of doublets in the region 5-7ppm as is expected from the different environments of these groups observed in the crystal structure (Figure 3). Distinguishing between the individual vinyl groups is difficult because the sets of doublets overlap. The four signals between 9.5 and 10.5ppm are assigned to the NH groups. These are clearly two pairs and distinguish the lactam NH's (N21 and N24) from the pyrrole NH's (N22 and N23). Due to fast exchange with H_2O present in the solvent, the COOH signals (expected around 12ppm) are flattened.

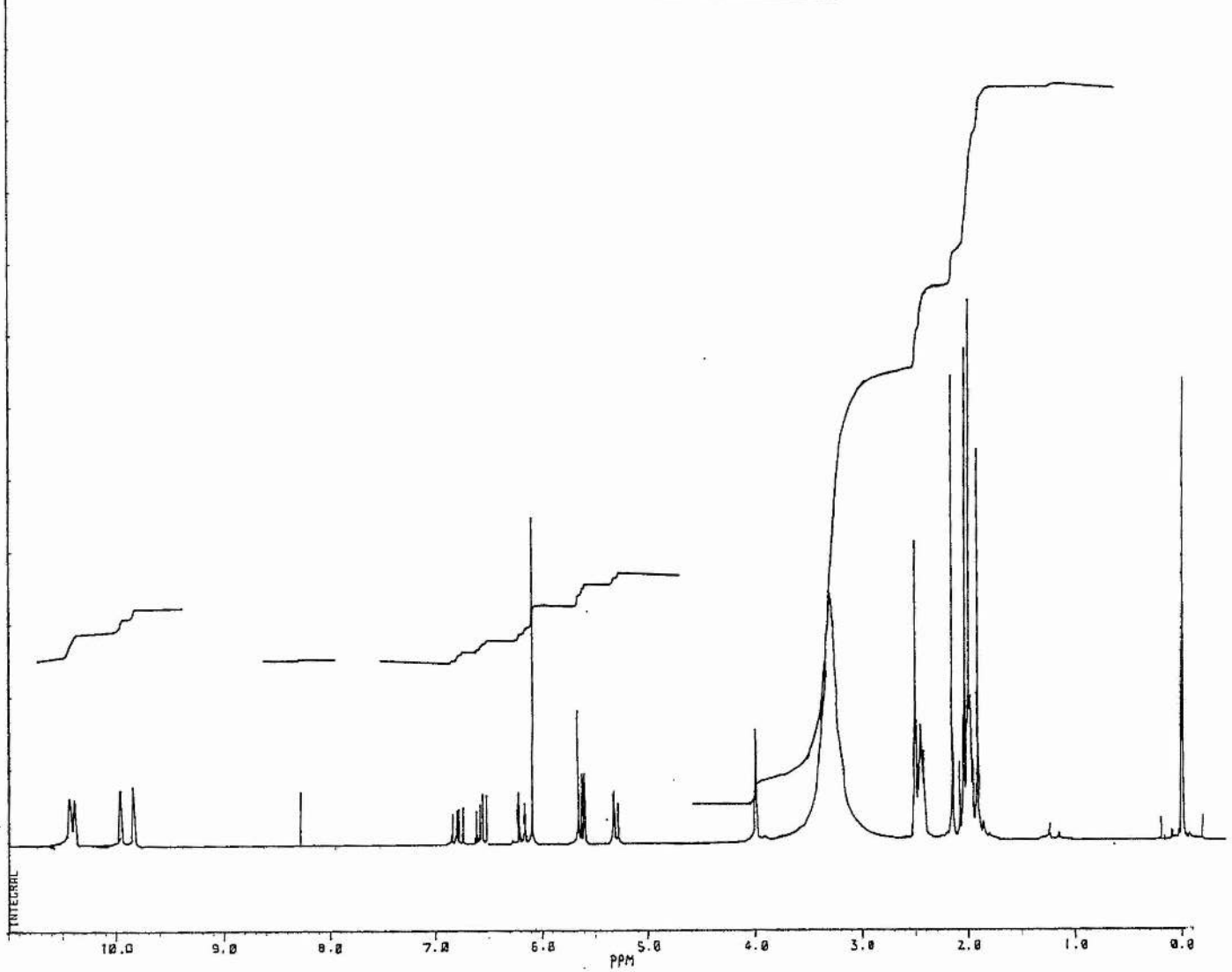

Figure 4.
^{1}H nmr spectrum.

Table 1.
^1H nmr assignments.

Chemical shift (in ppm)	**intensity**		**assignment**	
1.95	9	Singlet	CH_3	methyl
2.00	approx.30	Triplet	CH_2	CH_2CH_2 CO_2H
2.02		Singlet	CH_3	methyl
2.05		Singlet	CH_3	methyl
2.20	9	Singlet	CH_3	methyl
2.48	10	Triplet	CH_2	CH_2 CH_2CO_2H
4.00	6	Singlet	CH_2	methylene bridge(C10)
5.31	3	Doublet of doublets	CH	vinyl
5.63	6	Multiplet	CH_2	vinyl
6.10	6	Singlet	CH	unsat. bridges (C5, C15)
6.20	3	Multiplet	CH	vinyl
6.59	3	Doublet of doublets	CH	vinyl
6.80	3	Doublet of doublets	CH	vinyl
9.85	3	Singlet	NH	
9.98	3	Singlet	NH	
10.40	3	Singlet	NH	
10.55	3	Singlet	NH	

5.3 ^{13}C NMR SPECTROSCOPY

The ^{13}C nmr spectrum of bilirubin (Figure 5) contains 31 signals of which 15 occur in the region of unsaturated carbon-carbon double bonds (120 to 140ppm). The assignments are shown in Table 2. Not many of these signals can be positively identified from the straight ^{13}C spectrum therefore a DEPT (Distortionless Enhancement by Polarisation Transfer) spectrum was run in order to clarify the situation. This type of spectrum has not previously been reported for bilirubin. The DEPT pulse sequence produces a spectrum in which the CH_2 signals are inverted and the quaternary carbon signals disappear. The CH and CH_3 signals appear as normal but are generally easily distinguished because they appear in different regions of the spectrum. The DEPT spectrum of bilirubin identified the signals at 9.29, 9.41 and 9.52ppm as CH_3's, those at 19.45, 23.79, 34.48, 117.37 and 122.18ppm as CH_2's and those at 99.43, 100.20, 127.17 and 127.48ppm as CH's. The remaining signals which do not appear in the DEPT spectrum correspond to the quaternary carbons of the pyrrole rings. The ^{13}C assignments obtained from the DEPT experiment are also indicated in Table 2. From their chemical shifts the peaks at 127.48 and 127.17ppm are identified as the vinyl CH's and the peaks at 100.20 and 99.43ppm are assigned to the bridging carbons C5 and C15. Similarly the CH_2's at 117.37 and 122.18ppm are part of the vinyl groups. The remaining CH_2's could not, from these spectra, be confidently assigned as bridging (C10) or propionic (attached to C8 or C12).

5.4 ^{1}H-^{1}H CORRELATION SPECTROSCOPY

In order to assign fully the ^{1}H spectrum and, in particular, to resolve the complex vinyl splitting pattern, a homonuclear two-dimensional COrrelation SpectroscopY (COSY) experiment was carried out. This technique is the most

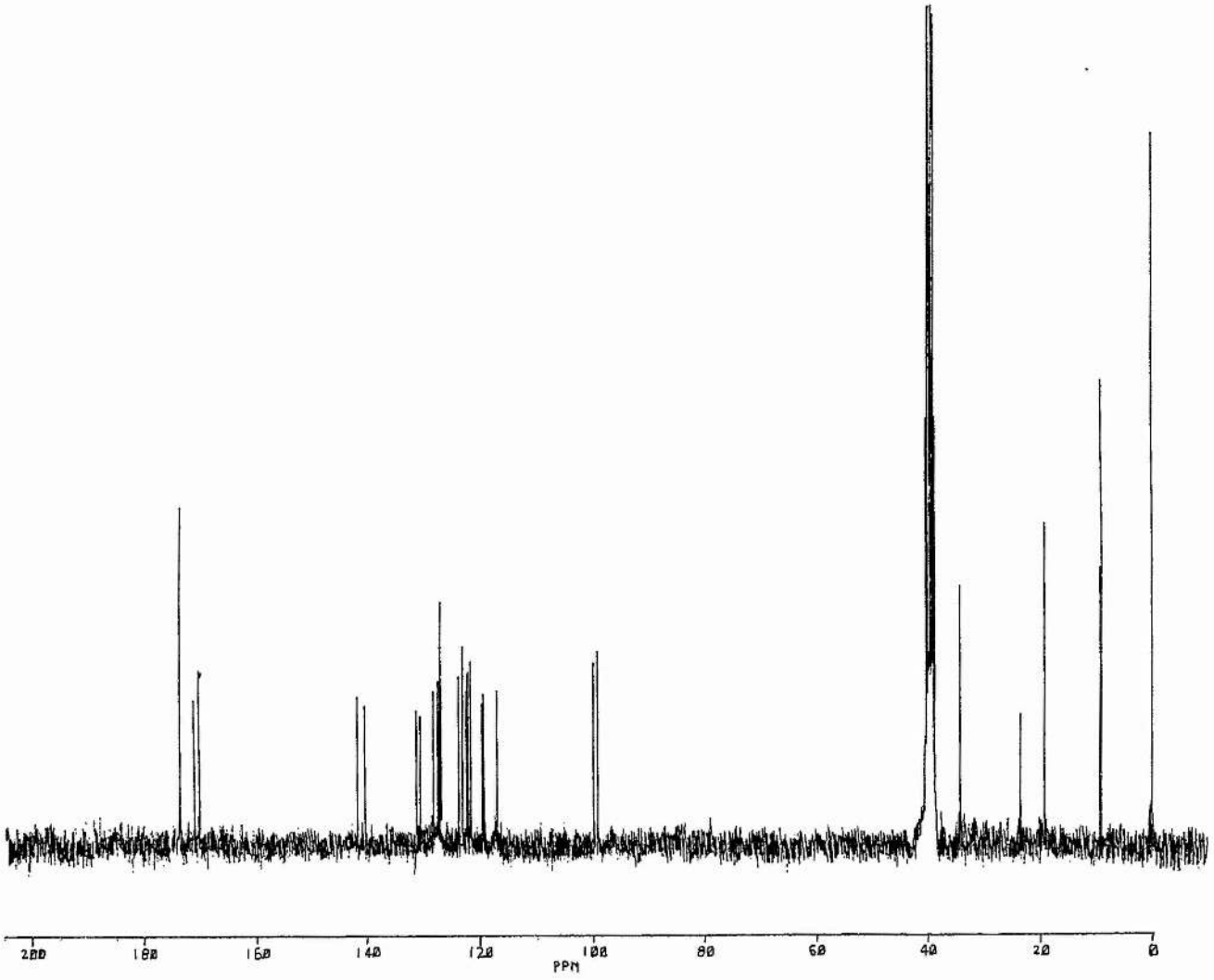

Figure 5.
^{13}C nmr spectrum.

Table 2.
^{13}C nmr assignments.

Chemical shift (in ppm)	intensity	assignment	DEPT intensity	assignment
173.85	8.970	COOH		
171.29	4.004	carbonyl		
170.36	4.551	carbonyl		
141.83	4.055	unsaturated		
140.45	3.804	carbons		
131.35	3.440			
131.24	2.285			
130.70	2.138			
130.60	3.323			
128.37	3.968			
127.58	4.271			
127.32	6.705		5.134	CH vinyl C3 or C18
126.99	6.140		4.900	CH vinyl C3 or C18
123.96	4.454			
123.32	4.688			
123.28	5.220			
122.52	4.162			
122.34	4.777			
122.16	4.695			
121.88	4.824		-3.347	CH_2 vinyl C3 or C18
119.81	3.858			
119.59	3.799			
117.12	4.057		-2.621	CH_2 vinyl C3 or C18
99.94	4.721		4.246	CH C5 or C15
99.15	5.040		4.482	CH C5 or C15
34.29	6.883	CH_2	-5.253	CH_2
23.60	3.347	CH_2	-2.844	CH_2
19.25	8.508	CH_2	-6.811	CH_2
9.32	7.245	CH_3	4.898	CH_3
9.20	6.810	CH_3	5.699	CH_3
9.09	12.227	CH_3	10.003	CH_3

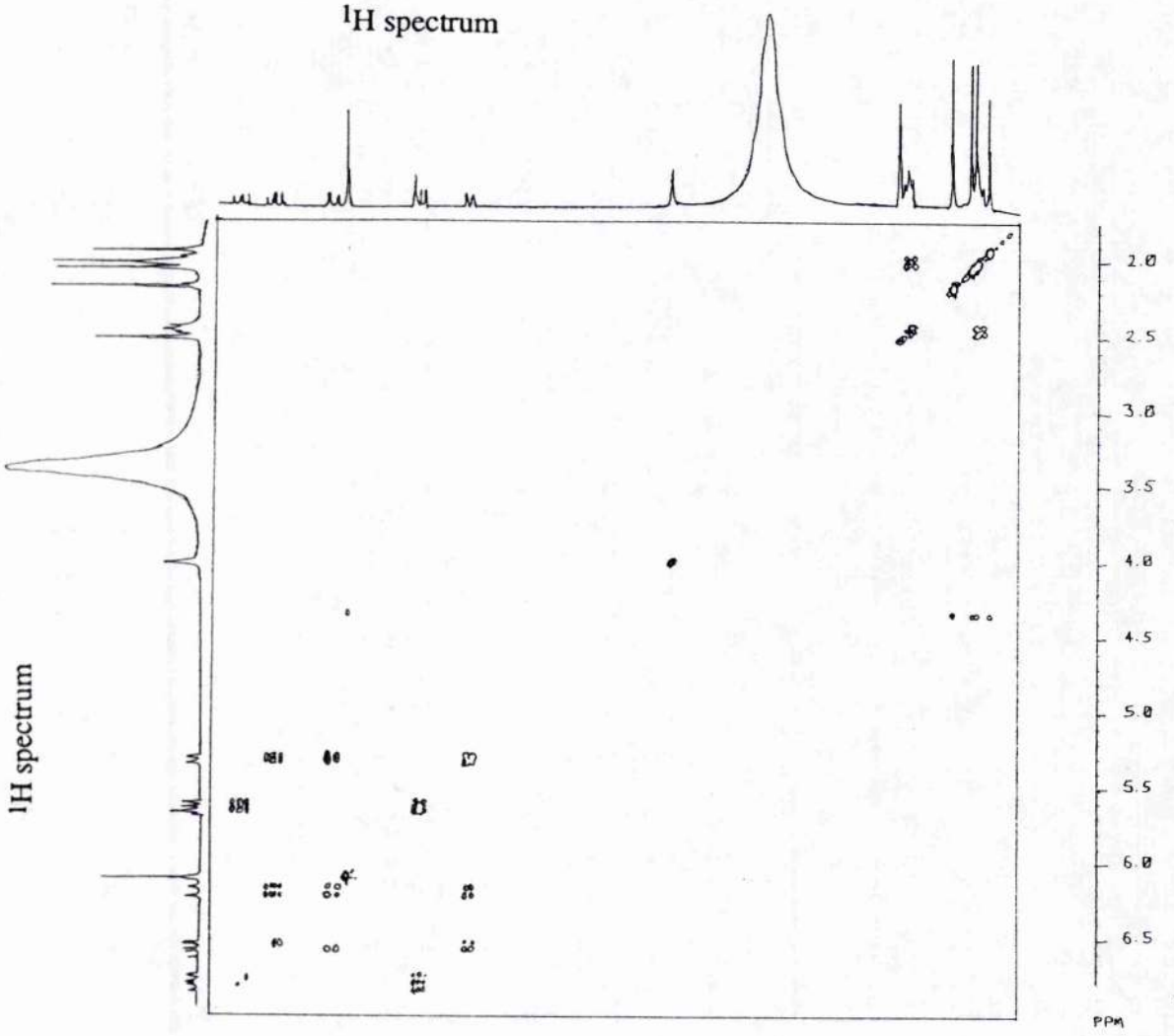

Figure 6.
^{1}H-^{1}H correlation spectrum.

commonly and easily used of the two dimensional experiments and establishes the connectivities between the various protons in a molecule. The COSY plot consists of a data matrix in which both axes carry the ^1H nmr spectrum. Each proton appears in its appropriate position on the diagonal such that a cross-section taken along the diagonal would correspond to the ^1H nmr spectrum. The off-diagonal (cross) peaks are caused by spin-spin coupling between two protons. To identify the chemical shifts of two protons, a horizontal and a vertical line are drawn through a cross-peak. The intersections of the horizontal and vertical lines with the x- and y-axes identify the chemical shifts of the coupling protons. The full ^1H-^1H COSY spectrum of bilirubin is shown in Figure 6. Off-diagonal peaks can be seen in the region between 2 and 2.5ppm arising from coupling of the two CH_2 groups on the propionic acid side chains attached to C8 and C12. The region of 5-7ppm also contains off-diagonal peaks resulting from the coupling of the vinyl protons. Figure 7 shows an expansion of this area of the COSY spectrum. The couplings between protons at 6.19ppm and those at 5.32 and 6.57ppm are indicated on the spectrum. The remaining vinyl protons couple to each other. The relationship between these two sets of vinyl protons is shown in Table 3. From the crystal structure of bilirubin (Figure 3) it can be deduced that the vinyl system containing three ABX protons in very different environments is likely to be that attached to C18. The CH_2 of this group is adjacent to a methyl group on one side and a lactam hydrogen bonding system on the other. Thus each H in the CH_2 group is situated in a different environment. The CH_2 vinyl group attached to C3 is situated between the two methyl groups on C2 and C7 and therefore both H's are in similar environments.

5.5 ^{13}C-^1H CORRELATION SPECTROSCOPY

This is a similar experiment to the homonuclear correlation described above except that ^1H-^{13}C couplings are involved instead of ^1H-^1H couplings. The

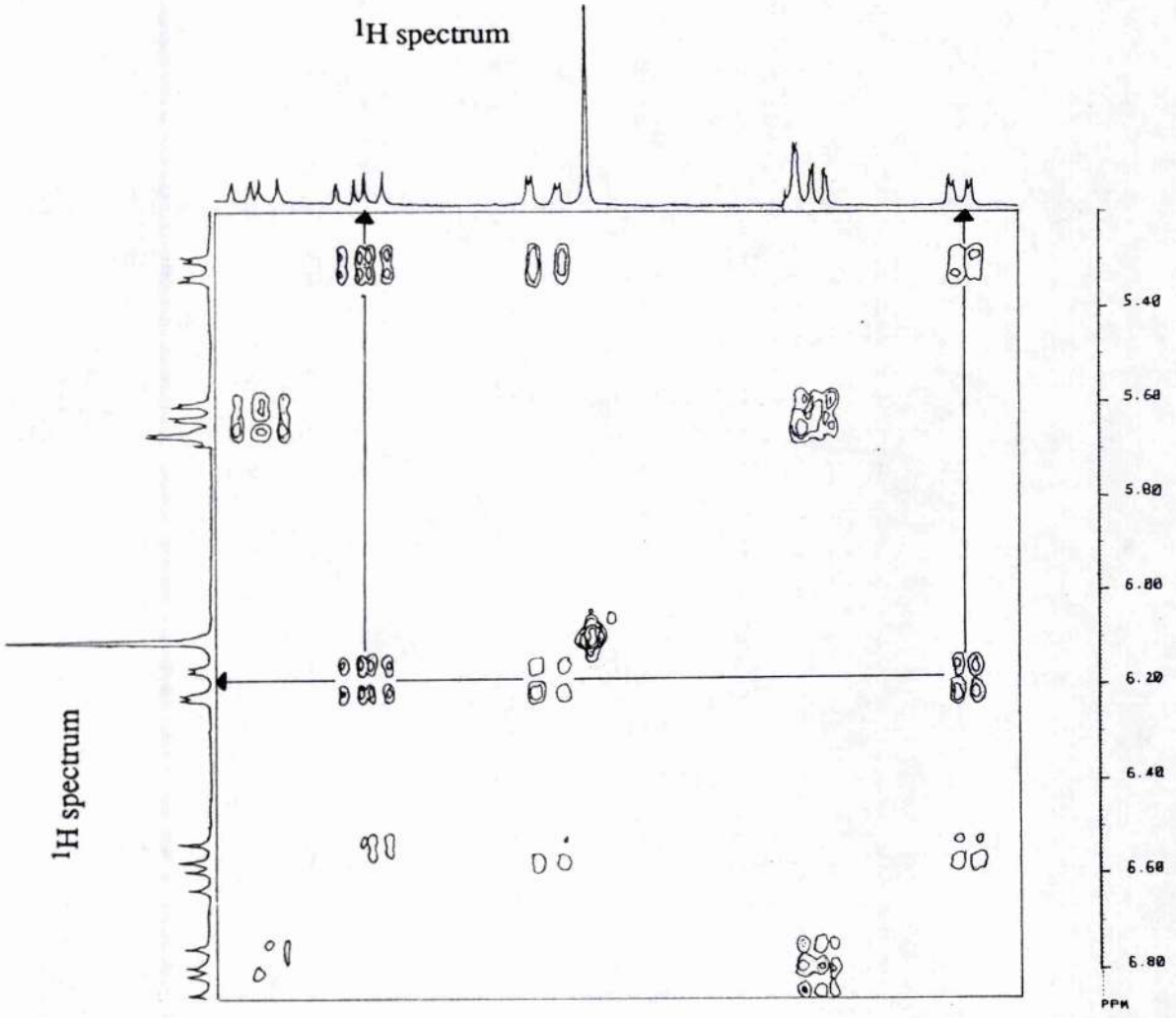

Figure 7.
Expansion of ^{1}H-^{1}H correlation spectrum.

Table 3.
^{1}H-^{1}H Correlations.

Chemical shift (in ppm)			**previous assignment**		**observed correlations**
2.00	Triplet	CH_2	2.48	T	$CH_2CH_2CO_2H$
2.48	Triplet	CH_2	2.00	T	$CH_2CH_2CO_2H$
5.31	Doublet of doublets	CH	6.20 6.59	DofD DofD	CH vinyl 18 CH vinyl
5.63	Multiplet	CH	6.80	DofD	CH vinyl 3
6.20	Multiplet	CH	5.31 6.59	DofD DofD	CH vinyl 18 CH vinyl
6.59	DofD	CH	6.20 5.31	DofD DofD	CH vinyl 18 CH vinyl
6.80	DofD	CH	5.61	DofD	CH vinyl 3

DofD = Doublet of doublets

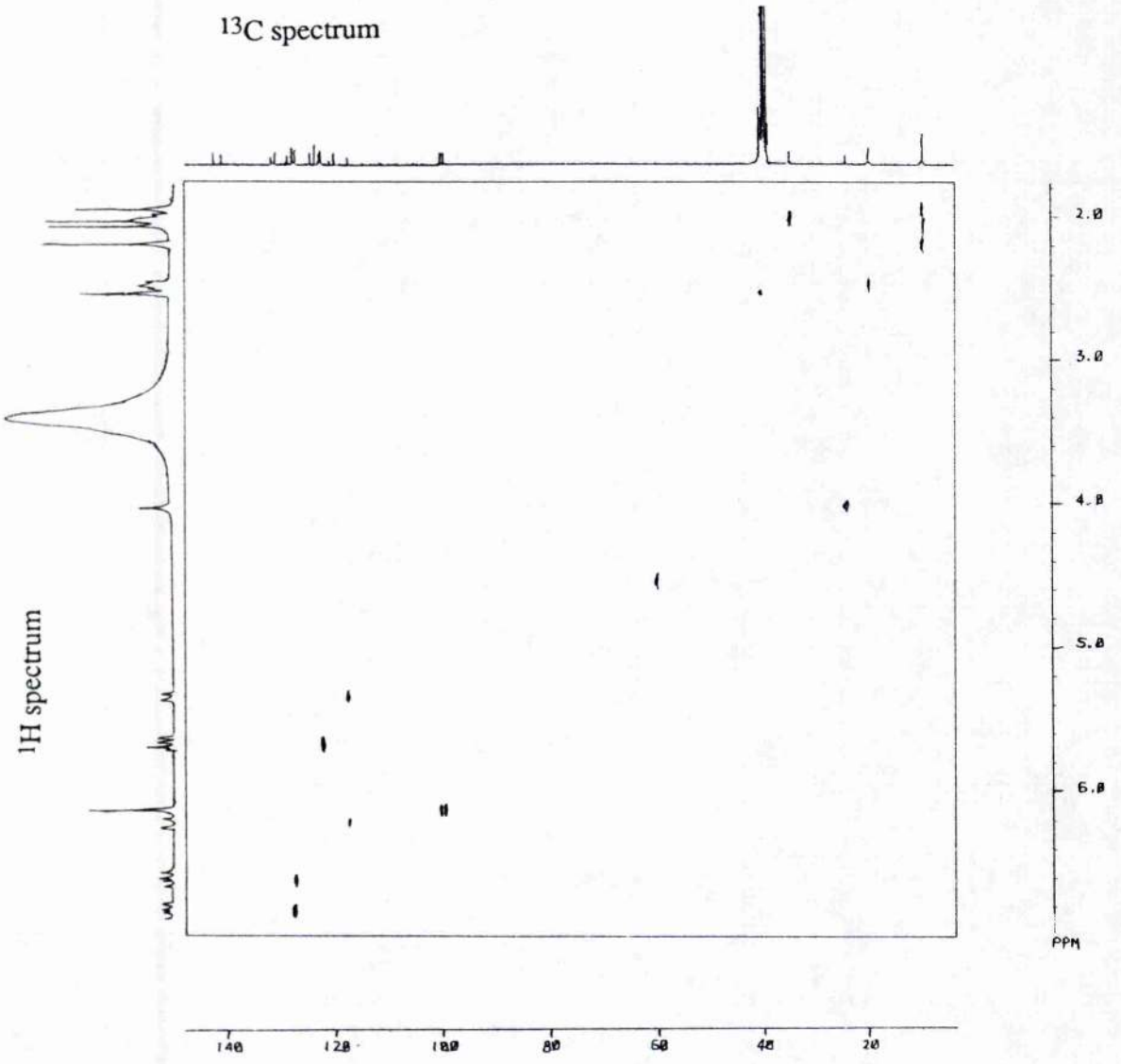

Figure 8.
^{13}C-^{1}H correlation spectrum.

experiment shows directly which protons are attached to which carbons. The full contour plot for bilirubin is shown in Figure 8. The x-axis contains ^{13}C chemical shifts and the y-axis contains ^{1}H chemical shifts. By drawing horizontal and vertical lines through the peaks on the contour plot and tracing them back to the ^{1}H and ^{13}C chemical shifts, it is possible to assign all the carbon atoms which have directly bonded protons and identify to which protons the carbons are coupled. Thus, from the expansion in Figure 9, it can be clearly seen that the vinyl protons at 5.64ppm are bonded to the carbon at 121.88ppm and those at 6.78ppm are bonded to the carbon at 127.32ppm. It is known from the ^{1}H-^{1}H correlation that these two groups of proton signals belong to the same vinyl system so by identifying the carbons bonded to these protons, the vinyl system is fully assigned as being the one attached to C3. The other vinyl group attached to C18 is assigned similarly (Table 4). The protons attached to each methyl group can also be identified although the position of attachment of the methyl group to the tetrapyrrole backbone is still not clear. Correlations between the carbons and protons of the propionic acid side chains are also observed in the region between 1.5 and 2.5ppm. The side chains have now been assigned and the next step is to build up a structure for the rest of the molecule by establishing the positions of the side chains on the tetrapyrrole backbone.

5.6 NOE DIFFERENCE SPECTRA

One important application of the Nuclear Overhauser Effect (NOE) is in ^{13}C spectroscopy where the ^{13}C signal of a carbon coupled to a proton is enhanced. This effect is caused by the decoupling of the protons creating a distortion in the energy levels of the carbon, resulting in an increase in the probability of upwards transitions for the ^{13}C nucleii and therefore a more intense signal is observed than would be found if there was no decoupling. There are two principles of ^{1}H-^{1}H NOE which enable it to be a useful technique in structural analysis. Firstly it arises only during

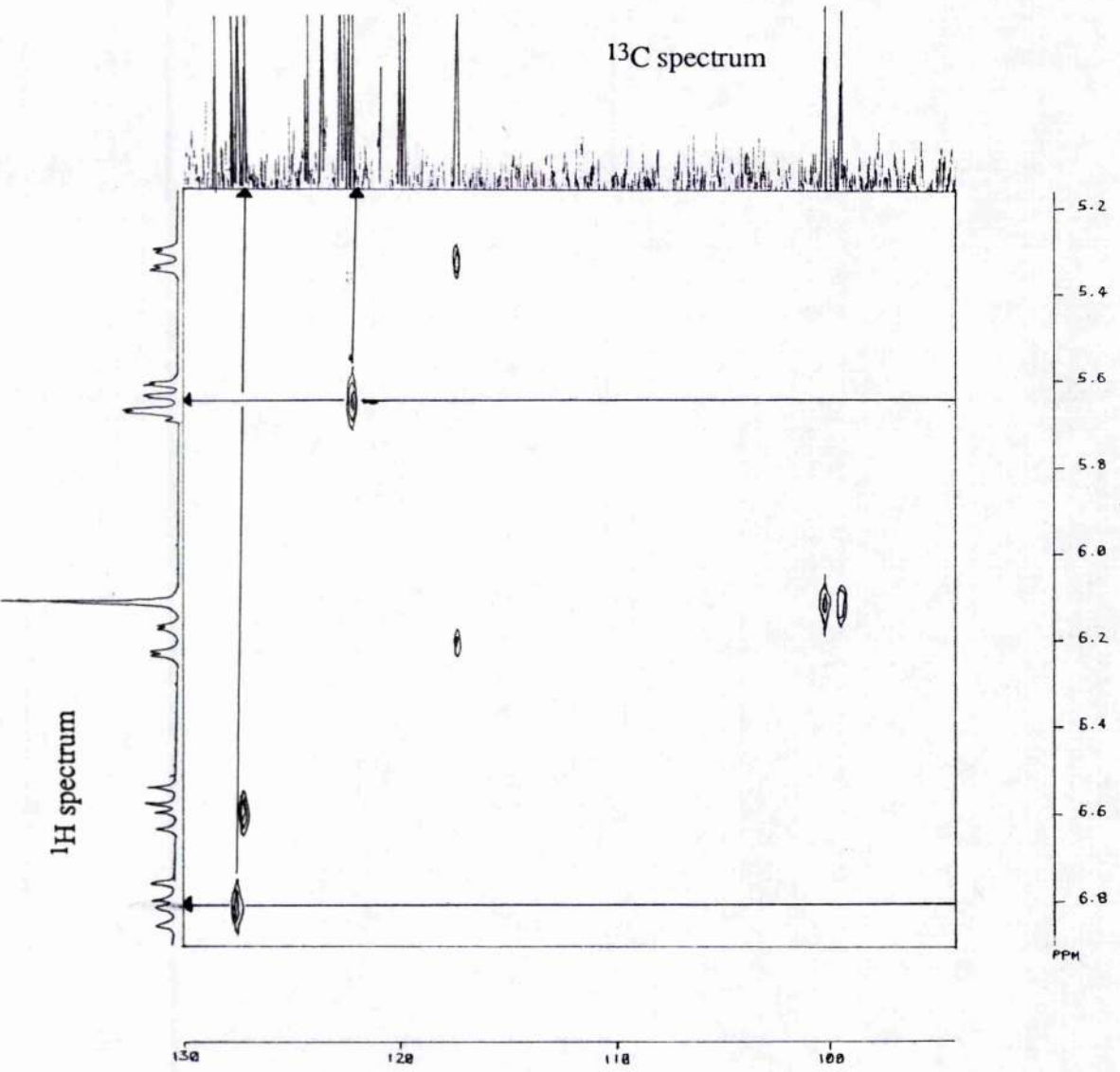

Figure 9.
Expansion of ^{13}C-^{1}H correlation spectrum.

Table 4.
^{13}C-^{1}H Correlations.

^{13}C Chemical shift	Correlation to ^{1}H			
9.09	2.02	S		
	2.05	S		
9.20	2.20	S		
9.32	1.95	S		
19.25	2.48	T	$CH_2CH_2\mathit{CH_2}CO_2H$	
34.29	2.00	T	$CH_2\mathit{CH_2}CH_2CO_2H$	
23.60	4.00	S	CH_2	C10
99.15	6.10	S	CH	C5 or C15
99.94	6.10	S	CH	C5 or C15
117.12	5.31	DofD	CH_2	C18
	6.20	DofD	CH_2	C18
121.88	5.63	DofD	CH_2	C3
127.00	6.59	DofD	CH	C18
127.32	6.80	DofD	CH	C3

Table 5.
Observed NOE of ^1H resonances.

Irradiation point	assignment	(%)	enhanced signals	
1.95	methyl		5.61	CH_2 vinyl C3
			5.66	
			6.80	CH vinyl C3
2.02	methyl		6.10	CH C5 or C15
			4.00	CH_2 C10
2.05	methyl		6.10	CH C5 or C15
			4.00	CH_2 C10
2.20	methyl		6.59	CH vinyl C18
			6.10	CH C5 or C1
6.09	CH (C5,C15)	(-6)	6.59	CH vinyl C18
		(-2.5)	2.20	methyl
		(-1.5)	2.02	methyl
		(-1.5)	2.05	methyl
9.85	NH	(-3)	10.55	NH
		(-1)	4.00	CH_2 C10
9.98	NH	(-2)	10.40	NH
10.40	NH	(-2)	9.98	NH
10.55	NH	(-3)	9.85	NH

the double irradiation of one nucleus and affects another nucleus which must be close spatially but is not neccesarily coupling with the irradiated nucleus. Secondly, it is associated with dipolar relaxation mechanisms.

Initial NOE experiments were carried out on d_6-DMSO solutions of bilirubin. The observed enhancements are shown in Table 5. In d_6-DMSO the enhancements are negative due to slow molecular motion. Irradiation at 1.95ppm (methyl resonance) produced an enhancement of the vinyl resonances assigned already to C3. The proton resonances assigned to the other vinyl system on C18 were enhanced by irradiation at 2.20ppm (methyl resonance). These observed enhancements identify the peak at 1.95ppm as the methyl on ring A and the peak at 2.20ppm as the methyl on ring D. Further experiments on d_6-DMSO solutions of bilirubin were recorded by the high-field nmr service at the University of Edinburgh. No enhancements were observed on irradiation of the vinyl proton resonances. The pattern of enhancements of the NH signals identify two pairs corresponding to the lactam and pyrrolic forms. The bridging protons on C5, C10 and C15 were all enhanced by irradiation at the methyl resonances on the middle rings, B and C (2.02 and 2.05ppm).

5.7 LONG RANGE COUPLING CORRELATION

The proton nmr spectrum has now been fully assigned apart from the coincident bridging CH's (C5 and C15), two methyl resonances (C7 and C13) and the four NH's. The carbon spectrum, however, still requires assignment of the quaternary carbons of the pyrrole rings. The assignment of such carbons is more complex because there are no directly bonded hydrogens available to give additional information. A more complex two-dimensional experiment, the COLOC (COrrelation via LOng range Coupling) pulse sequence optimised to J approximately 10Hz, was used to identify carbons by means of correlation with

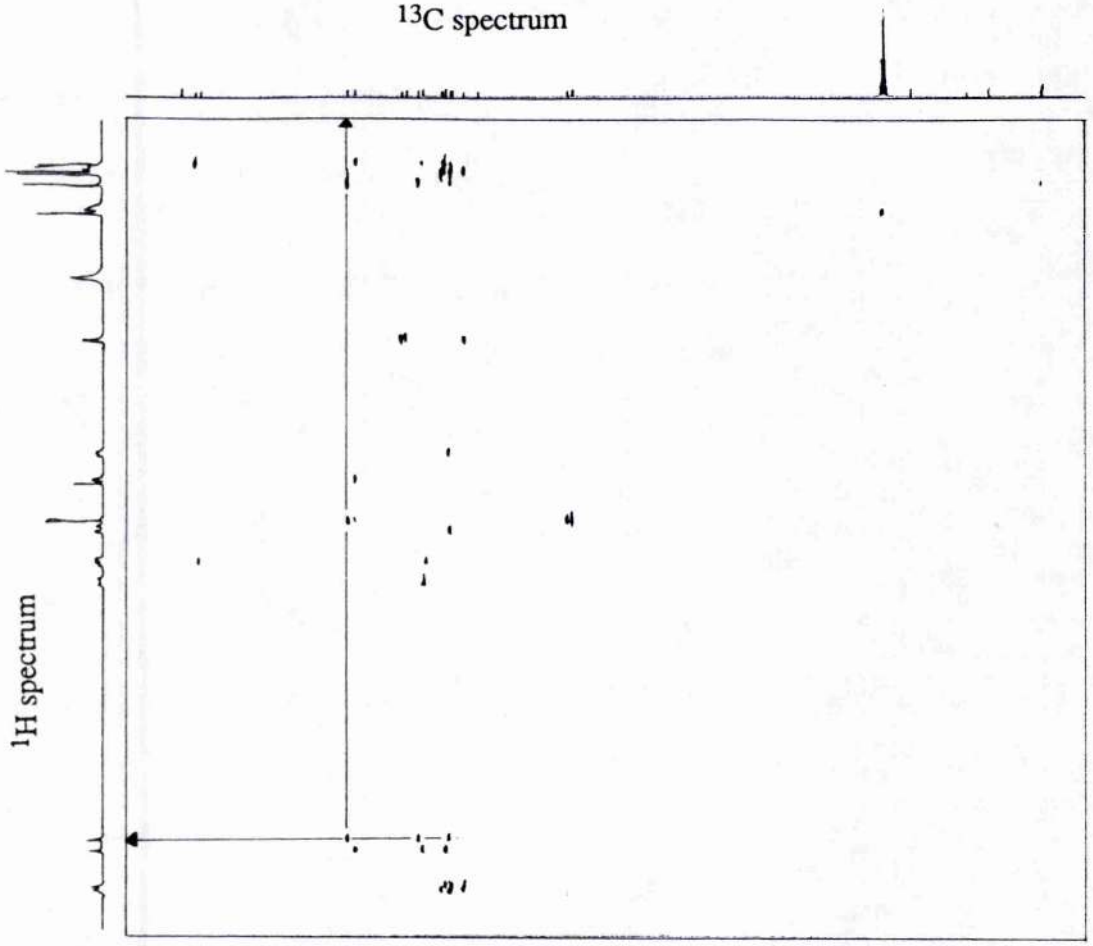

Figure 10.
Full COLOC spectrum.

protons at a distance of more than one bond. The contour plot obtained from the COLOC experiment on bilirubin is shown in Figure 10. The signals arise from couplings between carbons and protons separated by more than one bond and intensities vary with the distance and angles of separation. Coupling constant effects noted for systems examined in previous studies were used to help in the assignments[23,24].

Each of the four NH groups couples with different quaternary carbons. This gives rise to the four sets of correlations observed in the region 9.5 to 11ppm. Taking one of these sets as a starting point, the chemical shift of each of the correlated carbons is found by drawing horizontal and vertical lines through the signals as illustrated in Figure 10. The carbon chemical shifts are read off the ^{13}C spectrum along the top of the plot. These carbons are also themselves correlated to other protons on the side chains attached to the pyrrole ring. The chemical shifts of these protons can, in turn, be read off the ^{1}H spectrum along the side of the plot. Analysing all the correlations allows each set of ring carbons to be assigned as shown in Table 6. An expansion of the full contour plot is shown in Figure 11 with some of the assignments illustrated. A detailed description of the assignment of quaternary carbons in ring A from the COLOC spectra is given now. The proton chemical shift of the NH at 9.98ppm correlates to three carbon signals at 140.5, 127.6 and 123.3ppm. The carbons resonating at these chemical shifts are therefore in the same ring as the NH resonating at 9.98ppm. The peak at 140.5ppm correlates with protons at 5.61 and 6.80ppm. From the previous experiments, it has been shown that these are the protons of the vinyl system attached to C3. This correlation indicates that the carbon at 140.5ppm is in the same ring as the vinyl at C3, that is ring A. Similarly the carbons at 127.6 and 123.3ppm must also be in ring A. The carbon at 140.5ppm also correlates to the methyl protons at 1.95ppm. These protons have been shown by ^{1}H-^{1}H NOE to be attached to C2 in ring A confirming that 140.5ppm is the shift of a carbon in this ring. The carbon at 127.6ppm has a very

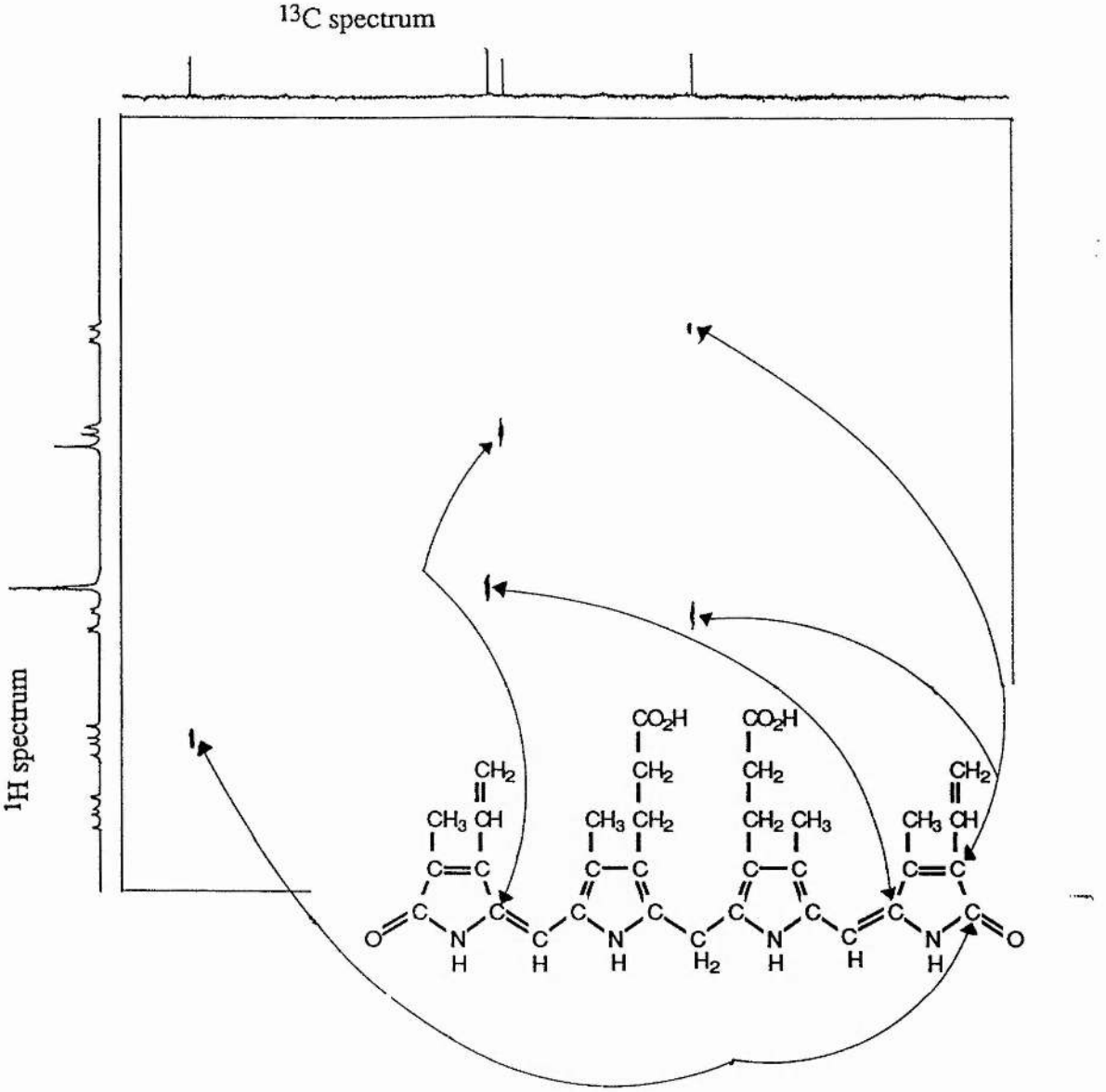

Figure 11.
Expansion of COLOC spectrum.

Table 6.
COLOC assignments.

Ring A

Group	^{1}H Chemical shift
NH	9.98
CH_3	1.95
CH_2 (C3)	5.63

Quaternary Carbon Shifts
123.32
127.58
140.45
171.29

Ring B

Group	^{1}H Chemical shift
NH	10.40

Quaternary Carbon Shifts
119.59
122.16
123.28
130.60

Ring C

Group	^{1}H Chemical Shift
NH	10.55
CH_3	2.20

Quaternary Carbon Shifts
119.81
122.34
123.96
131.35

Ring D

Group	^{1}H Chemical shift
NH	9.85

Quaternary Carbon Shifts
122.52
128.37
141.83
170.36

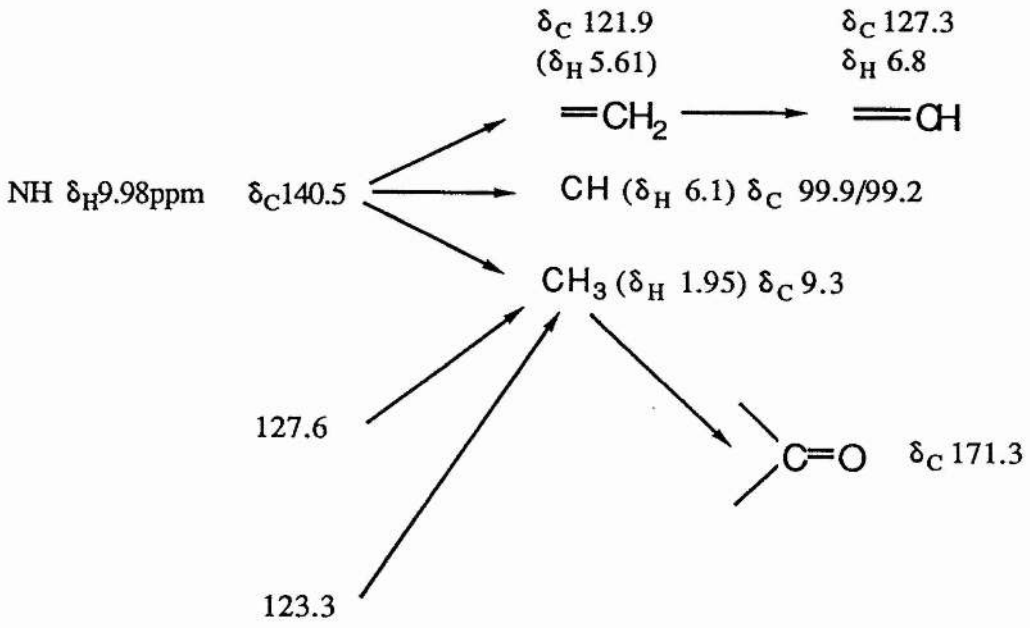

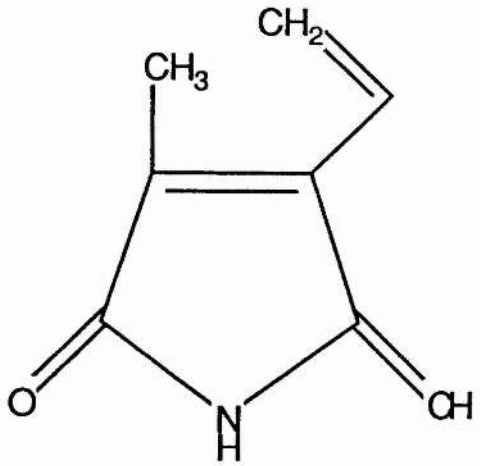

RING A

Figure 12.

weak correlation to the methyl protons at 1.95ppm. A more intense correlation is observed between the methyl protons at 1.95ppm and the carbon resonating at 123.3ppm. Most importantly the methyl protons at 1.95ppm correlate strongly with the carbonyl carbon at 171.3ppm. The four quaternary carbons in ring A therefore are those with chemical shifts of 171.3, 140.5, 127.6 and 123.3ppm. Having established the chemical shifts of the ring A carbons it now remains for the position of each carbon in the ring to be deduced. Obviously the carbonyl carbon C1 has a chemical shift of 171.3ppm but the other three carbons are distinguished by the intensities of their various correlations. On the full COLOC spectrum it can be seen that the methyl protons at 1.95ppm correlate with all four of the ring A carbons with various intensities. After the carbonyl correlation, the strongest correlation occurs between 1.95and 123.3ppm. This suggests that 123.3ppm is the chemical shift of the carbon to which the methyl carbon is directly attached, that is C2. The weakest correlation is observed between 1.95 and 127.6ppm suggesting that this latter carbon signal arises from the carbon C4, the ring carbon furthest from the methyl protons. The remaining carbon signal at 140.5ppm must arise from C3. This agrees well with the strong correlation observed between this carbon and the vinyl protons adjacent to C3 and suggests that correlation intensities are reduced when correlation is observed along a double bond. A diagram illustrating the assignment of ring A is shown in Figure 12. By a very similar process of assigning carbon chemical shifts within the ring system and comparison of correlation intensities, ring D, starting from the proton shift of the NH at 9.85ppm can be fully assigned. It is expected that carbons of similar electron density will resonate at similar chemical shifts. This is clearly demonstrated by the signals at 140.5 and 141.83ppm which both arise from carbons in conjugated systems at similar distances from carbonyls.

Rings B and C are rather more ambiguous than A and D. A set of quaternary carbon shifts for each ring can be ascertained starting from the NH proton chemical shifts of 10.40 and 10.55ppm. The assignment of carbons within each ring

is rather more tentative and based mainly on intensity effects similar to those observed in rings A and D. For example, one of the central rings is found to contain quaternary carbons at 123.3, 122.2, 119.6 and 131.4 or 130.6ppm. Assignments are made by examination of the intensities of the correlations between these carbons and the methyl proton at 2.02. The strongest correlation is observed between 2.02 and 123.3ppm so this latter carbon is deemed to be that adjacent to the methyl carbon. The carbon adjacent ot the unsaturated CH bridge has a double bond between it and the methyl carbon and it is therefore likely to show a weak correlation to this carbon. The weakest correlation to the methyl protons is shown by the carbon at 119.6ppm. The carbons at 131.4/130.6ppm correlate to the protons at 4.00ppm and are assigned to the carbon adjacent to the central methylene bridge. The remaining carbon at 122.2ppm is therefore assigned to the carbon adjacent to the propanoic acid side chain. The other set of quaternary carbon is assigned in a similar manner. It is not possible, however, to determine to which of the central pyrrole rings, B or C, the signals at 131.4 and 130.6ppm belong. Nor is it certain which of the central rings is in position B and which is C. This problem arises mainly because the two unsaturated CH bridges are coincident and there is no way of correlating rings B or C with rings A or D. It is also not possible to see any correlations between ring B and ring C themselves. Nevertheless, a detailed assignment of bilirubin in d_6-DMSO has been acheived without comparison with model compounds.

5.8 EXPERIMENTAL

Samples for nmr were prepared by making a saturated solution of bilirubin in d_6-DMSO or $CDCl_3$. All chemical shifts were referenced to tetramethylsilane (TMS). All the two-dimensional experiments and some of the NOE experiments were run on a Bruker AM-300 spectrometer at 40°C. Other NOE experiments were

Table 7.
Final ^1H nmr assignments.

Chemical shift (in ppm)	assignment	
1.95	CH_3	C2
2.00	CH_2	$CH_2CH_2CO_2H$
2.02	CH_3	C7
2.05	CH_3	C13
2.20	CH_3	C17
2.48	CH_2	$CH_2CH_2CO_2H$
4.00	CH_2	(C10)
5.30 5.32	CH	H_A C18
5.60 5.62	CH	H_A C3
5.66	CH	H_B C3
6.10	CH	(C5, C15)
6.18 6.22	CH	H_B C18
6.59	CH	H_X C18
6.80	CH	H_X C3
9.85	NH	N24
9.98	NH	N21
10.40	NH	N22
10.55	NH	N23

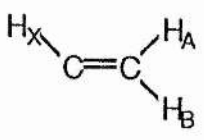

Table 8.
Final ^{13}C assignments.

Carbon	Chemical shift/ppm
1	171.29
2	123.32
3	140.45
4	127.58
5	99.15
6	122.16
7	119.59
8	123.28
9	130.60
10	23.60
11	131.35
12	123.96
13	119.81
14	122.3
15	99.94
16	128.37
17	141.83
18	122.52
19	170.36
2'	9.32
3'	127.32
3"	122.16
7'	9.09
8'	19.25
8"	34.29
8"'	173.85
12'	19.25
12"	34.29
12"'	173.85
13'	9.09
17'	9.20
18'	126.99
18"	117.12

run on a Bruker WH-360 spectrometer at the SERC high field nmr service at the University of Edinburgh.

5.9 REFERENCES

1. R. Schmid and A.F. McDonagh in *'The Porphrins'*, Vol.6, p258, (D. Dolphin, Ed.), 1979, Academic Press.
2. D.A. Lightner and A.F. McDonagh, *Acc. Chem. Res.*, 1984, **17**, 417.
3. A.W. Nichol and D.B. Morell, *Biochim. Biophys. Acta*, 1969, **177**, 599.
4. C.C. Kuenzle, M.H. Weibel, R.R. Pelloni and P. Hemmerich, *Biochem. J.*, 1973, **133**, 364.
5. D. Kaplan and G. Navon, *Isr. J. Chem.*, 1983, **23**, 177.
6. C.C. Kuenzle, *Biochem. J.*, 1970, **119**, 395.
7. D.W. Hutchinson, B. Johnson and A.J. Knell, *Biochem. J.*, 1971, **123**, 483.
8. P. Manitto and D. Monti, *J. Chem. Soc. Chem. Commun.*, 1976, 122.
9. D. Kaplan and G. Navon, *J. Chem. Soc. Perkin Trans. II*, 1981, 1374.
10. D.A. Lightner and J.-S. Ma, *Spectros. Lett.*, 1984, **17**, 317.
11. A.R. Holzwarth, E. Langer, H. Lehner and K. Schaffner, *Photochem. Photobiol.*, 1980, **32**, 17.
12. D.A. Lightner, T.C. Adams and J.-S. Ma, *Tetrahedron*, 1984, **40**, 4253.
13. D. Kaplan and G. Navon, *Org. Magn. Res.*, 1980, **13**, 59.
14. D. Kaplan and G. Navon, *Org. Magn. Res.*, 1981, **17**, 79
15. G. Severini-Ricca, P. Manitto, D. Monti and E.W. Randall, *Gazz. Chim. Ital.*, 1975, **105**, 1273.
16. D. Kaplan, R. Panigel and G. Navon, *Spectros. Lett.*, 1977, **10**, 881.
17. D.Kaplan and G.Navon, *Biochem. J.*, 1982, **201**, 605.
18. D.Kaplan and G.Navon, *Org. Magn. Reson.*, 1980, **14**, 319.
19. P.E. Hansen, H. Thiessen and R. Brodersen, *Acta Chem. Scand.*, 1979, **B33**, 281.
20. V. Wray, A. Gossauer, B. Gruning, G. Reifenstahl and H. Zilch, *J. Chem. Soc. Perkin Trans. II*, 1979, 1558.

21. R. Bonnett, J.E. Davies, M. B. Hursthouse and G.M. Sheldrick, *Proc. R. Soc. London, Ser. B*, 1978, **202**, 249.

22. R.Bonnett, J.E.Davies and M.B.Hursthouse, *Nature*, 1976, **262**, 326.

23. F.W. Wehrli, A.P. Marchand and S. Wehrli, *'Interpretation of ^{13}C nmr Spectra'*, (2nd. Edition), Wiley, England, 1983, Chapter 2, p71.

24. F.J. Weigert and J.D. Roberts, *J. Am. Chem. Soc.*, 1968, **90**, 3543.

Chapter 6

Effect of Binding on the Reactivity of Bilirubin

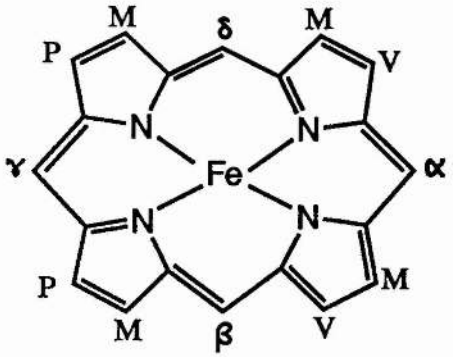

HAEM

heme oxygenase

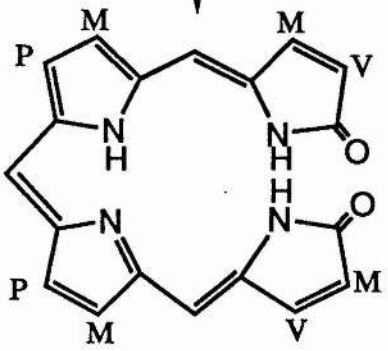

BILIVERDIN

biliverdin reductase

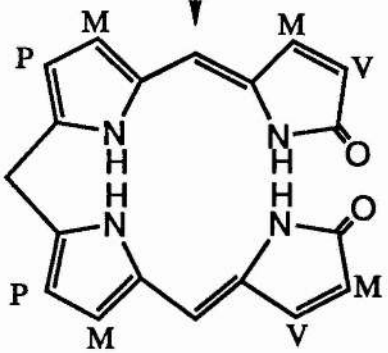

BILIRUBIN

REDUCED BILE PIGMENTS

Scheme 1. Formation of bilirubin

6.1 INTRODUCTION

In mammalian systems all of the bilirubin produced is derived from haem by oxidative cleavage of the α-methene bridge resulting in formation of the immediate tetrapyrrolic precursor of bilirubin, biliverdin; a blue-green pigment[1] (Scheme 1). The cleavage reaction is accompanied by formation of one mole of carbon monoxide per mole of haem degraded. Biliverdin has no known function in mammals and once formed is rapidly reduced by biliverdin reductase to bilirubin. The asymmetrical arrangement of side chains around the haem molecule means that, in principle, degradation could lead to the formation of four possible biliverdin, and hence bilirubin, isomers, depending on which one of the α-, β-, γ- or δ-methene bridges of haem are attacked. However the regioselectivity of haem catabolism results in the α-isomer being almost exclusively found in mammalian bile[2].

The high degree of hydrogen bonding present in bilirubin (see Chapter 5) renders it highly insoluble in water at physiological pH. In order to be transported in plasma, bilirubin binds strongly to certain proteins, particularly serum albumin. Although serum albumin is the major carrier, other proteins such as the α and β globulins have also been found to associate with bilirubin[3]. Jacobsen[4] found that bilirubin is bound to lysine residue 240 at its high affinity site on human serum albumin. Kinetic studies of bilirubin oxidation using horse-radish peroxidase[6] determined the dissociation constant for the binding of bilirubin to human serum albumin at a high affinity site. Binding at two other lower affinity sites was also observed with dissociation constants 10 to 100 times lower than the first.

Protein-bound bilirubin is not easily excreted and cannot efficiently pass out of the circulation across either of the selective barriers, kidney and liver, into urine or bile[6]. This problem is circumvented in nature by conjugation of bilirubin, that is by attaching polar substances such as glucoronic acid to the carboxylic acid groups of bilirubin. A glucuronyl transferase enzyme esterifies the carboxylic acid groups of

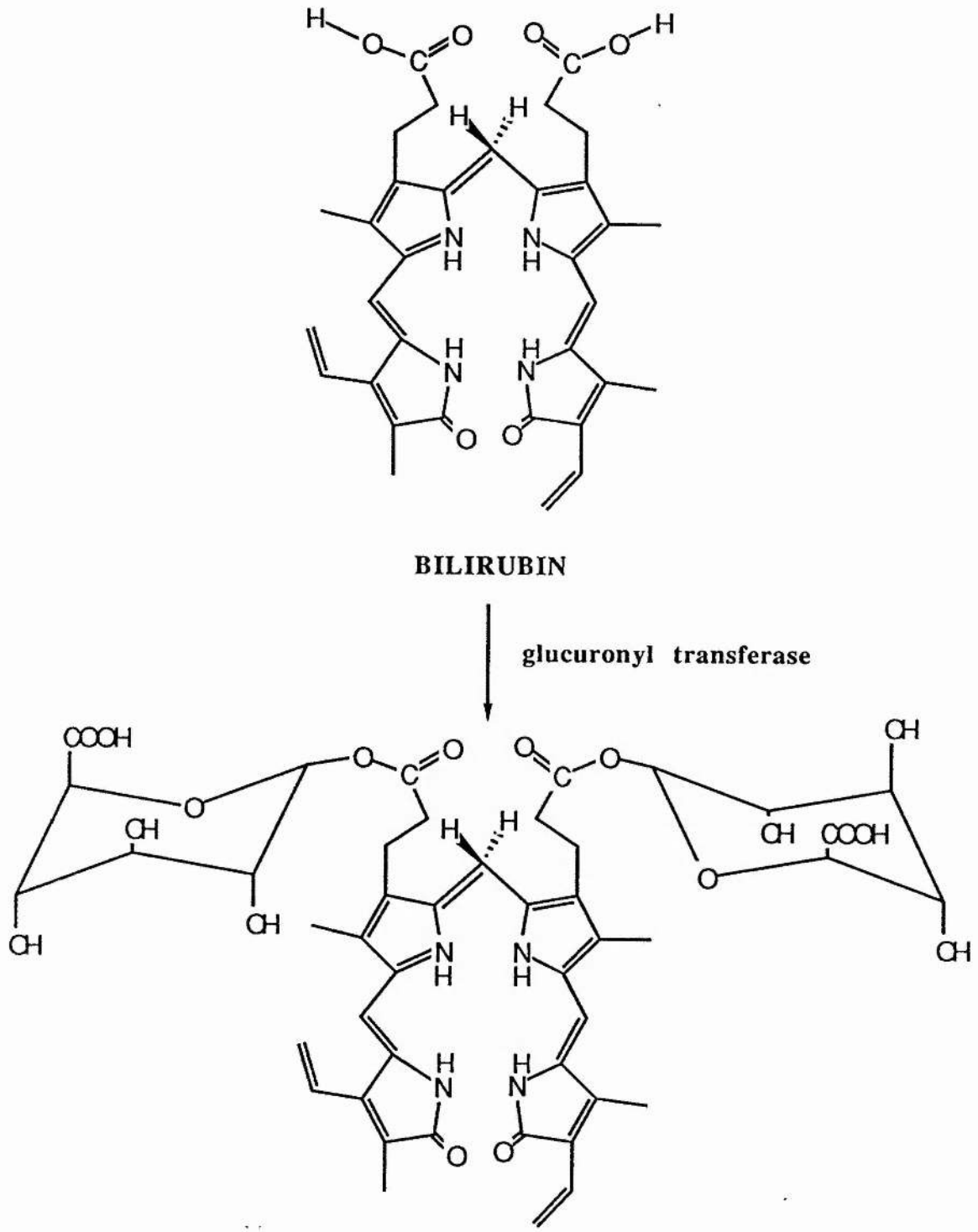

Scheme 2. Conjugation of bilirubin with glucuronic acid.

bilirubin giving a mixture of mono- and di-glucuronides (Scheme 2). These glucuronides, which are synthesised mainly in the liver, are more polar than bilirubin and can be readily excreted in bile. Conjugated bilirubin exists mainly in serum as the diglucuronide, a form in which it is water-soluble and non-toxic. It can then be excreted through the liver cells in the bile capilliaries. Excretion through the bile into the intestines is followed by further bacterial cleavage and reduction in the intestine before final excretion.

The bilirubin production rate in the healthy adult is about 250mg per day and the bilirubin concentration in the plasma is at most 15μM[7]. This amount can be dealt with efficiently by healthy liver but diseased liver, in which one or more of the processes between bilirubin production and excretion is disrupted, leads to the development of elevated levels of bilirubin in the serum, known as hyperbilirubinemia. The increased amounts of pigment result in the characteristic yellow colouring of the skin, referred to as jaundice. Jaundice and hyperbilirubinemia are not diseases in themselves but symptoms of a number of liver disorders which result in abnormally high levels of serum bilirubin. Hyperbilirubinemia is particularly prevalent amongst newborn babies where levels of the glucuronyl transferase enzyme involved in the formation of bilirubin diglucuronide are very low. In the fetus this is not a problem because the lipophilic bilirubin can pass readily across the placenta from the fetal to the maternal circulation where it is glucuronidated and excreted by the mother's liver. This cannot occur in the newborn, however, so after birth levels of bilirubin in serum begin to rise, resulting in hyperbilirubinemia. The problem may be aggrevated by administration of drugs which bind preferentially to albumin at the bilirubin binding site thereby increasing the amount of free bilirubin in the blood. In neonates this condition is transient, abating as bilirubin glucuronyl transferase activity in the liver increases. Usually within 7-14 days the baby is able to synthesise and excrete bilirubin glucuronides with complete efficiency. However, while the hyperbilirubinemia lasts,

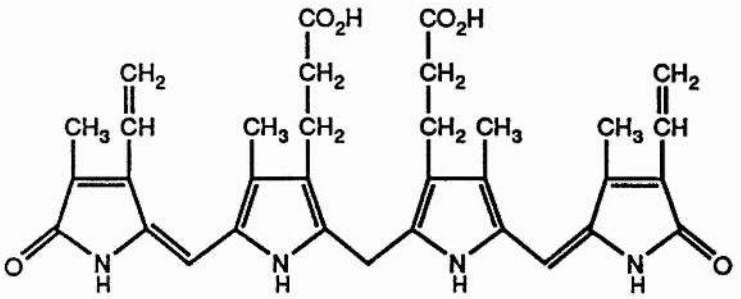

BILIRUBIN

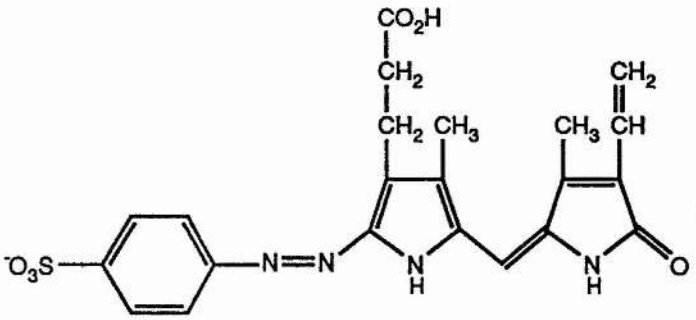

AZODIPYRROLE I

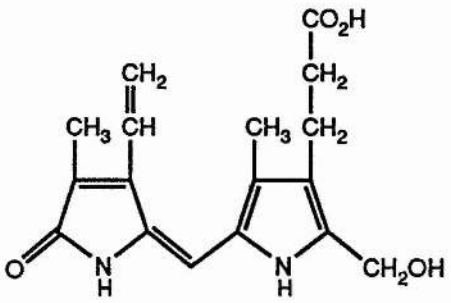

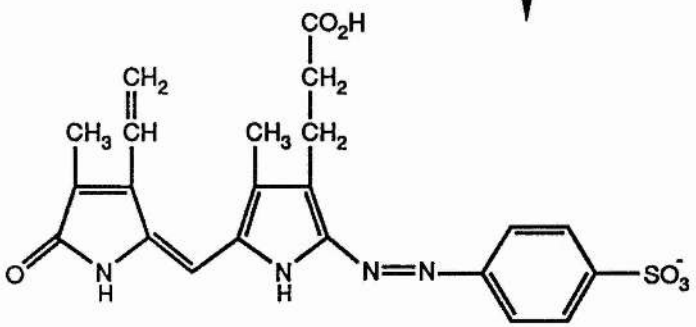

+ CH_2O

AZODIPYRROLE II

Scheme 3. Reaction of bilirubin with diazotised sulphanilic acid.

the toxicity of bilirubin may lead to irreversible cell damage, even brain damage if bilirubin crosses the blood-brain barrier.

The most usual and effective form of treatment of hyperbilirubinemia in newborns is phototherapy. The patient is exposed to ultra-violet light for several hours, or even days, until the jaundiced yellow colouring disappears. The way in which phototherapy works to reduce free bilirubin is not entirely clear although studies have been undertaken to investigate possible mechanisms[8]. Evidence has established that bilirubin undergoes rapid reversible carbon-carbon double bond configurational isomerisation to unstable 4E and 15E isomers when irradiated in solution[9] and it seems likely that photoisomerisation of bilirubin, disrupting hydrogen bonds, and forming a more soluble configuration, increases the efficiency of transportation and excretion of the pigment. Structural and conformational isomers of bilirubin have been detected in serum and bile from babies undergoing irradiation[3]. McDonagh and Lightner also note that binding of bilirubin to albumin does not inhibit photoisomerisation. Indeed, in human albumin the rates of structural and configurational isomerisation are higher than in the presence of organic solvents.

The clinical diagnostic test for serum bilirubin is based on a method devised at the end of the nineteenth century. Ehrlich[10] found that the reaction of bilirubin with diazotised sulphanilic acid produces stable red to violet azo pigments. These colours are due to the formation of the diazotised dipyrroles I and II shown in Scheme 3[11]. Only a few of the azo pigments derived from the reaction of bilirubin with diazotised aromatic amines have been fully characterised but many have been isolated, purified and at least partially characterised by a variety of techniques[12], including nmr spectroscopy[13]. The diazotisation reaction proceeds in two steps giving rise to one mole equivalent of each azodipyrrole[12]. The central methylene bridge is released as formaldehyde[11]. This chemical reaction was successfully used to detect and estimate bilirubin levels, initially in urine and later, more usefully in the

clinical situation, in serum.

It was thought that binding of bilirubin to albumin prevented reaction with diazotised sulphanilic acid, so before the test was carried out alcohol was added to the sample to remove all the protein. Under mildly acidic conditions, appropriate for the diazotisation of sulphanilic acid, a red azo pigment was obtained. In later studies two azo reactions were observed suggesting that two types of bilirubin occur naturally in serum[14]. The first reaction occurred almost instantaneously, the second only after addition of alcohol. It is generally accepted that the first reaction is due to the direct reaction of 'free' or unbound bilirubin. In contrast, bilirubin bound to albumin only reacts quickly once it has been solubilised by the addition of alcohol. The estimation of the total bilirubin content of a sample is therefore established by measuring the amount of direct-reacting bilirubin and adding to this the amount of indirect-reacting bilirubin detected after the addition of alcohol to the sample. This technique is not entirely satisfactory, however, because co-precipitation of bilirubin to the protein leads to under estimation of the total bilirubin content. A further refinement of the van den Bergh test for clinical analysis was the use of a variety of substances which increase the rate at which the diazotisation reaction proceeds. These substances, known as accelerators or promoters, include caffeine, sodium benzoate, sodium acetate, urea and mixtures of these. The ability of these substances to enhance both the rate of reaction and colour intensity has been investigated[15] and various mixtures proposed based on Jendrassik and Grof's[16] original procedure. These procedures claim to be quantitative but do not always agree with each other, emphasising the difficulties of practical application of the test. However, in spite of the chemical uncertainty of the processes involved, the van den Bergh test, using accelerators, is routinely used for clinical estimation of total bilirubin content in plasma. The determination of total bilirubin content by the diazo reaction is crucial in the detection and diagnosis of jaundice and the need to quantify the test has lead to many modifications[17].

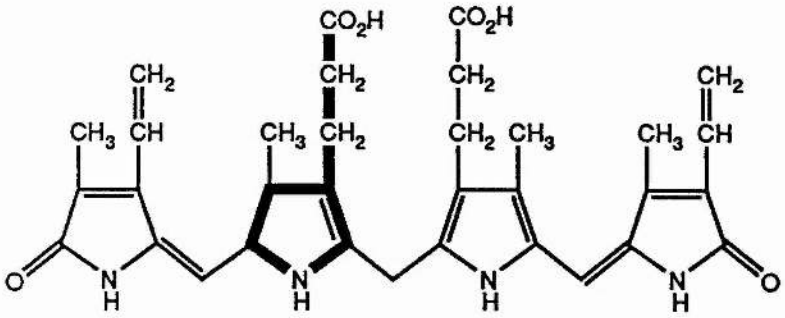

BILIRUBIN

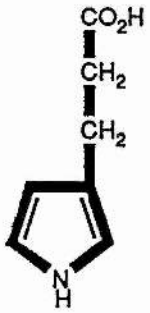

PYRROLE-3-PROPANOIC ACID

Figure 1.

Practically all plasma bilirubin exists in the form of non-glucuronidated pigment bound to albumin and this will affect the clinical estimation of bilirubin. Binding of albumin to bilirubin has long been thought to prevent reaction of bilirubin with diazotised sulphanilic acid and the clinical assays were modified accordingly, noteably by the use of accelerators which were thought to enhance the rate of reaction by facilitating attack of the diazonium ion on bilirubin. The diazo reaction is used for estimating bound and unbound bilirubin ratios but, because of poor methodology, significant errors can occur in the reported values for unbound and total bilirubin concentrations[18]. This assumption leads to incorrect estimation of total bilirubin content in serum and requires further development of the van den Bergh test for clinical use. In the clinical situation the test is carried out on a serum sample which contains a large number of substances other than the two of interest here, bilirubin and albumin. To simplify the situation and in the hope of obtaining an insight into the chemistry of the diazo reaction, a kinetic study of the effect of the binding of bilirubin to albumin was undertaken in a buffered system. The use of a buffer of physiological pH should enable the reaction to be studied under conditions which mimic those in a clinical sample but in a system which contains only the substances of interest.

Bilirubin is a large and rather complex molecule and for preliminary studies a smaller molecule, pyrrole-3-propanoic acid was chosen to serve as a model for the tetrapyrrolic pigment. As can be seen from Figure 1, pyrrole-3-propanoic acid has a structure very similar to the central pyrrole rings of bilirubin, having a propanoic acid side chain at the β-position. It would seem reasonable to assume that pyrrole-3-propanoic acid will have similar behaviour to bilirubin in its binding to albumin. Although smaller than bilirubin it contains the side chain most likely to be involved in binding.

Human albumin contains 609 amino acid residues and has a molecular

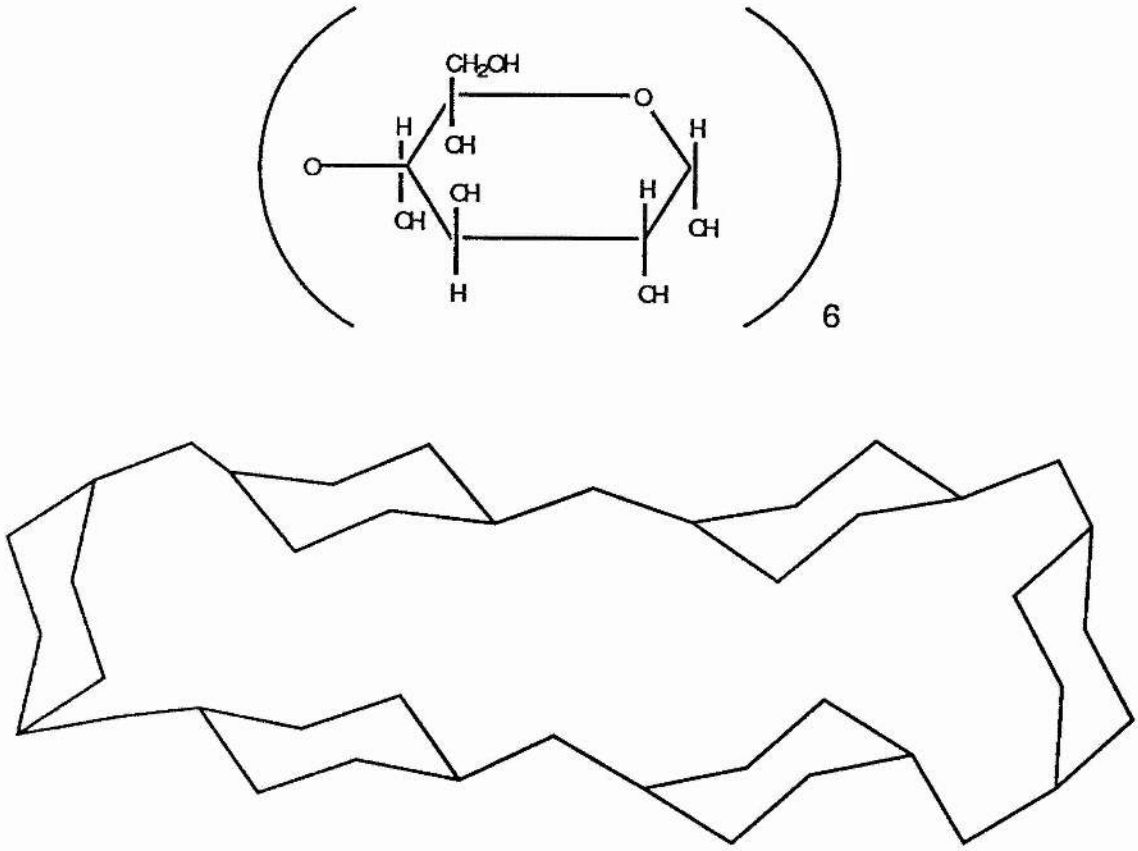

Figure 2. α-cyclodextrin - formula and configuration

weight of 69,365[19]. Many substances bind to this complex protein and although bilirubin will bind at its high affinity binding site, other molecules may interfere with the diazo reaction rate. This complication was eliminated by using a tris buffer of pH 7.0 as a medium for the reactions.

The cyclic oligosaccharides, α-, β- and γ-cyclodextrin and their ability to form inclusion complexes have been the subject of much investigation[20,21]. These sugar derivatives are composed of 6, 7, or 8 glucose units arranged in a crown-like formation (Figure 2). The cavity diameters and other physical properties vary according to the number of glucose units in the ring (Table 1)[22]. The cavity size of the host cyclodextrin dictates its selectivity for guest molecules and 1:1 stoichiometry is usually observed. A wide variety of molecules have been found to act as guests with aromatics being among the most exhaustively studied[20]. The best known type of inclusion complex for aromatics is termed 'axial'. The long axis of the aromatic lies parallel to the cyclodextrin axis. This is illustrated in Figure 3a. An alternative type of complexation has the short axis of the guest lying parallel to the cyclodextrin axis (Figure 3b). Recently, β-cyclodextrin complexes have been found by uv absorption and circular dichroism studies to exhibit a third type of inclusion, known as 'lid-type'[23]. In these complexes both axes of the guest molecule lie nearly normal to the cyclodextrin axis (Figure 3c). Cramer, Saenger and Spatz[21] investigated the inclusion complexes formed by a series of aromatic azo dyes and found the binding to be highly stereospecific. The mechanism of binding was examined by observing the influence on the rate of reaction of changing the substituent attached to the aromatic ring. From their thermodynamic and kinetic measurements, the authors deduced that nitrophenol and α-cyclodextrin form a 1:1 complex in which the aromatic molecule is entirely enclosed within the cyclodextrin cavity.

It has been demonstrated that bilirubin bound to albumin exhibits a bisignate

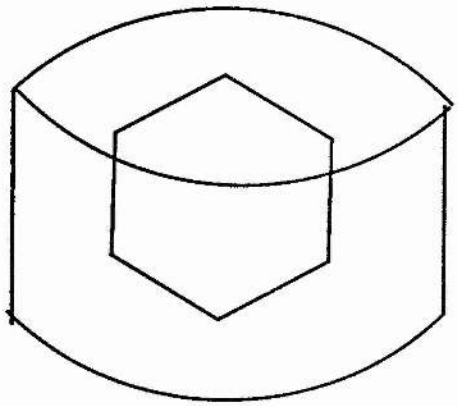

(a)

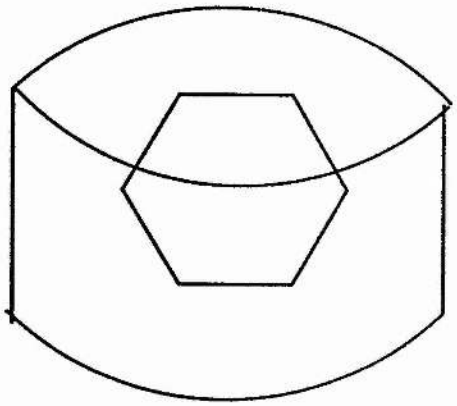

(b)

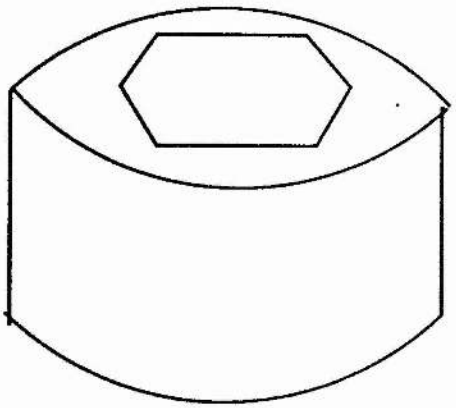

(c)

Figure 3. Types of β-cyclodextrin inclusion complex

Table 1.
Physical properties of cyclodextrins[21]

cyclodextrin	no. of units	molecular weight	water solubility[a]	cavity diameter[b]
α	6	972 a.m.u.	14.5	4.7-5.2
β	7	1135 a.m.u.	1.85	6.0-6.4
γ	8	1297 a.m.u.	23.2	7.5-8.3

a. g/100ml solution at room temperature.
b. as measured on CPK models.

circular dichroism spectrum in water[24,25]. Lightner[26] and his co-workers found that α-, β- and γ-cyclodextrins bound to bilirubin induce a similar effect. The mechanism of this enantioselective binding of bilirubin to cyclic oligosaccarides has recently been investigated by Kano et al[27]. This work suggested that bilirubin binds to cyclodextrin forming an inclusion complex comparable to that which it forms with albumin. As cyclodextrins are rather more simple molecules than albumin, the binding of bilirubin to α-cyclodextrin was examined and the effect of this binding on the reaction of bilirubin with diazotised sulphanilic acid investigated. Although α-cyclodextrin does not have the largest cavity diameter of the three widely known cyclodextrins, it is more soluble in water than β-cyclodextrin[22] and more commonly available than γ-cyclodextrin and was therefore the most convenient for this study. By studying the kinetics of the reactions of bilirubin and pyrrole with diazotised sulphanilic acid and observing the effect of albumin and α-cyclodextrin on the reaction, it was hoped to elucidate information concerning the binding processes involved. The nature of the binding could then be examined by nmr spectroscopy using the fully assigned bilirubin spectrum obtained previously (see Chapter 5).

6.2 EXPERIMENTAL

Bilirubin and other chemicals were obtained from Aldrich and Sigma. Tris buffer pH 7.0 at 25°C was prepared by mixing 0.1molar tris(hydroxymethyl) aminomethane (50ml) with of 0.1M HCl (46.6ml) and making the final volume up to 100ml with distilled water[28]. Diazotised sulphanilic acid was prepared according to the method of Starky[29]. Sulphanilic acid (0.025 moles) was dissolved in fluoroboric acid (10ml) in a 100ml beaker. The beaker was placed in an ice-bath and the solution was stirred. A solution of $NaNO_2$ (1.725g) in H_2O (5ml) was added dropwise. The solution was stirred for a further few minutes and filtered by suction

on sintered glass. The product was washed once with cold fluoroboric acid (5ml), twice with ethanol and several times with ether. The white solid was dried under vaccum. Pyrrole-3-propanoic acid was prepared from acrylonitrile and pyrrole according to the method of Blume and Lindwall[30]. Acrylonitrile (10ml) was added dropwise over a period of 30 minutes to a mixture of pyrrole (10g) and trimethylbenzylammonium hydroxide (1ml). The temperature was kept below 40°C. After one hour at room temperature, the crude nitrile was hydrolysed (without isolation) by refluxing for one hour with a solution of potassium hydroxide (10g) in water (15ml). The product was isolated by acidification with hydrochloric acid and extracted with ether. Recrystallisation from hexane gave off-white crystals.

Kinetic studies of the reaction of pyrrole-3-propanoic acid and diazotised sulphanilic acid were carried out on a Hi-Tech stopped-flow spectrophotometer and SF-40C photomultiplier, Data-Lab DC 901 transient recorder and a DT V12-14 Farnell oscilloscope. A solution of pyrrole-3-propanoic acid (0.0005M in 0.05M HCl) was placed in one arm and a solution of diazotised sulphanilic acid (0.01M in 0.05M HCl) in the other. Reactions were monitored at 450nm and 25°C. Data aquisition and processing were carried out by an Apple II Plus microcomputer using a Hi-Tech system software kinetics package. Rate constants were calculated by a computer program using the Kedzy-Swinbourne[31] method. Albumin and α-cyclodextrin were added in varying amounts (see results section) to the pyrrole-3-propanoic acid solution before it was mixed with the diazotised sulphanilic acid solution.

The reaction of bilirubin with diazotised sulphanilic acid was monitored on a Pye-Unicam SP8-100 spectrophotometer at 450nm and 25°C. Absorbancies were recorded over a period of time equivalent to at least two reaction half-lives. Rate constants were calculated according to the method of Kedzy and Swinbourne[31]. Solutions of bilirubin were prepared by dissolving a known amount of bilirubin in

dioxan (5ml) and diluting with tris buffer pH 7.0 to 50ml, resulting in an aqueous solution which was1% in dioxan. Concentrations of bilirubin in buffer ranged from $3.42x10^{-7}$ to $3.8x10^{-6}$M. The diazo reagent was prepared according to the method of Lucassen as reported by Heirwegh and Blanckaert[32]. Sulphanilic acid (0.5g) was dissolved, by warming, in H_2O (50ml) and HCl (1.5ml) in a 100ml volumetric flask. The solution was made up to the mark with distilled H_2O. Sodium nitrite solution was prepared by dissolving $NaNO_2$ (500mg) in distilled H_2O (100ml). The diazo reagent comprised a mixture of sodium nitrite solution (0.3ml) and sulphanilic acid solution (10ml). This mixture has a diazonium ion concentration of approximately 2mM. Samples contained 4ml bilirubin solution in tris buffer and 2ml diazo reagent. This was shaken and transferred into a plastic cell. Solutions containing albumin and α-cyclodextrin were prepared by adding the appropriate weight of albumin or α-cyclodextrin to 4ml bilirubin in buffer solution. Solutions contained various ratios ranging from an excess in bilirubin to an excess in albumin or α-cyclodextrin.

Inclusion complexes were prepared according to the guidelines given by Saenger[22]. Bilirubin was dissolved in chloroform and layered underneath a concentrated aqueous solution of α-cyclodextrin. Crystals formed at the interface were filtered off and washed with ethanol to remove any adhering substances. Bilirubin and α-cyclodextrin were used in equimolar quantities. The inclusion complex of pyrrole-3-propanoic acid with α-cyclodextrin was prepared by dissolving equimolar quantities of each substance in H_2O and filtering off the crystals formed. The ^{13}C and ^{1}H nmr spectra of these inclusion complexes were recorded on a Brucker AM-300 spectrometer at 25°C. Samples were either dissolved in d_6-DMSO and referenced to TMS or dissolved in D_2O and referenced to DSS.

Chem X structures were generated on a Tektronics t4107 colour graphics terminal. X-ray crystallographic data were obtained from the Daresbury databank.

6.3 RESULTS AND DISCUSSION

First order curves were obtained from stopped-flow kinetic experiments on the pyrrole-3-propanoic acid and diazotised sulphanilic acid system. α-Cyclodextrin was added to the system and the observed rate constants for a series of reactions involving an increasing amount of α-cyclodextrin are shown in Table 2. Figure 3 illustrates graphically the effect of α-cyclodextrin on the rate of the reaction. No marked effect was observed as the amount of α-cyclodextrin added was increased from a 5:1 pyrrole-3-propanoic acid:α-cyclodextrin ratio to a 1:2 ratio. To determine whether the α-cyclodextrin effect was due to the formation of an inclusion complex or simply caused by the presence of glucose units, a similar experiment was carried out using the same ratios of glucose to pyrrole-3-propanoic acid. Again there was little effect on the rate (Table 3). α-Cyclodextrin apparently has only a small effect on the attack of diazotised sulphanilic acid on pyrrole-3-propanoic acid. In a second set of experiments, human serum albumin was added to the solution of pyrrole-3-propanoic acid in the same proportions as the α-cyclodextrin in the previous experiments. The observed rate constants for this set of experiments are shown in Table 4 and illustrated graphically in Figure 4. Addition of increasing amounts of human albumin had a marked effect on the rate of reaction, reducing it by approximately half on addition of 0.001M albumin. From this evidence, diazonium ion attack is assumed to be hindered by the binding of albumin to pyrrole-3-propanoic acid but not completely prevented.

Looking at the proposed structures for the pyrrole-3-propanoic acid/α-cyclodextrin inclusion complex helps to clarify the kinetic results. There are

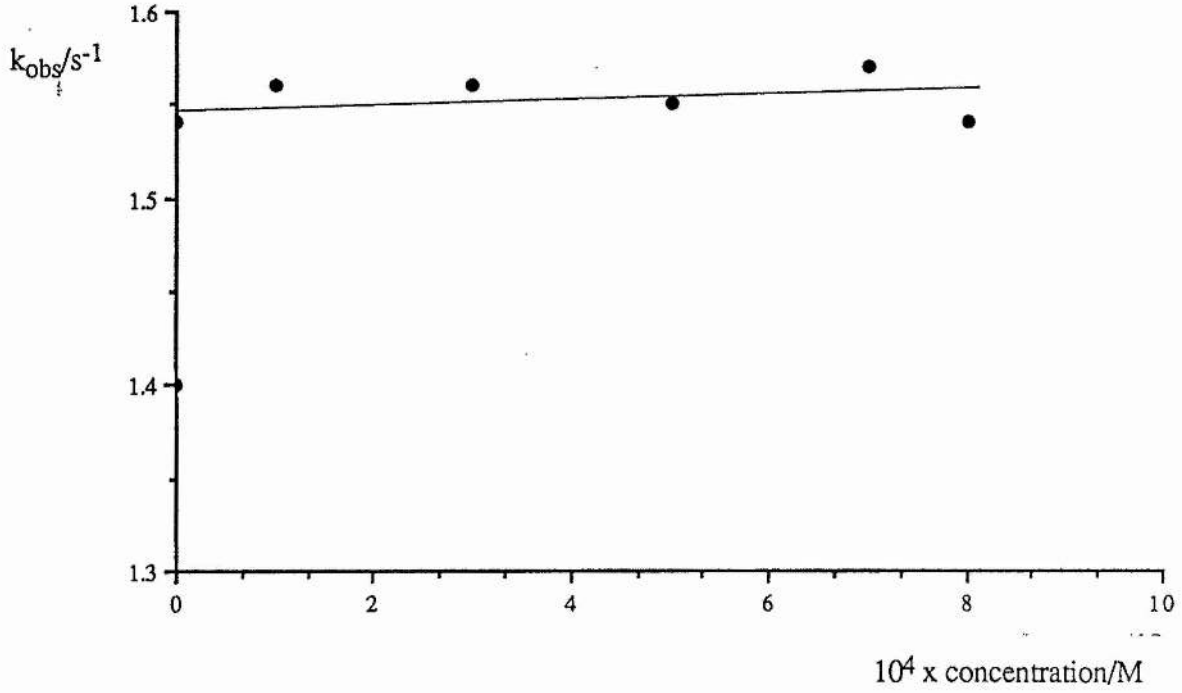

Figure 3.
Effect of α-cyclodextrin on rate of reaction of pyrrole-3-propanoic acid with diazotised sulphanilic acid.

Table 2.

Effect of addition of α-cyclodextrin on the rate of reaction of pyrrole-3-propanoic acid[a] with diazotised sulphanilic acid[b].

[α-cyclodextrin]/M	k_{obs}/s^{-1}
none	1.54
0.0001	1.56
0.0003	1.56
0.0005	1.55
0.0007	1.57
0.0008	1.54

a. 0.0005M in HCl.
b. 0.01M in HCl.

Table 3.

Effect of the addition of glucose to the reaction of pyrrole-3-propionic acid[a] with diazotised sulphanilic acid[b].

[glucose]/M	k_{obs}/s^{-1}
none	1.44
0.3	1.40
0.6	1.42
3.0	1.34

a. 0.0005M in HCl.
b. 0.01M in HCl.

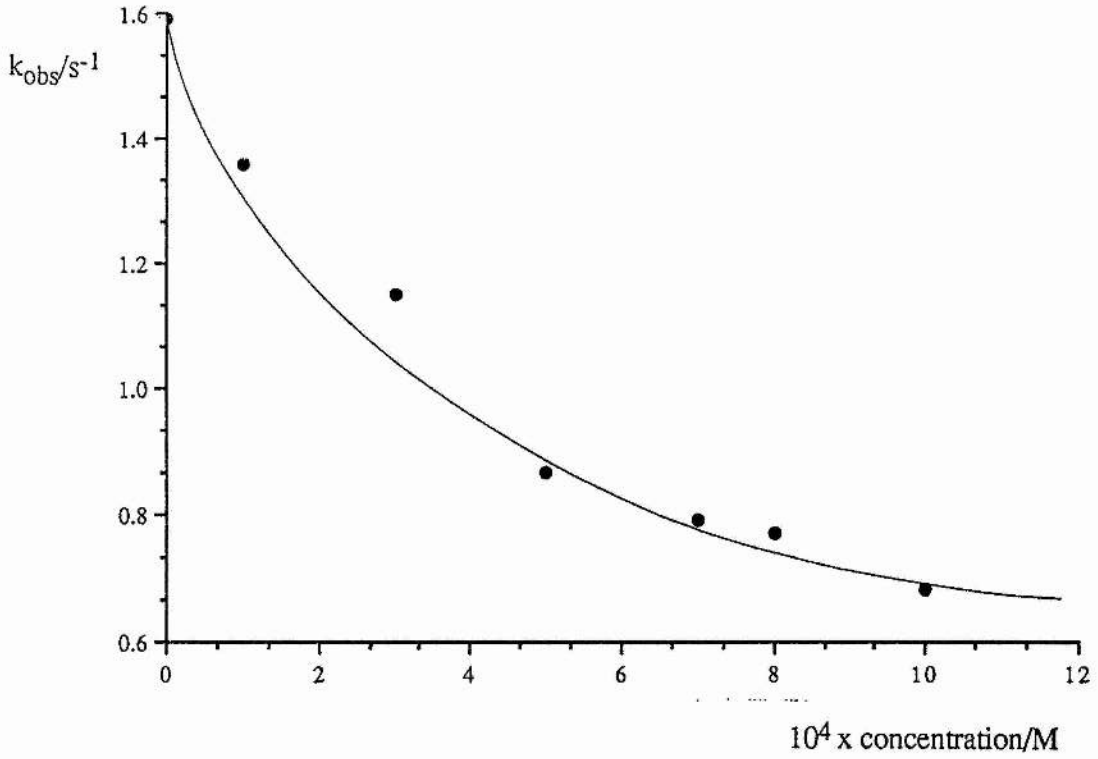

Figure 4.
Effect of human albumin on rate of reaction of pyrrole-3-propanoic acid with diazotised sulphanilic acid.

Table 4.
Effect of addition of human albumin to the rate of reaction of pyrrole-3-propionic acid[a] with diazotised sulphanilic acid[b].

[human albumin]/M	k_{obs}/s^{-1}
none	1.59
0.0001	1.36
0.0003	1.15
0.0005	0.866
0.0007	0.79
0.0008	0.77
0.001	0.684

a. 0.0005M in HCl.
b. 0.01M in HCl.

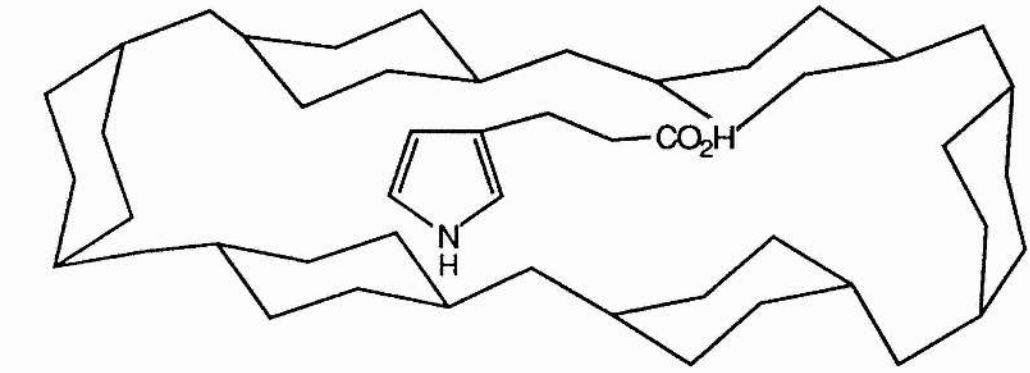

(a)

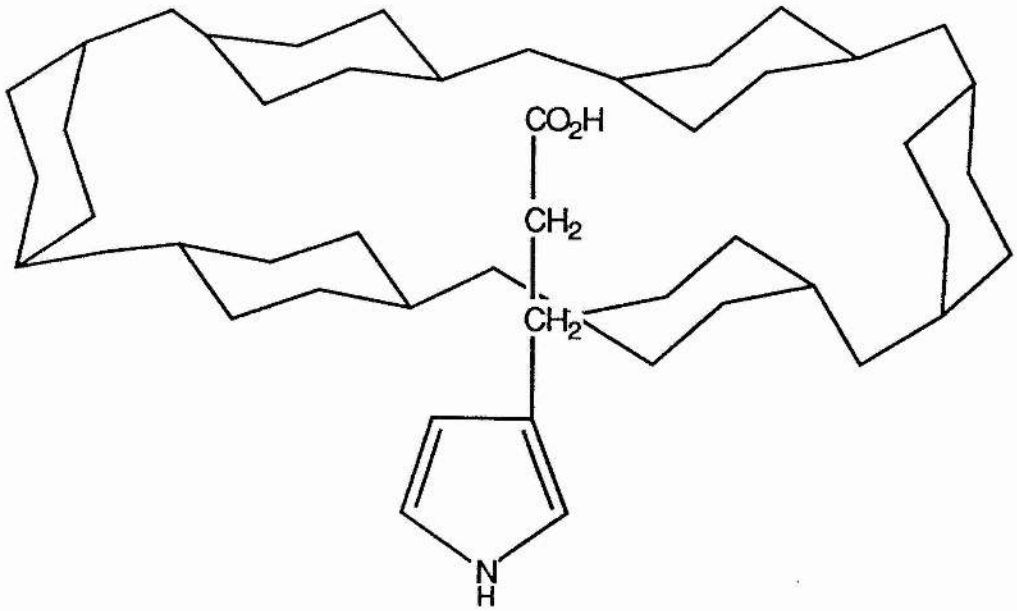

(b)

Figure 5. Possible inclusion complexes of α-cyclodextrin with pyrrole-3-propanoic acid.

two distinct ways in which the pyrrole-3-propanoic acid could fit inside the α-cyclodextrin cavity (Figure 5). In Figure 5a, the entire pyrrrole-3-propanoic acid molecule, both ring and side chain, are enclosed by the α-cyclodextrin cavity. Alternatively, in Figure 5b, only the propanoic side chain sits inside the cavity in a similar manner to that adopted by diazonium ions complexing with crown ethers[33,34]. In order to try and determine which of these structures is more likely, ^{13}C nmr spectra were run on the inclusion complex. A known amount of pyrrole-3-propanoic acid was dissolved in D_2O and the ^{13}C nmr spectrum recorded. To this sample was added an equimolar amount of α-cyclodextrin and a second ^{13}C nmr spectrum recorded. The relevant chemical shifts differences observed are displayed in Table 5. The largest differences observed are those corresponding to the three carbons of the propanoic acid side chain of the pyrrole. The carboxylic acid carbon exhibits the largest change in chemical shift, with the methylenes of the chain exhibiting slightly smaller changes. From these results one can imagine the inclusion complex of pyrrole-3-propanoic acid and α-cyclodextrin to be of the type illustrated in Figure 5b. This complex is also illustrated in Photograph 1, which shows the complex generated by Chem-X from the crystal structures of the components. This structure is also in accordance with the kinetic results which showed that α-cyclodextrin had little effect on the rate of reaction of pyrrole-3-propanoic acid with diazotised sulphanilic acid. From previous studies, it is known that attack of the diazonium ion will occur exclusively at the α-carbon (see Chapter 1 and references therein). From Figure 5b, it is clear that complexation of this type with the pyrrole-3-propanoic acid will not hinder attack of the diazonium ion at the α-carbon of the pyrrole ring which remains completely outside the α-cyclodextrin cavity. Thus the kinetic and ^{13}C nmr evidence is reconciled in the conclusion that pyrrole-3-propanoic acid does complex with α-cyclodextrin but not in a manner

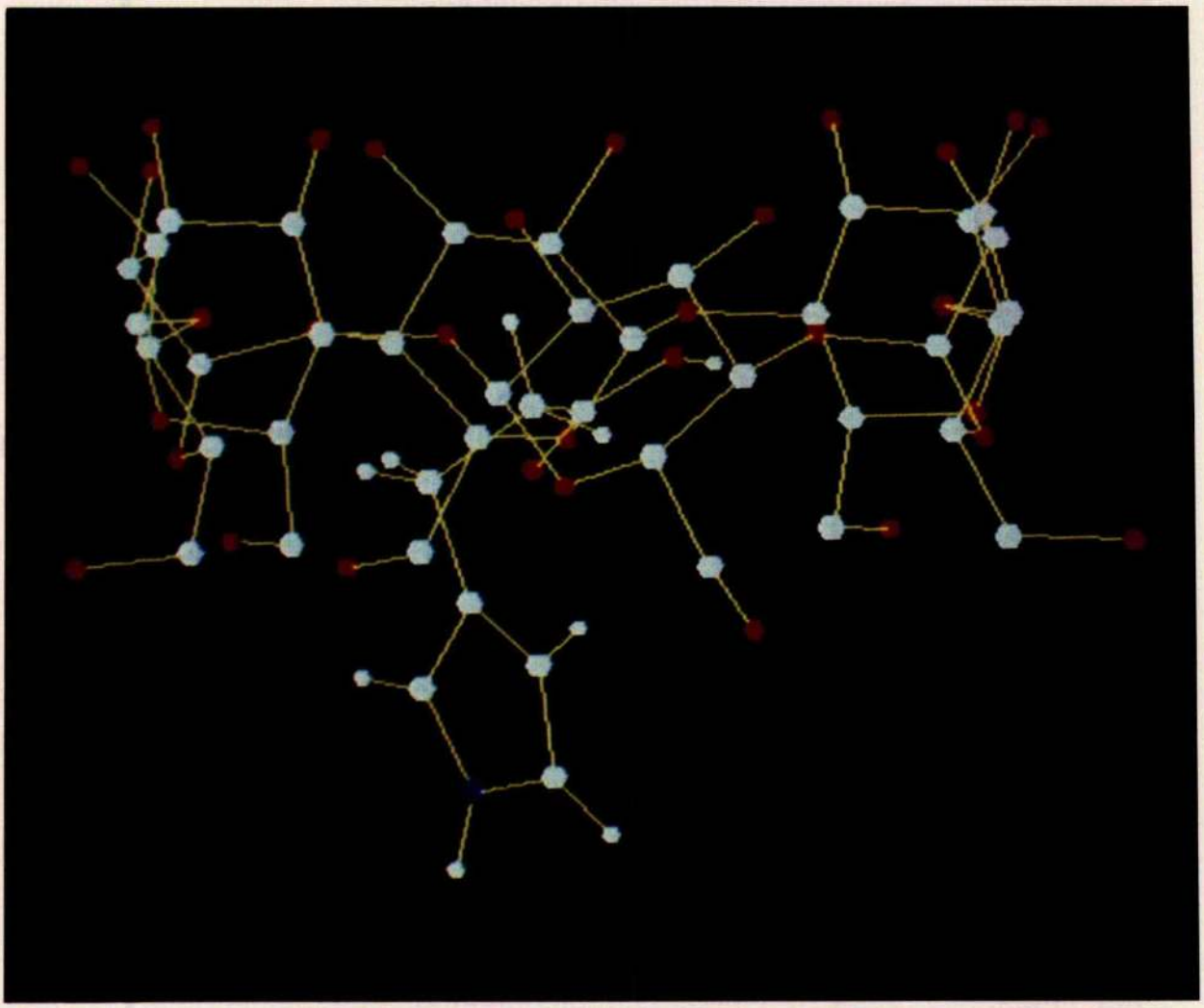

Photograph 1.
Chem-X generated structure of possible inclusion complex of pyrrole-3-propionic acid with α-cyclodextrin. Atoms labelled as follows: carbon-large white, hydrogen-small white, nitrogen-blue, oxygen-red.

Table 5.
Observed ^{13}C chemical shift differences[a] for pyrrole-3-propanoic acid/α-cyclodextrin complex.

Pyrrole	Complex	Difference
177.99	178.54	+0.55
123.48	123.56	+0.08
110.10	110.07	-0.03
46.84	47.12	+0.28
38.42	38.85	+0.43

(Solvent: D_2O)
a. chemical shifts recorded in ppm.

which affects reaction of the pyrrole with diazotised sulphanilic acid.

The reduction in rate caused by the addition of human albumin suggests that pyrrole-3-propanoic acid does also bind to albumin but in such a way as to inhibit attack of the diazonium ion on the pyrrole ring. It has not yet been possible to investigate the inclusion complex of pyrrole-3-propanoic acid and human albumin by ^{13}C nmr spectroscopy. Previous ^{13}C nmr studies involving human albumin indicate that isotopic labelling is necessary to identify the non-albumin signals in a mixture of albumin and any smaller molecule. In natural abundance experiments, without isotopic labelling, the albumin signals dominate the entire spectrum and no other peaks can be identified.

The reaction of bilirubin with diazotised sulphanilic acid with no accelerators added, is slower than the reaction of pyrrole-3-propanoic acid with diazotised sulphanilic acid and therefore was followed by conventional spectrophotometric techniques. Observed rate constants for reaction involving addition of α-cyclodextrin are displayed in Table 6 and illustrated graphically in Figure 7. It was found that adding α-cyclodextrin to the bilirubin in tris buffer increased the rate of reaction by a factor of three when the α-cyclodextrin is present in 10000 fold excess. This ratio of α-cyclodextrin to bilirubin is equivalent to an α-cyclodextrin concentration of about 0.03M, not in fact a high concentration at all. The concentrations are limited by the low solubility of bilirubin at the pH used here and the ratios give a clearer impression of the amounts of bilirubin and α-cyclodextrin present in solution. Addition of albumin to the reaction mixture at ratios of up to 1000:1 (albumin:bilirubin) decreased the observed rate of reaction (Table 7 and Figure 8) by a factor of approximately 7. The opposite effects of adding α-cyclodextrin and albumin to the reaction indicate rather different binding processes occuring between bilirubin and each 'host' molecule.

A possible structure for the complexation of bilirubin and α-cyclodextrin is

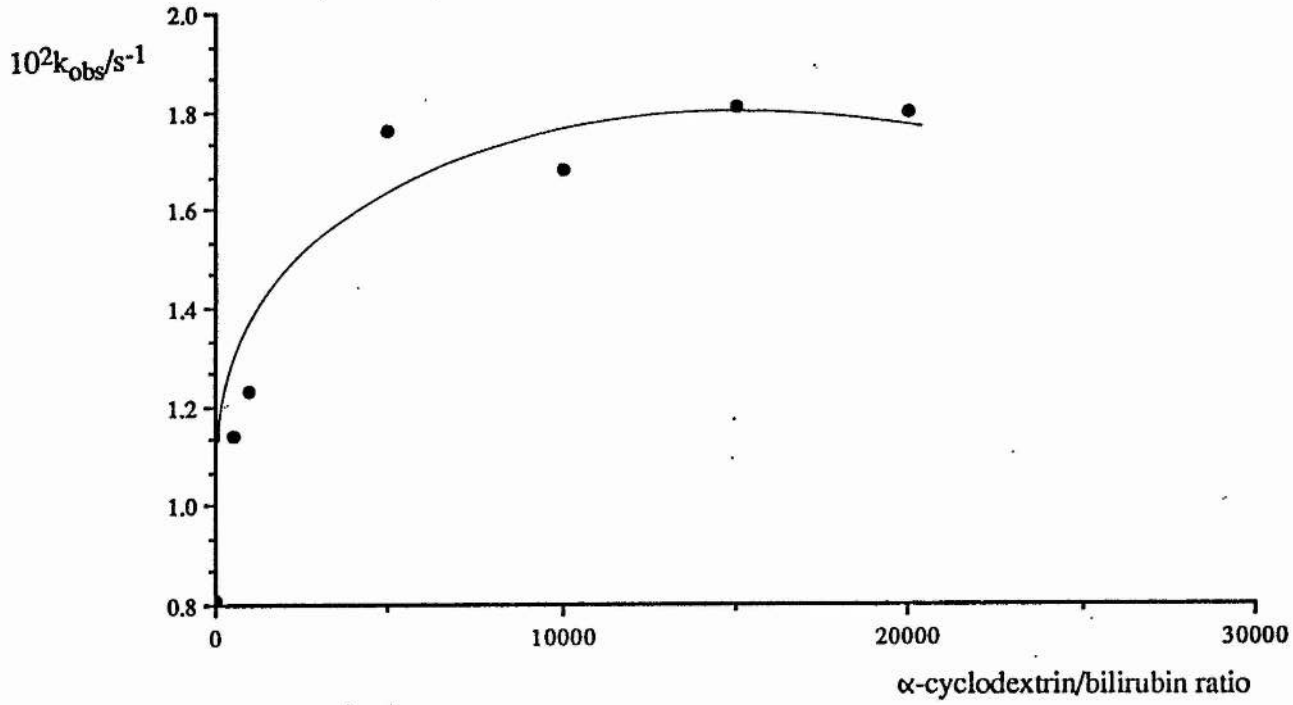

Figure 7.
Effect of α-cyclodextrin on rate of reaction of bilirubin with diazotised sulphanilic acid.

Table 6.

Effect of addition of α-cyclodextrin on the rate of reaction of bilirubin[a] with diazotised sulphanilic acid.

α-cyclodextrin:pyrrole	$10^2 k_{obs}/s^{-1}$
none	0.81
500:1	1.14
1000:1	1.23
5000:1	1.76
10000:1	1.68
15000:1	1.81
20000:1	1.80

a. in tris buffer at pH 7.0.

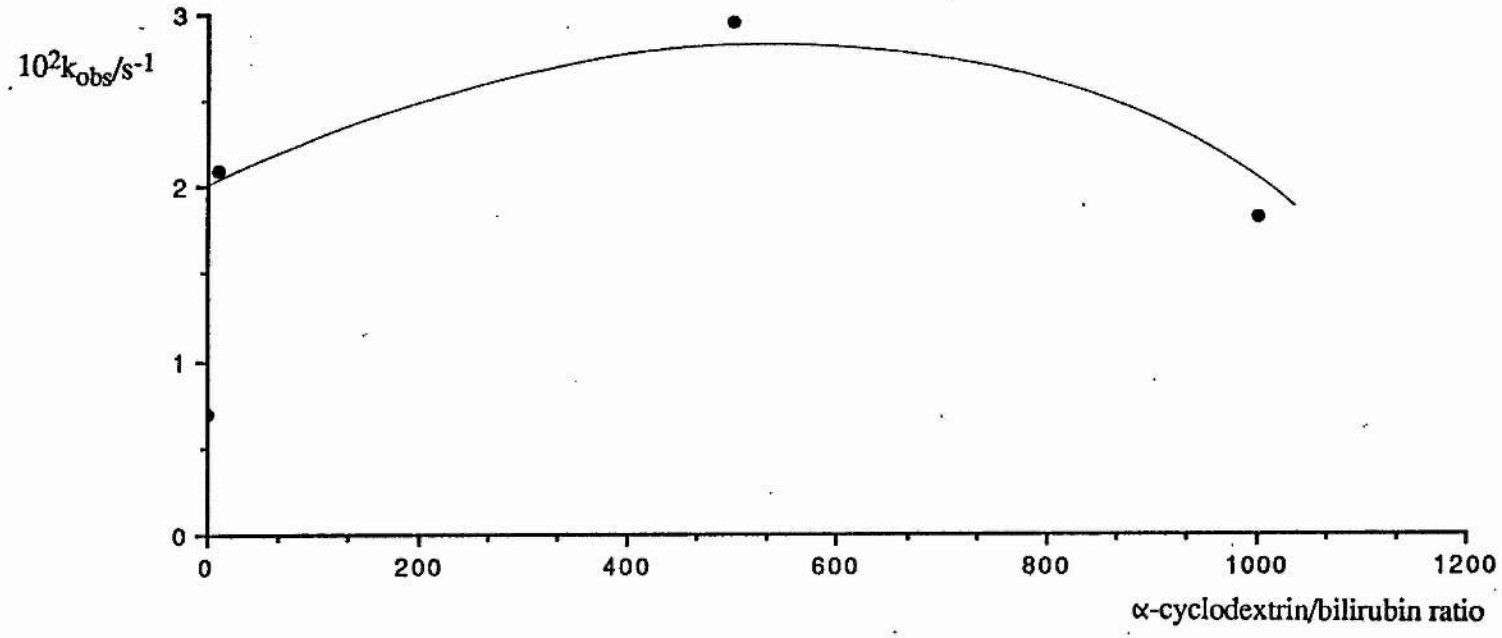

Figure 8.
Effect of human albumin on rate of reaction of bilirubin with diazotised sulphanilic acid.

Table 7.
Effect of addition of human albumin on the reaction of bilirubin[a] with diazotised sulphanilic acid.

human albumin:bilirubin	$10^2 k_{obs}/s^{-1}$
none	0.70
10:1	0.21
500:1	0.295
1000:1	0.182

a. in tris buffer pH 7.0.

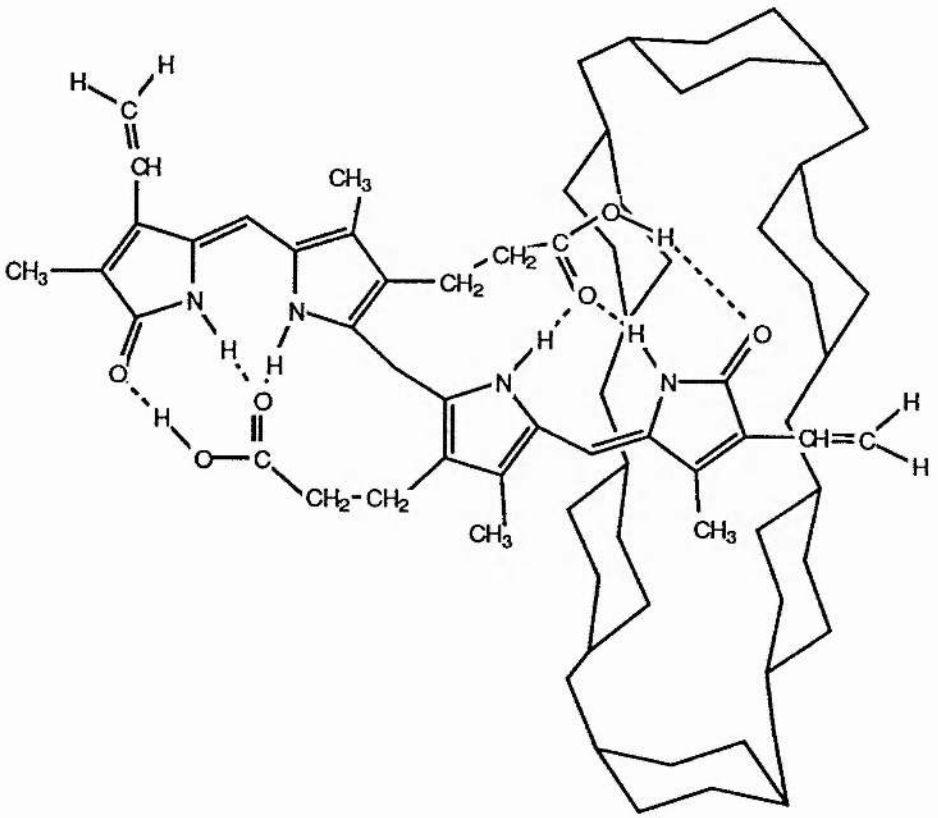

Figure 9. Possible complexation of bilirubin with α-cyclodextrin.

shown schematically in Figure 9. Photograph 2 illustrates the complex generated from crystal structure data using Chem-X. It is possible that a second α-cyclodextrin molecule could also fit onto the pyrrole ring at the other end of the tetrapyrrole creating an even more rigid complex. The initial site of attack by the diazonium ion on bilirubin is at the α-position of either of the two central pyrrole rings, both of which lie outwith the α-cyclodextrin cavities. It can be imagined that the rigid structure caused by the positioning of α-cyclodextrin molecules at either end of bilirubin holds the pigment in a configuration favourable for attack by the diazonium ion because the site of attack is easily found. This would explain the increase in reaction rate which is observed on addition of α-cyclodextrin to the bilirubin/diazotised sulphanilic acid reaction mixture.

Evidence for the structure in Figure 9 was sought by ^{13}C nmr spectroscopy. Bilirubin was dissolved in d_6-DMSO and the ^{13}C spectrum was run. Solubility problems were encountered on addition of α-cyclodextrin and as much α-cyclodextrin as would dissolve was added but the resulting sample was not a 1:1 mixture. A second nmr spectrum was recorded. Smaller chemical shift differences were observed for this sample compared with the pyrrole-3-propanoic acid/α-cyclodextrin sample. However, the largest observed differences in chemical shift were for the propanoic acid side chains of the central pyrrole rings of bilirubin (Table 8). This suggests that these side chains are involved in the binding of bilirubin to α-cyclodextrin. Clearly the real situation is not as simple as the structure depicted in Figure 9.

One possible explanation concerns the difference in structure between the crystalline and d_6-DMSO solution states of bilirubin. In the solid state six intramolecular hydrogen bonds hold the bilirubin structure in a very rigid conformation allowing α-cyclodextrin molecules to attach themselves at the ends of

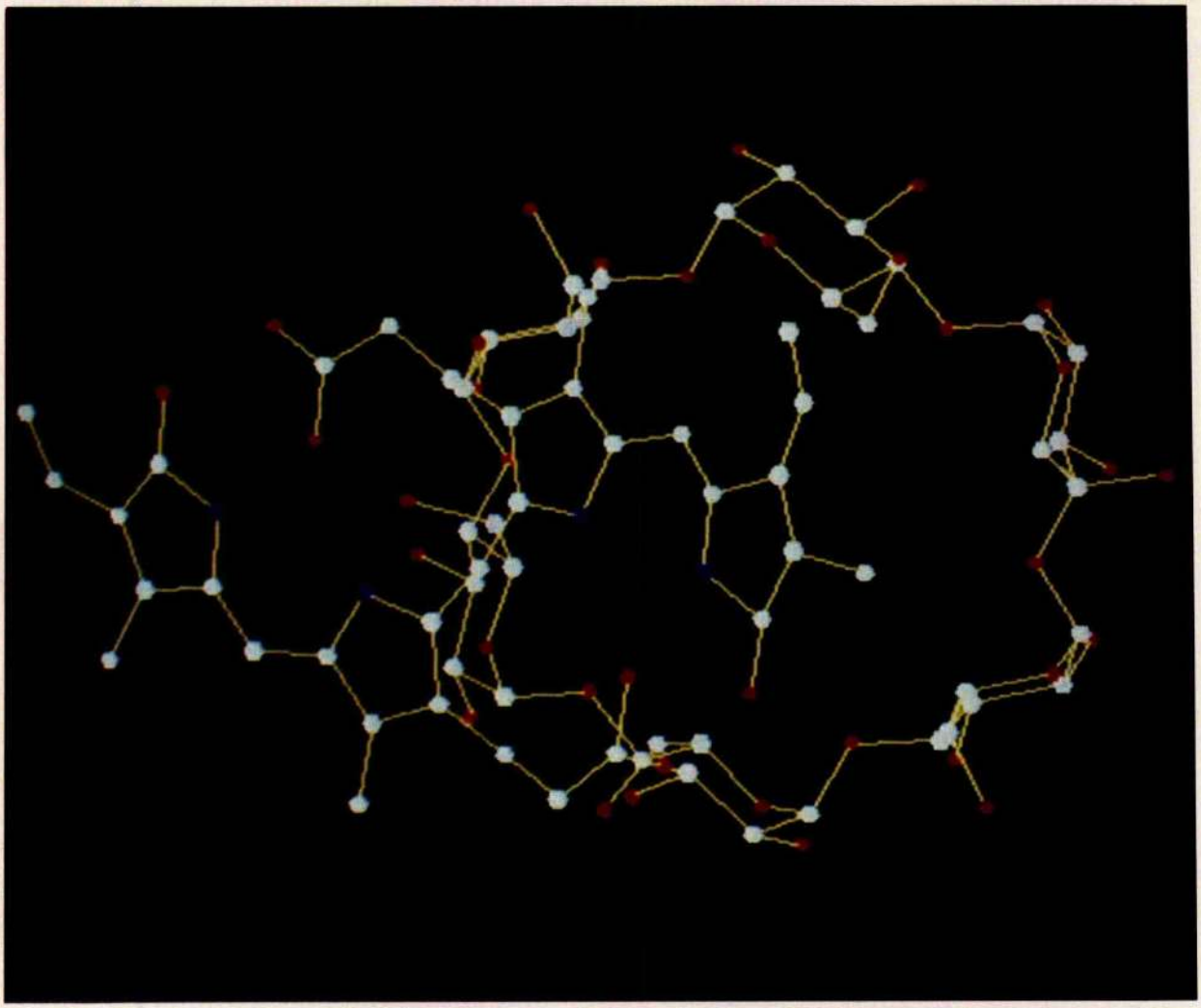

Photograph 2.
Chem-X generated structure of possible inclusion complex of bilirubin with α-cyclodextrin. Atoms labelled as follows: carbon-large white, hydrogen-small white, nitrogen-blue, oxygen-red.

Table 8.
Observed ^{13}C chemical shift differences[a] for propionic acid side chains in bilirubin/α-cyclodextrin complex[a].

Bilirubin		Complex	Difference
173.85	CO_2H	173.98	+0.13
34.15	CH_2	34.29	+0.14
19.25	CH_2	19.32	+0.07

(Solvent:d_6-DMSO)

a. Chemical shifts recorded in ppm

the bilirubin structure. The hydrogen bonding involves the carboxylic acid groups on the propanoic side chains and therefore is likely to prevent attachment of α-cyclodextrin molecules to the carboxylic side chains. In d_6-DMSO, the hydrogen bonding will be destroyed, possibly inducing a different arrangement of α-cyclodextrin molecules around the tetrapyrrolic structure. Addition of albumin to the reaction of bilirubin with diazotised sulphanilic acid decreases the rate of reaction but does not prevent reaction completely (Figure 8). This is contrary to previous assumptions that only 'free' bilirubin could react with diazotised sulphanilic acid[17].

The inclusion complex of bilirubin and albumin could not be examined by ^{13}C nmr spectroscopy because albumin signals completely dominate the spectrum. Low solubility of bilirubin means that the only way to circumvent this problem is to label bilirubin isotopically. Ideally this would involve synthesising bilirubin with a ^{13}C label on the carboxylic acid group. This is a distinctive signal, away from the more complicated part of the spectrum and should be easily identified. A chemical shift difference at this signal on addition of albumin to the sample would indicate possible involvement of the carboxylic acid side chains in the binding process. The labelling experiment would also be useful in clarifying the binding processes taking place between bilirubin and α-cyclodextrin.

The van den Bergh test detects the amount of free bilirubin in solution which reacts with diazotised sulphanilic acid. The way in which the test is used clinically requires it to detect two sorts of bilirubin in serum. The unbound bilirubin, which is thought to be the diglucuronide, reacts immediately. The other sort of bilirubin is bound to albumin. This type was thought not to react at all but the studies carried out in this work demonstrate that although binding of bilirubin to albumin slows down the reaction of the pigment with diazotised sulphanilic acid, reaction is not completely inhibited. It is possible that the slowness of the reaction of bound bilirubin, however, gives the impression that no reaction is occurring. Clinical

testing on a routine basis requires an almost instantaneous result in order to be effective and it is not possible to obtain a quick result from the reaction of bound bilirubin with diazotised sulphanilic acid. The use of accelerating substances is necessary to obtain an immediate estimation of the total amount of bilirubin content in plasma. The accelerators are thought to break down the binding of bilirubin to albumin, enabling the reaction of the now unbound bilirubin with diazotised sulphanilic acid. The use of accelerators to speed up the reaction releases more bilirubin, which will react with diazotised sulphanilic acid and thus lead to an over-estimation of the actual amount of unbound bilirubin present in a sample.

A greater understanding of the nature of bilirubin binding with albumin shows that the van den Bergh test does not give an entirely accurate indication of the bilirubin levels in serum when used in the clinical situation. It is vital to know the levels of the unbound bilirubin as it is this species which causes cell damage. Artificial acceleration of the test by addition of substances to the sample does not allow a true value of the amount of unbound bilirubin actually present in the circulation to be calculated. The value obtained by accelerator methods should be adjusted to allow for the fact that bilirubin is released from its binding with albumin as a result of the addition of the accelerators.

The nature of the binding of bilirubin to albumin is not only of interest from the standpoint of protein-ligand interactions but is of physiological importance too. Studies have indicated that bilirubin is less toxic when bound to albumin than when free in solution[35]. Protein-bound bilirubin is also easily transported in plasma and the pigment can therefore be distributed throughout the entire circulation. The physiological function of bilirubin and the reason for the reduction of non-toxic biliverdin to a potentially hazardous substance were unclear until recent studies by Stocker, Glazer and Ames[36]. These workers proposed that bilirubin may act as a physiological antioxidant. In vitro studies indicate that bilirubin bound to albumin at normal plasma concentrations protects albumin-bound linoleic acid from peroxy

radical-induced oxidation. Each molecule of albumin-bound bilirubin donates two hydrogens to scavenge two molecules of peroxy radicals, resulting in bilirubin being reduced to albumin-bound biliverdin.

The bilirubin-albumin complex competes successfully with other known radical scavengers in the blood circulation and its importance is expected to rise under conditions of low concentrations of other scavengers. It is also possible that bilirubin bound to proteins other than albumin may have similar beneficial properties. The further investigation of bilirubin binding processes may lead to an explanation of the otherwise mysterious production of a toxic substance from a non-toxic precursor.

6.4 REFERENCES

1. R.Schmid and A.F.McDonagh in 'The Porphrins', Vol.6, p258, (D.Dolphin, Ed.), 1979, Academic Press.
2. S.B.Brown and R.F.Troxler in 'Bilirubin', Vol.2, p3, (K.P.M.Heirwegh and S.B.Brown, Eds.), CRC Press, 1982.
3. N.H.Martin, *J. Am. Chem. Soc.*, 1949, **71**, 1230.
4. C.Jacobsen, *Biochem. J.*, 1978, **171**, 453.
5. J.Jacobsen, *FEBS Lett.*, 1969, **5**, 112.
6. D.A.Lightner and A.F.McDonagh, *Acc. Chem. Res.*, 1984, **17**, 417.
7. P.Berthelot, Ph.Duvaldestin and J.Fevery in 'Bilirubin', Vol.2, p175, (K.P.M.Heirwegh and S.B.Brown, Eds.), CRC Press, 1982.
8. A.F.McDonagh, L.A.Palma, F.R.Trull and D.A.Lightner, *J. Am. Chem. Soc.*, 1982, **104**, 6965.
9. A.F.McDonagh, D.A.Lightner and T.A.Wooldridge, *J. Chem. Soc. Chem. Commun.*, 1979,110.
10. P.Ehrlich, *J. Liebigs Ann. Chem.*, 1883, **8**, 140.
11. D.W.Hutchinson, B.Johnson and A.J.Knell, *Biochem. J.*, 1972, **127**, 907.
12. W.Kufer and H.Scheer, *Tetrahedron*, 1983, **39**, 1887.
13. F.Compernolle, G.P.Van Hees, J.Fevery and K.P.M.Heirwegh, *Biochem. J.*, 1971, **125**, 811.
14. A.A.Heyman van den Bergh and P.Muller, *Biochem. Z.*, 1916, **77**, 90.
15. P.H.Loleka and K.Limparithayakul, *Clin. Chem.*, 1977, **23**, 778.
16. L.Jendrassik and P.Grof, *Biochem. Z.*, 1938, **297**, 81.
17. H.T.Malloy and K.A.Evelyn, *J. Biol. Chem.*, 1937, **119**, 481.
18. A.F.McDonagh in 'The Porphrins', Vol.6, p358, (D.Dolphin, Ed.), 1979, Academic Press.
19. P.Q. Behrens, A.M. Spiekerman and J.R. Brown, *Fed. Proc.*, 1975, 34, 591.
20. M.J.Gridley and S.M.Bociek, *J. Am. Chem. Soc.*, 1988, **110**, 3820.

21. F.Cramer, W.Saemger and H-Ch.Spatz, *J. Am. Chem. Soc.*, 1967, **89**, 14.

22. W.Saenger, *Angew. Chem. Int. Ed. Engl.*, 1980, **19**, 344.

23. N.Kobayashi, *J. Chem. Soc. Chem. Commun.*, 1988, 918.

24. C.D.Tran and G.S.Beddard, *J. Am. Chem. Soc.*, 1982, **104**, 6741.

25. D.A.Lightner, M.Reisinger and G.L.Landen, *J. Biol. Chem.*, 1986, **261**, 6034.

26. D.A.Lightner, J.K.Gawronski and K.Gawronska, *J. Am. Chem. Soc.*, 1985, **107**, 2456.

27. K.Kano, KYoshiyasu and S.Hashimoto, *J. Chem. Soc. Chem. Commun.*, 1988, 801.

28. CRC 'Handbook of Chemistry and Physics', p1719.

29. E.B.Starky, 'Organic Synthesis', Collective Vol.2, Wiley, New York, 1943, p225.

30. R.C.Blume and H.G.Lindwall, *J. Org. Chem.*, 1945, **10**, 255.

31. F.J.Kedzy, J.Jaz and P.Bruylants, *Bull. Soc. Chim. Belges*, 1958, **67**, 687.

32. K.P.M.Heirwegh and N.Blanckaert in 'Bilirubin', Vol.2, p133, (K.P.M.Heirwegh and S.B.Brown, Eds.), CRC Press, 1982.

33. P.N.Jun and R.A.Bartsch, *J. Org. Chem.*, 1979, **44**, 143.

34. T.Kuokkanen and P.O.I.Virtanen, *Acta Chem. Scand.*, 1979, **B33**, 725.

35. J.A.T.P.Meuwissen and K.P.M.Heirwegh in 'Bilirubin', Vol.2, p39, (K.P.M.Heirwegh and S.B.Brown, Eds.), CRC Press, 1982.

36. R.Stocker, A.N.Glazer and B.N.Ames, *Proc. Natl. Acad. Sci.*, USA, 1987, **84**, 5918.